Real Time Full Circuit Driving Simulation System

N.H.Louw

Thesis presented in partial fulfilment of the requirements for the M.Sc Eng. degree in Mechanical Engineering at the University of Stellenbosch

Supervisor: Dr. A.B. Taylor

December 2004

Declaration

I, the undersigned, hereby declare that the work contained in this thesis is my own work and that I have not previously in its entirety or in part submitted it at any university for a degree.

Abstract

The requirements regarding the quality of engines and vehicles have increased constantly, requiring more and more sophisticated engine testing. At the same time, there is a strong demand to reduce lead time and cost of development. For many years steady state engine testing was the norm using standard principles of power absorption. Since the mid 1980's increasing importance has been attached to the optimisation of transient engine characteristics and the simulation of dynamic real world driving situations on engine test stands. This has led to the use of bi-directional DC or AC regenerative dynamometers a practice now known as dynamic engine testing.

Interfacing a computer with vehicle simulation software to an engine on a dynamic test stand and using "hardware in the loop" techniques, enables the simulation of real world driving situations in a test facility. In dynamic engine testing a distinction can be made between simulation testing and transient testing. In simulation testing the set point values are predetermined whereas in transient testing a model generates set point values in real time. Speeds and loads are calculated in real time on the basis of real time measurements. The model can be in the form of a human or driver simulation.

This project involved the application of dynamic engine testing to simulating a racing application. It is termed Real Time Full Circuit Driving Simulation System due to the simulation of a race car circling a race track, controlled by a driver model and running the engine on a dynamic test bench in real time using "hardware in the loop" techniques. By measuring the simulated lap times for a certain engine configuration on the test bench in real time, it is possible to select the optimal engine set-up for every circuit. The real time nature of the simulation subjects the engine on the test bench to similar load and speed conditions as experienced by its racing counterpart in the race car yielding relevant results. The racing simulation was achieved by finding a suitable dynamic vehicle model and a three dimensional race track model, developing a control strategy, programming the software and testing the complete system on a dynamic test stand.

In order to verify the simulation results it was necessary to conduct actual track testing on a representative vehicle. A professional racing driver completed three flying laps of the Killarney racing circuit in a vehicle fitted with various sensors including three axis orientation and acceleration sensors, a GPS and an engine control unit emulator for capturing engine data. This included lap time, vehicle accelerations, engine speed and manifold pressure, an indicator of driver input. The results obtained from the real time circuit simulation were compared to actual track data and the results showed good correlation.

By changing the physical engine configuration in the hardware and gear ratios in the software, comparative capabilities of the system were evaluated. Again satisfactory results were obtained with the system clearly showing which configuration was best suited for a certain race track. This satisfies the modern trend of minimizing costs and development time and proved the value of the system as a suitable engineering tool for racing engine and drive train optimisation.

The Real Time Full Circuit Driving Simulation System opened the door to further development in other areas of simulation. One such area is the driveability of a vehicle. By expanding the model it would be possible to evaluate previously subjective characteristics of a vehicle in a more objective manner.

Opsomming

Die vereistes om die kwaliteit van enjins en voertuie te verhoog, word daagliks hoër. Meer gesofistikeerde enjintoetse word daarom vereis. Terselfdertyd is dit 'n groot uitdaging om die tydsduur en koste van ontwikkeling so laag as moontlik te hou. Gestadigde toestand enjintoetse, wat op die prinsiep van krag absorpsie werk, was vir baie jare die norm. Vanaf die middel tagtigerjare het die optimering van dinamiese enjinkarakteristieke en die simulasie van werklike bestuursituasies op enjintoetsbanke van al hoe groter belang geword. Die gevolg was die gebruik van twee rigting wissel- of gelykstroomdinamometers en staan vandag bekend as dinamiese enjintoetsing.

Deur 'n rekenaar met simulasiesagteware aan 'n enjin op 'n dinamiese toetsbank te koppel, word die moontlikheid geskep om enige werklike bestuursituasies van 'n voertuig te simuleer in die enjintoetsfasiliteit. Dinamiese enjintoetse kan opgedeel word in simulasietoetse en oorgangstoestandtoetse. By laasgenoemde genereer 'n "bestuurdersmodel" die beheerwaardes intyds deur te kyk na intydse metings terwyl by simulasietoetse die beheerwaardes vooraf bepaal word. Die "bestuurder" kan in die vorm van 'n persoon of rekenaarsimulasie wees.

Die projek behels die toepassing van dinamiese enjintoetse vir renbaansimulasie en staan bekend as 'n Intydse, Volledige Renbaansisteem weens die simulasie van 'n renmotor om 'n renbaan, onder die beheer van 'n bestuurdersmodel. Dit geskied terwyl die enjin intyds op 'n dinamiese enjintoetsbank loop en gekoppel is aan die simulasie. Deur die intydse, gesimuleerde rondtetye te analiseer, word die moontlikheid geskep om die enjinkonfigurasie te optimeer vir 'n sekere renbaan. Dit is bereik deur die keuse van 'n gepaste dinamiese voertuigmodel, 'n driedimensionele renbaanmodel, ontwikkeling van 'n beheermodel, programmering van die sagteware en integrasie van die dinamiese enjintoetsstelsel.

Die simulasieresultate verkry is gestaaf deur werklike renbaantoetse. 'n Professionele renjaer het drie rondtes van die Killarney renbaan voltooi in 'n verteenwoordigende voertuig wat toegerus was met verskeie sensors o.a. drie as versnellings- en orientasiesensors, GPS en 'n enjinbeheereenheidemmuleerder vir die verkryging en stoor van enjindata. Die sensors het data versamel wat insluit rondtetyd, voertuigversnellings, enjinspoed en inlaatspruitstukdruk. Die korrelasie tussen die simulasie waardes en werklik gemete data was van hoë gehalte.

Deur die fisiese enjinkonfigurasie te verander in die hardeware en ratverhoudings in die sagteware, is die vergelykbare kapasiteite van die renbaansimulasie geevalueer. Die resultate was weer bevredigend en die simulasie was in staat om die beste enjinkonfigurasie vir die renbaan uit te wys. Dit bevredig die moderne neiging om koste en ontwikkelingstyd so laag as moontlik te hou. Sodoende is bewys dat die stelsel waarde in die ingenieurswêreld het.

'n Intydse, Volledige Renbaansisteem die skep die geleentheid vir verdere ontwikkeling op verskeie terreine van simulasie. Een so 'n veld is die bestuurbaarheid van 'n voertuig. Deur die model verder te ontwikkel word die moontlikheid geskep om voorheen subjektiewe karakteristieke van 'n voertuig meer wetenskaplik te analiseer.

Acknowledgements

I would like to thank the following parties for their involvement in my project and their assistance in this work:

- Dr A.B. Taylor, my supervisor for his guidance, knowledge and motivation during the duration of my studies.

- All CAE personnel who helped and supported me in various ways, especially Gerhard Lourens whose assistance I greatly value.

- The Western Province Motor Club for the use of the Killarney race circuit.

- Racing driver Deon Joubert for the Killarney track testing.

Table of contents

List of tables

List of figures

List of symbols

A	Frontal area	[m^2]
a_x	Longitudinal vehicle acceleration	[m/s^2]
a_y	Lateral acceleration	[m/s^2]
B	Stiffness factor	
b	Longitudinal distance from front axle to centre of gravity	[m]
C	Shape factor	
c	Longitudinal distance from centre of gravity to rear axle	[m]
C_d	Coefficient of drag	
D	Peak factor	
e(t)	Error signal	
E	Curvature factor	
F_c	Friction circle radius	[N]
F_d	Aerodynamic drag force	[N]
F_g	Gradient force	[N]
f_m	Mass factor	
F_{nf}	Normal force front	[N]
F_r	Rolling resistance force	[N]
f_r	Rolling friction coefficient	
F_{res}	Resistance force	[N]
F_x	Longitudinal force	[N]
F_{xmax}	Maximum longitudinal force	[N]
F_y	Lateral force	[N]
F_{yf}	Lateral force on front axle	[N]
G_f	Final drive ratio	
G_{tf}	Overall transmission ratio	
h	Height of centre of gravity above ground	[m]
J_d	Dynamometer inertia	[kgm^2]
J_e	Engine inertia	[kgm^2]
J_v	Equivalent vehicle angular inertia	[kgm^2]
K_i	Integral gain	
K_p	Proportional gain	
L	Vehicle wheel base	[m]
M	Vehicle Mass	[kg]
M_f	Mass on front axle	[kg]
m_r	Mass ratio	
N	Dynamometer rotational speed	[rpm]
$\dot{N}$	Dynamometer speed gradient	[rpm/s]
N_e	Engine speed	[rpm]
N_{emax}	Maximum engine speed	[rpm]
N_{fd}	Final drive speed	[rpm]
R_c	Corner radius	[m]
R_w	Wheel radius	[m]
S_h	Horizontal shift	
S_v	Vertical shift	
s	Distance	[m]
t	Time	[s]
Δt	Time increment	[s]
T_c	Clutch torque	[Nm]

T_d	Time derivative constant	
T_e	Engine torque	[Nm]
T_l	Load Torque	[Nm]
T_{lc}	Load cell torque	[Nm]
T_t	Traction torque	[Nm]
T_v	Total vehicle load as seen at the clutch	[Nm]
$u(t)$	Controller output	
V	Vehicle speed	[km/h]
V_{new}	New vehicle speed	[km/h]
V_{old}	Old vehicle speed	[km/h]
W	Vehicle weight	[N]
W_{fd}	Dynamic weight on front axle	[N]
W_{fe}	Extra weight on front axle	[N]
W_{fs}	Static weight on front axle	[N]
x	Slip angle or longitudinal slip	[degrees]
X	x after adding shift factor	
X_i	Initial track position	[m]
$y(x)$	Side force/brake force/self aligning torque	[N]/[N]/[Nm]
$Y(X)$	y after adding shift factor	
α_d	Dynamometer angular acceleration	[rad/s^2]
α_e	Engine angular acceleration	[rad/s^2]
α_v	Equivalent vehicle angular acceleration	[rad/s^2]
η	Drive train efficiency	
η_{tf}	Total drive train efficiency	
Φ	Gradient	[radians]
ρ	Air density	[kg/m^3]
θ	Bank angle	[radians]
μ	Friction coefficient	
ω_e	Engine speed	[rad/s]
CAD	Computer Aided Design	
CAE	Stellenbosch Automotive Engineering	
CircuitSim	Real Time Full Circuit Driving Simulation System software	
CPU	Central Processing Unit	
ECU	Engine Control Unit	
ETA	CAE's dynamometer control software	
ETK	Engine control unit emulator	
PLC	Programmable Logical Controller	
RAM	Random Access Memory	
WAAS	Wide Area Augmentation System	
WOT	Wide Open Throttle	

1. Introduction

In recent years motor manufacturers have been placed under increasing pressure to produce highly efficient and clean burning engines while being expected to decrease both their development time and costs. Despite this customers still demand lively performance from their vehicles. These requirements have forced manufacturers to look at more sophisticated ways of testing engines, resulting in one of the latest aids in engine development, the ***Dynamic Engine Testing Facility.***

This facility enables manufacturers to subject their engines to dynamic conditions and yields results superior to the conventional steady state testing techniques. These dynamic conditions include simulation of in-vehicle dynamic events. The cornerstone of the facility is a regenerative AC or DC dynamometer with computer based control systems, which insures dynamic loading and repeatable results.

Although this technology is mostly used for emission regulation testing, it is clear that a lot of potential is still overlooked. One of the applications for the ***Dynamic Engine Testing Facility*** is motor racing. This industry could benefit tremendously in both performance and cost, by optimising the race set up, before the actual race track testing is carried out.

The dynamic real time engine testing makes it possible to test different drive train configurations on a controlled engine test stand. Running the simulation in real time and under transient conditions gives more realistic results than steady state testing and eliminates the human factor present in on-track testing.

Any vehicle simulation is only as good as the dynamic vehicle model and track model incorporated within the simulation software. The real time nature of the simulation must be taken into account when choosing a dynamic vehicle model. Models that use iterative methods when calculating certain vehicle parameters may be too time consuming. The accuracy of the simulation is dependent on the length of time increment of the numerical integration process and comprehensiveness of the dynamic vehicle model. This last requirement will invariably lead to a compromised solution.

The track model consists of a three dimensional representation of the actual circuit. It will include the gradients, bank angles, length of straights and radii of corners. The precise collection and representation of the data in the software will contribute to the representativeness of the simulation.

This document commences with a need identification and objectives section followed by a literature study. Thereafter the process of developing the driving simulation is discussed. The implementation of the simulation focuses on the test system components. Results achieved by track testing were used for the correlation analysis. The document concludes with a recommendation and conclusion section.

The end result of this study was the implementation of a **Real Time Full Circuit Driving Simulation System** that could be used effectively for race car engine development and optimisation.

2. Need identification and objectives

In the world of ever increasing pressure for faster development, decreased cost and shorter lead times, there is a need for effective optimisation of the internal combustion engine. The dynamic testing facility combined with the AC or DC dynamometer has played its part, especially in the field of emission regulation.

One area of application for this facility is racing. To optimise a race engine for a circuit takes immense resources, including personnel, funds and time. Typically when a race team wants to test a new engine configuration, it will books the track including the test driver. Several test laps are completed. Human error and ever-changing track conditions leave the test team with very expensive yet unreliable results.

The objective of this work was to investigate the advantages of using dynamic engine testing to improve race engine optimisation by cutting cost, shortening lead times and by producing repeatable results. The scope of the project was as follows:

Scope:
- The development of a dynamic vehicle model.
- The development of a race track model.
- The development and implementation of a traction control strategy.
- Integrate the above in a Real Time Full Circuit Driving Simulation System.
- Refine the engineering tool to simplify engine and drive train optimisation for a certain circuit.

In order to reach the goals of this project certain outcomes were envisaged:

Outcomes:
- Develop software that includes racetrack and dynamic vehicle models.
- Include a traction model in the software.
- Link software with an AC or DC dynamometer to form a "hardware in the loop" simulation.
- Run real time simulations in order to measure lap times.
- Correlate results with actual race data.
- Run comparative tests to evaluate the system for accuracy and to determine the value as an engineering tool.

3. Literature study

In order to achieve the goals of this project it was necessary to carry out an extensive literature study on dynamic engine testing and race track simulation. Only when the theory of dynamic engine testing and lap time simulation techniques were fully understood could they be combined in a real time "hardware in the loop" simulation.

The hardware of the system was the dynamic engine testing facility consisting of a test bench and a DC or AC dynamometer with computer control. To understand the process the following were researched.

3.1 Dynamic engine testing

According to Voos (1992) the demand from industry for more sophisticated engine testing began in the middle 1980's. Cassidy and Rillings (1972) realised as early as 1972 that by placing an engine on a test bench under computer control, combines the advantages of on-road testing and dynamometer testing. Increased importance was attached to optimisation of the transient engine characteristics and it was the purpose of the test equipment to simulate actual driving conditions. This led to the development of a typical dynamic engine testing facility as illustrated in Figure 3.1. Leonhardt et al. (1992) stated that the dynamical test stand might be used as an advanced tool for combustion engine optimisation and control.

Figure 3.1 Dynamic engine test facility (http://www.mech.kuleuven.ac.be)

3

3.1.1 Definitions of steady state and dynamic engine testing

3.1.1.1 Steady state engine testing

Steady state engine testing is the most commonly used method for testing engines and makes use of fluid or eddy current absorption dynamometers (Voos, 1992). These type of dynamometers are capable of providing adequately stable loads at constant speeds. These conditions are representative of those experienced by a vehicle driven on a road at constant speed and are therefore frequently used to conduct durability tests. In steady state engine testing the control of the engine is based upon set values, which are constant for longer periods of time.

3.1.1.2 Dynamic engine testing

According to Voos (1992) the control in dynamic engine testing is based upon closed loop control where the set point values change continuously. Direct presetting of set point values for torque and speed in dynamic engine testing changes the test stand into a transient test stand. If the set point values are not directly preset but are determined with the help of a model prior to testing Voos (1992) speaks of a simulation test stand as illustrated in Figure 3.2.

```
            ┌─────────────────────────┐
            │  Dynamic engine testing │
            └─────────────────────────┘
             ╱                       ╲
            ╱                         ╲
┌──────────────────────┐    ┌──────────────────────┐
│  Transient test stand│    │ Simulation test stand│
└──────────────────────┘    └──────────────────────┘
```
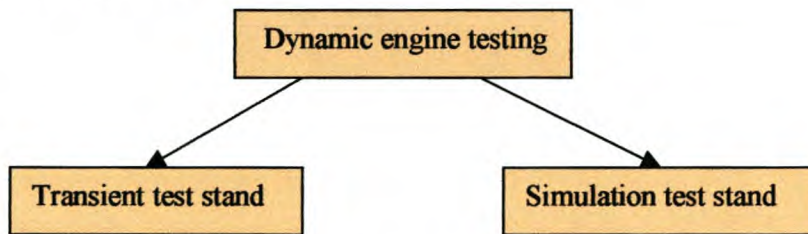
Figure 3.2 Types of dynamic engine test stands

3.1.2 The DC or AC Dynamometer

The basis of the dynamic engine testing facility is the DC or AC dynamometer (Voigt, 1991) During the last number of years the introduction of the AC or DC electric motor in the field of engine testing represented a quantum leap forward. For many years the classical dynamometer worked on the principle of eddy current absorption and was used as the loading (brake) unit in engine test stands. These are still in use today and play an important role in steady state engine testing.

The advancement in power electronics and increased maximum speeds of DC and AC machines have boosted the application of DC and AC thyristor drives in engine testing. In the past this was done for engine motoring applications as in friction tests, simulation of inertia motoring as well as energy recovery. As experience was gained it became apparent that this set-up could be utilized for dynamic engine testing.

4

3.1.3 Benefits of dynamic engine testing

The benefit of dynamic testing is that one can reproduce more realistic loads on the test engine by varying the load to simulate real operating conditions. According to Hong (1995) the main difference between static and dynamic tests are caused by the effect of inertia. There are three forms of inertia evident in an internal combustion engine.

- Flow inertia.

The internal combustion engine operates as an air pump with a throttle to limit the airflow to the engine in spark ignition engines. Sudden changes in throttle angle during dynamic engine testing events will influence the amount of air that reaches the cylinders due to the inertia of the air. This is normally termed "throttle lag".

- Thermal inertia.

Almost a third of the power developed in the cylinder is lost through heat transfer. Heat transfer is a function of the convection coefficient, the heat transfer area and the temperature difference between the combustion gas and the cylinder walls (Conradie, 2001). The thermal inertia present during dynamic engine testing events influences the energy balance at the cylinder wall boundary.

- Mechanical inertia.

The mass of the rotating parts in the drive train manifests itself as mechanical inertia during dynamic engine testing events. The above will play very little part in static engine testing where time dependent variables are allowed to stabilize before readings are taken. In dynamic engine testing inertia will have a noticeable effect on engine performance, which is a more realistic representation of the engine in an actual vehicle where acceleration is involved.

Gallacher and Krebi (1995) considered the benefits of dynamic engine testing and found that the dynamic test stand is not only capable of producing road conditions through road load and driver simulation, but also capable of reproducing gear shifts, throttle tip-ins and acceleration with the aid of electrical inertia simulation.

3.1.4 Applications for dynamic engine testing

New technologies are required to meet the demands of engine optimisation for low fuel consumption, strict emissions control and driveability. Currently the dynamic test stands are mostly used in the field of research and development and cover the following test objectives as stipulated by Voos (1992):

- Testing the control response and drivability of the components for ignition and fuel supply, for example the change in throttle position.
- Dynamic endurance testing with load and speed characteristics corresponding to actual driving conditions.
- Comparative measurements of fuel consumption and exhaust emission in the early phases of development to provide data that is necessary for modifications of design and engine optimisation.
- Acceptance tests under the EPA Heavy-Duty Transient Cycle.
- Optimisation of engine management systems.
- Noise measurement on exhausts systems during acceleration and inertia motoring.

The main advantages of dynamic engine test stands are that they enable the simulation of testing on the road, in particular:

- Ease of changing vehicle parameters via the simulation computer for example gearbox ratios, vehicle mass and drive train efficiency.
- Reduction of development periods because the engine characteristics and the influence of vehicle parameters on the engine characteristics are defined on the engine test stand.
- Repeatability of results.

The above advantages also apply to the Real Time Full Circuit Driving Simulation System. Changing the vehicle parameters in the simulation closely resembles the race track situation where the optimal race set-up is sought. Race engineers will experiment with different gear ratios, tyre pressures, suspension set-up and engine calibration in order to minimize lap time. This can easily be done in the software of the simulation without the cost and time penalty.

6

3.2 Lap time simulation

Considerable effort has gone into modelling the performance of a race car by engineers in professional motor sport teams (Siegler et al., 2000). This allows for optimisation of vehicle parameters to be achieved in a more cost and time efficient manner. Although track testing cannot be replaced by simulation packages, it improves the efficiency of physical testing.

The purpose of lap time simulation is to optimise all vehicle parameters to suit a certain race track, even if the vehicle has never operated on the track before. A race simulation package consists of a dynamic vehicle and track model that represents the actual race car and race track. By employing a driver model the simulation "drives" the virtual vehicle around the virtual track in order to measure lap times. Lap time is the deciding factor that determines if one set up configuration results in a higher speed than another. The faster the lap time the better the configuration.

3.2.1 Lap time simulation methods

The most common and widely used method for lap time simulation has been described by Milliken (1995). It involves using the corners of the race track as the limiting factors. The maximum speed a vehicle can negotiate a certain corner with known radius, bank angle and approximate friction coefficient can be found. This maximum speed is independent of the speeds along the straights of the circuit. With the maximum entry and exit speed of every corner known, it is possible to find the vehicle's speed along the straights.

Siegler et al. (2000) looked at a method where the whole lap is divided into small segments and an analysis made of the vehicle at each segment point, using the external forces acting on the vehicle. They also looked at three methods by which the vehicles performance in the corners could be modelled.

3.2.1.1 Steady state strategy

The first step is to use a steady state model where the vehicle's longitudinal and lateral acceleration performance is modelled separately, meaning that the vehicle brakes and then turns. Thus, only lateral performance of the vehicle is taken into consideration during cornering.

The steady state solution occurs when the system is in equilibrium and the time dependent variables constant. This can be done by using a Newton-Rhaphson technique. This technique is based on negotiating the corner at a fixed velocity, steer angle, path radius and maximum lateral acceleration. This is theoretically only possible through a constant radius turn.

7

3.2.1.2 Quasi-static modelling strategy

Quasi-static modelling is similar to the steady state strategy but in this case the corner is split up into a series of constant radius segments. Larger number of corner segments improves the accuracy of the solution. At each path segment the vehicles acceleration is found by allowing the simulation to settle down to its steady state values. The lateral tyre force needed to maintain this acceleration can be found using the friction circle concept (explained later). The remaining tyre force available is then used to calculate the longitudinal acceleration of the vehicle. This ensures that the total combined lateral and longitudinal forces generated by the tyre are equivalent to what a real tyre is capable of producing. The minimum path radius and speed at the apex is again found by the Newton-Rhaphson iteration technique.

3.2.1.3 Transient modelling strategy

In this strategy a transient solution is sought. This is found when a vehicle is undergoing non-steady linear and/or angular accelerations. In reality, as the vehicle corners, it is never in equilibrium as the vehicle is always accelerating in a combination of the lateral, longitudinal or normal directions and/or the rotational pitch, roll or yaw directions.

The transient solution takes into account the response time (Siegler et al., 2000) of the vehicle in changing its attitude and direction of travel. Consequently, complex transient simulations can be performed which include the effect of dynamic yaw on the model.

3.2.1.4 Conclusion on cornering strategies

Siegler et al. (2000) has found that the difference in overall time for a j-turn varied between 2.71s and 2.85s for the different solution techniques. However, the quasi-static and especially the transient solution takes into account vehicle factors not included in the steady state solution such as dynamic yaw. This will allow the accurate optimisation of a greater number of vehicle parameters. The disadvantage is more complex governing equations, which may slow down the computational process in real time. All three solutions can be used to optimise vehicle parameters to minimize lap time.

8

3.3 Tyres

Tyres are the primary source of the forces and torques, which provide control and stability of the vehicle (Milliken, 1995). This includes tractive, braking, and cornering forces. Tyres are also designed to resist external forces such as road disturbances and wind. For these beneficial effects there is a compromise in terms of rolling resistance and drag.

3.3.1 Tyre model

A tyre model represents the forces and loads experienced by the actual tyres of a vehicle in a software model. The following characteristics are important in a tyre model (Milliken, 1995):

3.3.1.1 The print and "grip"

The area of the tyre that is in contact with the ground is called the footprint of the tyre or the contact patch. The term "grip" refers to the interaction of the rubber elements of the tyre and surface of the road at the contact patch. The rubber interacts with the road by various mechanisms including mechanical gearing to the texture of the pavement and molecular adhesion to the surface. Fortunately it is not necessary to understand the physical interaction but only the associated forces. The acceleration performance of a race car in any direction is limited by the tyre contact forces.

3.3.1.2 Lateral forces

A vehicle turns because of an applied lateral force. According to Vehicle Dynamics Terminology (SAE J670e, 1976) a lateral tyre force originates at the centre of the contact patch, lies in the horizontal road plane and is perpendicular to the direction in which the wheel is headed if no inclination or camber angle exists. Lateral force may be thought of as a result of slip angle. Slip angle is the angle between the travelled direction and tyre heading.

9

A typical lateral force vs. slip angle diagram can be seen in Figure 3.3.
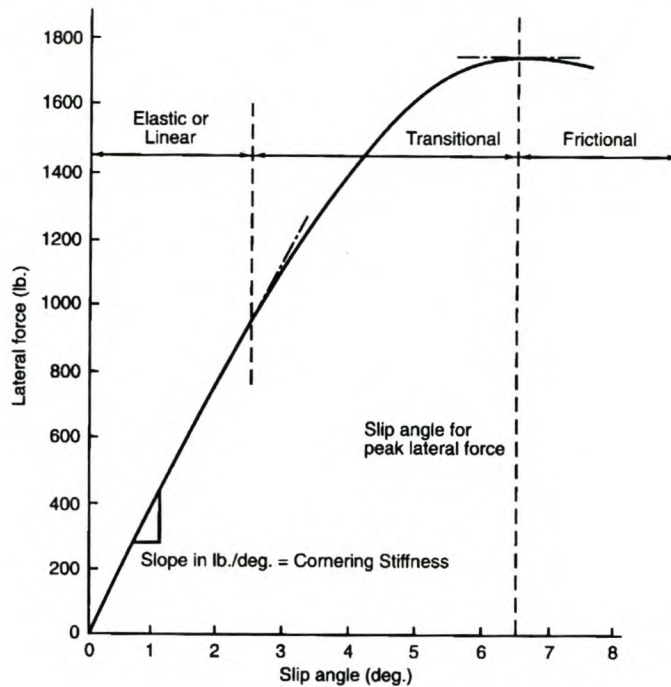
Figure 3.3 Lateral force vs. slip angle (Milliken, 1995)

3.3.1.3 Aligning torque and pneumatic trail

Aligning torque describes the tendency of a tyre to steer about a vertical axis through the centre of the contact patch. This usually happens at low or medium slip angles where the tyre tends to align its heading with its path. The torque originates from the form of the deformed footprint of a tyre when cornering. This gives an uneven lateral force distribution that gives rise to an aligning torque. The asymmetric footprint is called pneumatic trail as illustrated in Figure 3.4. This is the distance from the fore-aft centre of the footprint to the vertical steering axis. The aligning torque is the lateral force multiplied by the pneumatic trail.
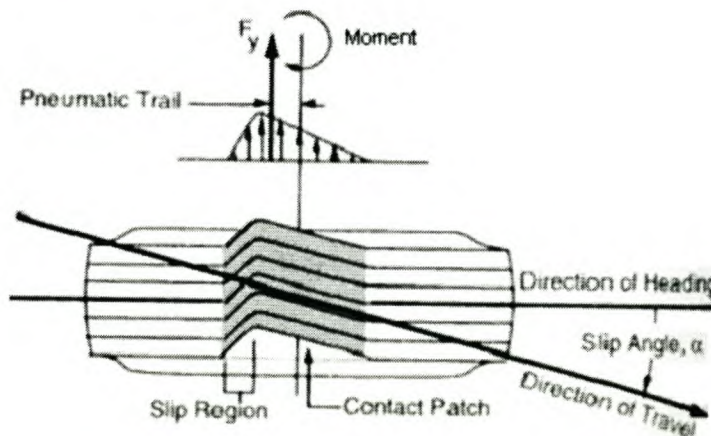
Figure 3.4 Pneumatic Trail (Gillespie, 1992)

3.3.1.4 Longitudinal force

For a vehicle to accelerate and brake in a straight line, a longitudinal force must be present at the tyre contact patch. The magnitude of this force is in accordance to Newton's second law that incorporates the change in vehicle momentum. Applying a driving force to the wheels by means of a drive train and engine combination generates a tractive force. This force can only be generated at the driven wheels. Applying a braking torque to a wheel generates a braking force. Slip ratio is the ratio between the angular velocity of a driven or braked wheel and a free rolling wheel.

3.3.1.5 Camber effects

Camber is the angle between the tilted wheel and the vertical axis. Positive camber means the top part of the wheel leans to the outside relative to the vehicle. Camber force or camber thrust is the force in the direction of tilt. This usually occurs during zero slip angles. This is again due to a distorted footprint. In a race car the suspension set up may include camber angles to assist the handling of the car for certain corners on a racetrack.

3.3.1.6 Tyre pressure

One of the easiest and most common changes to a race car is the tyre pressure. This is mostly done to alter the over steer / under steer handling characteristics of the race car. If the tyre pressure is increased the carcass will get stiffer and cornering stiffness will increase. Therefore, lateral forces will increase. Rolling resistance will also decrease with increasing pressure. The "ride" of the vehicle is on the other hand adversely affected by increasing the pressure although this is not that important in a race car.

3.3.1.7 Tyre temperature

Temperature directly influences the force producing capabilities and life expectancy of a tyre. Race car tyres tread compounds have an optimum temperature range for maximum grip. If the tyre is too cold the traction will be low and if too hot it will wear excessively.

3.3.2 Tyre force strategies

3.3.2.1 Friction circle/ellipse strategy

All lap time simulation models use a strategy to determine the tyre forces of the vehicle. A popular method is the friction circle concept as mentioned by Milliken (1995). A combination of the possible lateral and longitudinal forces can be drawn in an ellipse diagram as Figure 3.5 illustrates, where one axis represents lateral forces and the other longitudinal forces. If the vehicle is only accelerating or braking in a straight line then the "force point" will lie on the longitudinal axis, similarly if a vehicle is cornering at a constant velocity (ignoring drag, rolling and gradient resistance), then the "force point" will lie on the lateral axis. The outer part of the

11

ellipse represents the maximum force possible for a certain tyre. When a vehicle is braking into a corner the tyre experiences a combination of lateral and longitudinal forces.
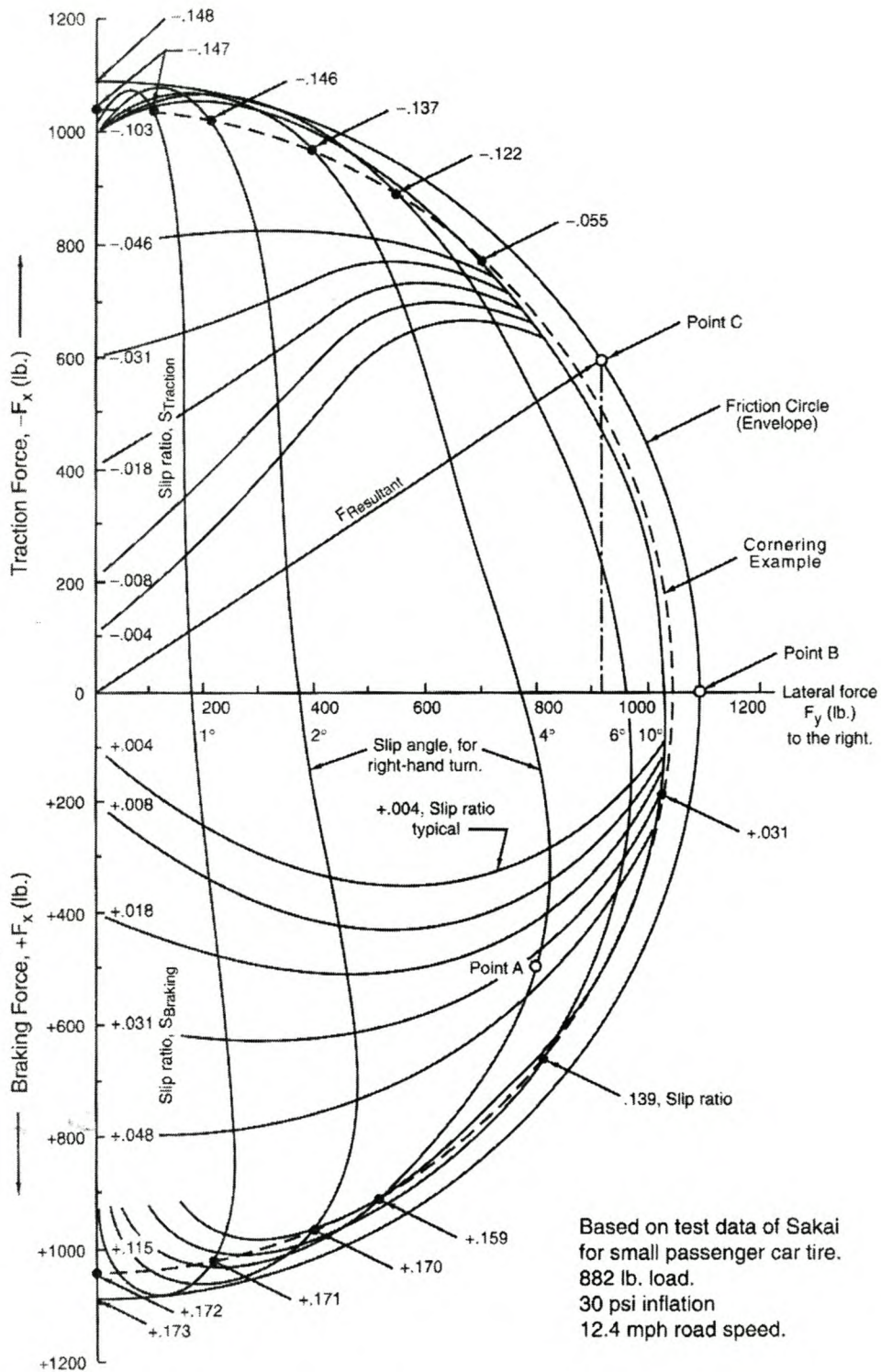
Figure 3.5 Friction Ellipse (Milliken, 1995)

The racing driver strives to drive on the outer limit of this ellipse in order to achieve maximum total acceleration and therefore the fastest possible lap time. Total acceleration includes acceleration, deceleration and cornering. This diagram usually forms the basis of any tyre model.

Milliken (1995) also showed that the vehicle's tyre forces can be represented by four ellipses, one at each wheel as seen in Figure 3.6. The ellipse's size then depends on the normal force present at each wheel. The total force available is the sum of all the individual forces.
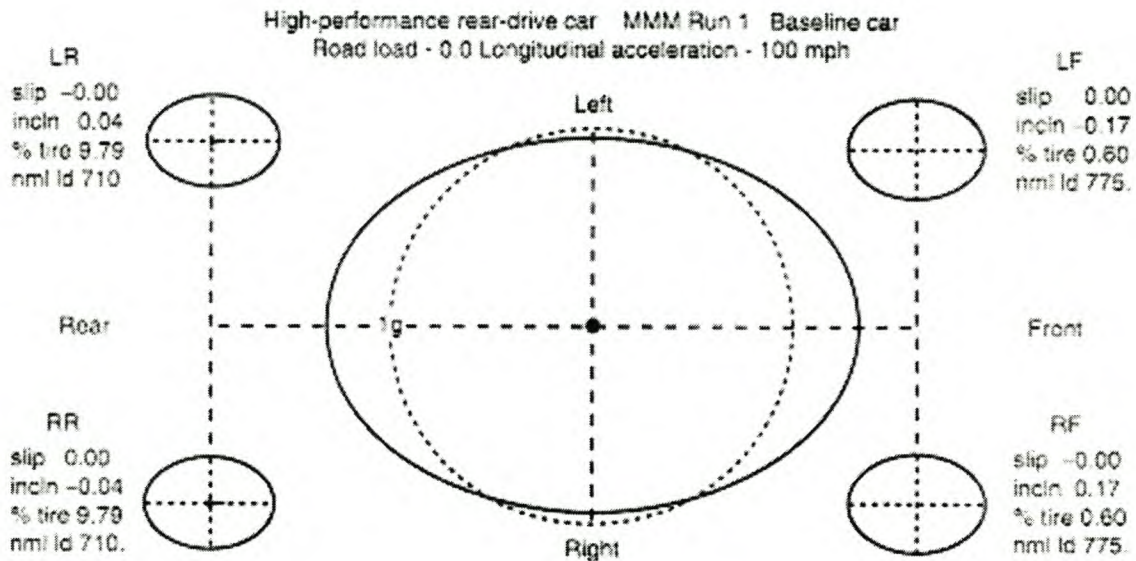
Figure 3.6 Independent tyre ellipses (Milliken, 1995)

3.3.2.2 Pacejka's tyre formula

To determine tyre forces is a complex problem. Tyre data are difficult to obtain and even if the data are available then it is quite difficult to represent it mathematically in a simulation model.

Pacejka et al. (1989) has derived a formula that correlates the actual tyre data obtained through a series of tests on the road in stationary conditions. The equations are in the form of:

$$y(x) = D\sin(C\arctan(Bx - E(Bx - \arctan(Bx)))) \tag{3.1}$$

$$Y(X) = y(x) + S_v \tag{3.2}$$

$$x = X + S_h \tag{3.3}$$

with

- x [degrees] denoting the slip angle or longitudinal slip
- y(x) representing either the side force [N], brake force [N] or self aligning torque [Nm]
- X [degrees] denoting the slip angle or longitudinal slip after adding shift factor
- Y(X) representing either the side force [N], brake force [N] or self aligning torque [Nm]after adding shift factor
- B = stiffness factor
- D = peak factor
- E = curvature factor
- S_h = horizontal shift
- S_v = vertical shift

The coefficients of the formula represent some of the typifying quantities of the tyre and the formula is capable of describing all characteristics of side force, brake force and self-aligning torque with great accuracy. The influence of ply steer, conical shape, rolling resistance and camber is also accounted for. Figure 3.7 shows the side force characteristics of a tyre as described by the formula in comparison with the measured data.
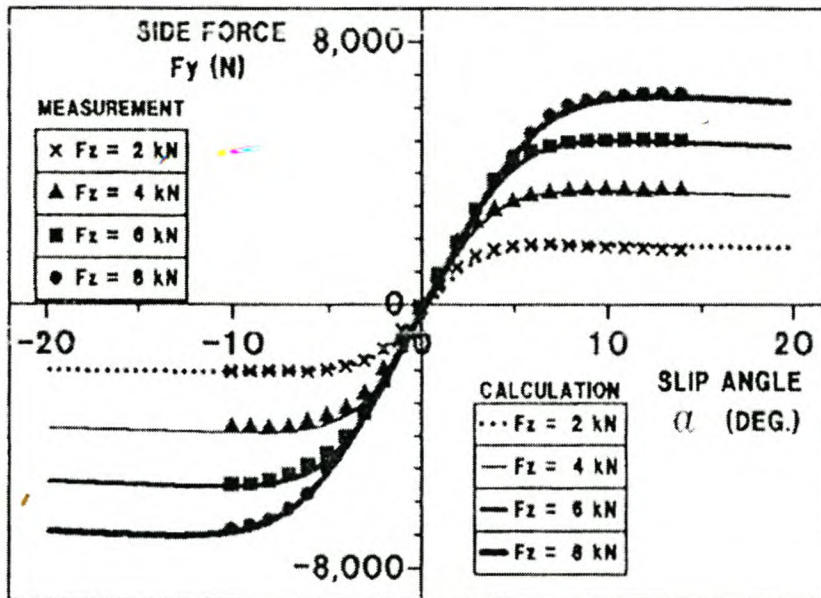
Figure 3.7 Side force characteristics using the tyre formula compared with measured data (Pacejka, 1989).

14

3.4 Dynamic vehicle model

3.4.1 External vehicle forces

The dynamic vehicle model is responsible for reproducing all the loads (see Figure 3.8) seen by the actual vehicle in the simulation. The general external forces are the same for all dynamic vehicle models and are fully described in the software development chapter.
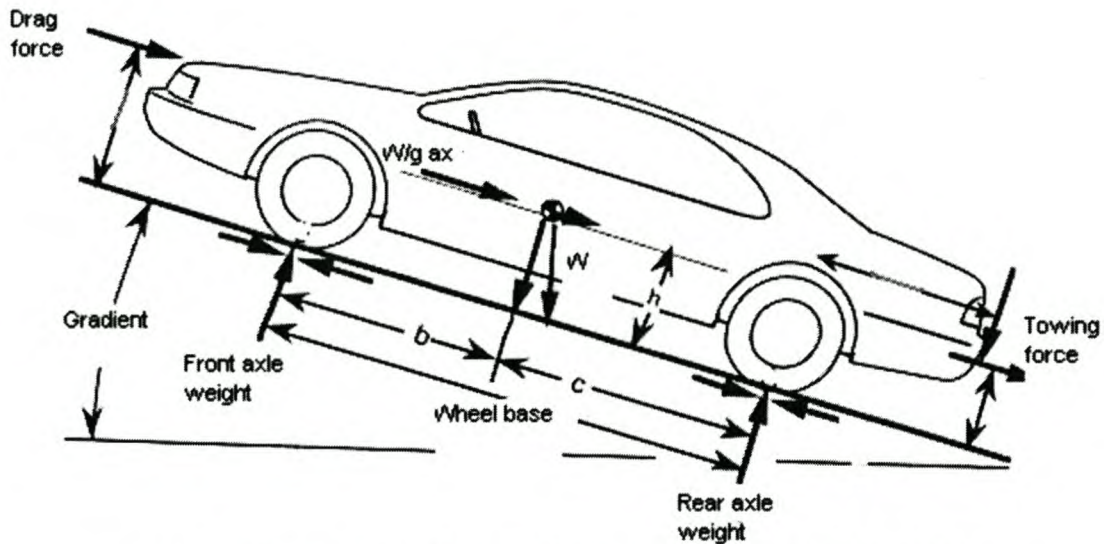
Figure 3.8 Summary of external vehicle forces (Gillespie, 1992)

3.4.2 Drive train and suspension

The drive train of a vehicle provides the torque at the driven wheels, which in turn leads to the tractive force that accelerates the vehicle. Although many of the actual drive train components are absent from the test stand, it is important to model their presence in the simulation software.

3.4.2.1 Engine

The engine in a car converts the fuel energy into a drive moment. The difference between a normal simulation model and a real time dynamic engine testing simulation is that the real time simulation uses the real time torque output of the engine on the test bench as an input.

3.4.2.2 Clutch

The clutch disconnects the engine from the drive train. Although the clutch is attached to an engine on a test bench, its primary function is to help damp drive train vibration. The clutch is seldom depressed during a real time simulation. Therefore any clutch action should be programmed in the simulation software and forms part of the dynamic vehicle model.

3.4.2.3 Gearbox

The primary function of the gearbox is to multiply the engine torque while matching the pre-differential shaft speed to the engine speed. There are usually no actual gear changes during a real time simulation and the normal technique of programming the gear ratios in the control software will have to suffice. The added advantage to race car simulation is that different gear ratios can be tested for a specific circuit.

3.4.2.4 Final drive and differential

The final drive has the same function as the gearbox, to multiply torque by reducing speed but this is done at a fixed ratio. This ratio is an important input into a dynamic vehicle model. Depending on the complexity of the vehicle model the differential action can also be included to distinguish between each driven wheel's speed and torque.

3.4.2.5 Suspension

The art of optimising the contact between the tyre and road surface of a race car can be summarized in one word: suspension (Milliken, 1995). Although there have been several patents over the years, the basic elements of a suspension remains the spring and damper as illustrated in Figure 3.9. Most suspensions can be simplified by a spring damper system for simulation purposes.
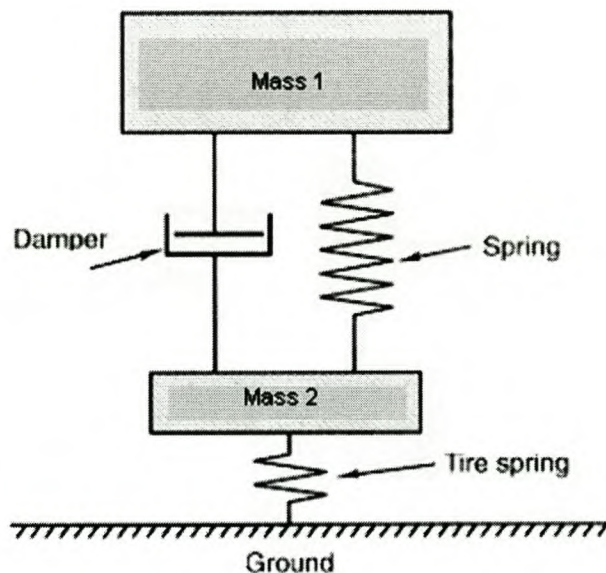
Figure 3.9 Spring-mass system (Milliken, 1995)

16

3.4.3 Vehicle control models

One of the basic design requirements of a race car is the provision of stability and control characteristics that enable a racing driver to drive near the outer limits of the tyre traction ellipse mentioned earlier. The basic flowchart of driver steering control over a vehicle is shown in Figure 3.10.
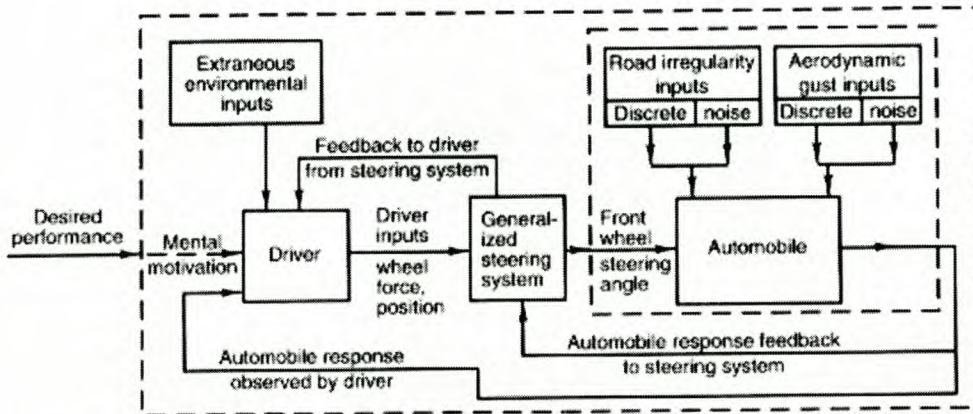
Figure 3.10 Driver steering control over vehicle (Milliken, 1995)

In open loop simulation the user is responsible for supplying the "driver" commands to follow a specific path. This is a trial and error procedure and would rarely be used in any simulation.

A superior method to the open loop simulation is the closed loop simulation. The "driver" in this case consists of a mathematical model. This model is responsible for assessing the error between the simulated and measured path and making the necessary corrections to the driver inputs. In synthesizing a first-approximation linear differential equation model of the human driver, two properties are immediately suggested by intuition (Gillespie, 1992):

- Reaction time delay

Several experiments show that the absolute minimum reaction time of humans is in the order of 0.15s. This must be incorporated in the model.

- Feedback control

Due to the closed loop nature of the simulation a feedback is necessary to correct the error signal. A common feedback controller used is the PID controller that is discussed in a later section.

When the objective of dynamic engine testing is to optimise an engine configuration for a certain race track then it is of immense importance that the driver control model delivers repeatable results. The choice of vehicle control model is discussed in the next chapter.

17

4. Development of the driving simulation

4.1 Introduction

Although the Real Time Full Circuit Driving Simulation System was a "hardware in the loop" simulation, the only physical part of the vehicle that was utilized was the engine. The rest of the vehicle and racetrack was represented by software. A decision had to be taken on the use of available software or the programming of new software. The possible use of an existing dynamic vehicle model found in Adams, a product of MSC Software, was investigated but found to be unsuitable due to the following reasons:

- Complex dynamic vehicle models demand a lot of computing time for a simple manoeuvre such as a lane change. The accuracy of a real time simulation, which uses numerical integration, is compromised by large time steps.
- No real time calculation capability.
- No interfacing module or unit that couples software to existing hardware.

For this specific application a new software program had to be developed. This was achieved by following the process described in the rest of the chapter.

4.2 Choice of programming language

It was important to choose a programming language that best suited the application. Some of the factors, which were considered in the choice of programming language, were:

- Interfacing with hardware.

The CAE dynamic engine testing facility (Stellenbosch Automotive Engineering) consisted of a DC dynamometer coupled to a software programme named ETA via a PLC. The software had to communicate with the PLC in order to control the dynamometer and engine. This was done through an Eagle PC30 data acquisition card developed by Eagle Technology.

- Real time capability

During real time simulation the speed of the calculations was a critical factor as it influenced the accuracy of the simulation directly. The programming language, CPU speed and available RAM played a vital role in the processing speed.

- Ease of programming

Object orientated languages were considered as they speed up programming and make a user-friendly graphical interface easily attainable.

- Availability

The language has to be available to the student.

In the end it was decided to use **Delphi,** a Borland product, as the preferred language as it met all the above requirements and was successfully used by Conradie (2001) in the development of the CAE dynamic engine testing facility.

The student got accustomed to the programming language by studying relevant material and experimentation. The development of the software program called **CircuitSim** took an estimated 6 months.

4.3 Software components

The software consisted of the following components:

4.3.1 The dynamic vehicle model

The main software component of the real time full circuit simulation is the dynamic vehicle model (see Figure 4.1 below for an Adams model). It is clear that the accuracy of the simulation model is directly related to the appropriateness of the vehicle dynamic model and the interface between the computer based control systems and the hardware. The accuracy of the chosen model was only proven after the correlation between actual and simulated race data were done.
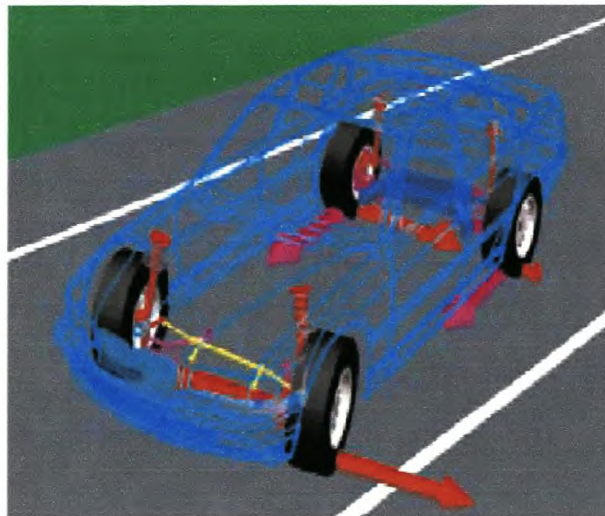
Figure 4.1 Adams dynamic vehicle model (http://www.adams.com)

4.3.1.1 Choice of vehicle model

As with the choice of programming language the appropriateness of the model depends on certain factors:

- Simplicity of the dynamic vehicle model.

It is important to keep the model as simple as possible without compromising the accuracy of the simulation. This is due to the real time nature of the simulation where calculation speed is very important. Complex equations can consume computing time to solve especially if iterations are necessary to reach convergence.

It must be mentioned that the prediction of absolute lap time is not the main focus of this project. If the engine behaviour on the test stand is similar to that of its counterpart in the race car, then it will be feasible to look at comparative lap times. It is still important that the absolute predicted lap time falls within 5% of the expected lap time.

- Appropriateness of model

The model must be representative of a race car. A vehicle model that models the behaviour of off-road vehicles will focus on different aspects of the vehicle and may not be appropriate.

According to Milliken (1995) a race car tends to be non-rolling and pitching due to a very stiff suspension set up and can be simplified to a two-degree of freedom system called the "bicycle" model as illustrated in Figure 4.2. The basic model is defined as follows:

- No lateral load transfer
- No longitudinal load transfer
- No rolling or pitching motions of the body
- Linear range tyres
- Constant forward velocity
- No chassis or suspension compliance effects

In order to use this model effectively in a racing simulation it had to be modified in the following way:

- Include longitudinal load transfer

By defining the position of centre of the gravity (COG) it was possible to calculate the force transfer between the front and rear wheels. This played a part in calculating the maximum traction force on the driven wheels.

20

- Include vehicle acceleration

The model represented a race car that experienced longitudinal and lateral accelerations and this almost led to a continuous change in forward velocity. This model formed the basis of CircuitSim's vehicle model.
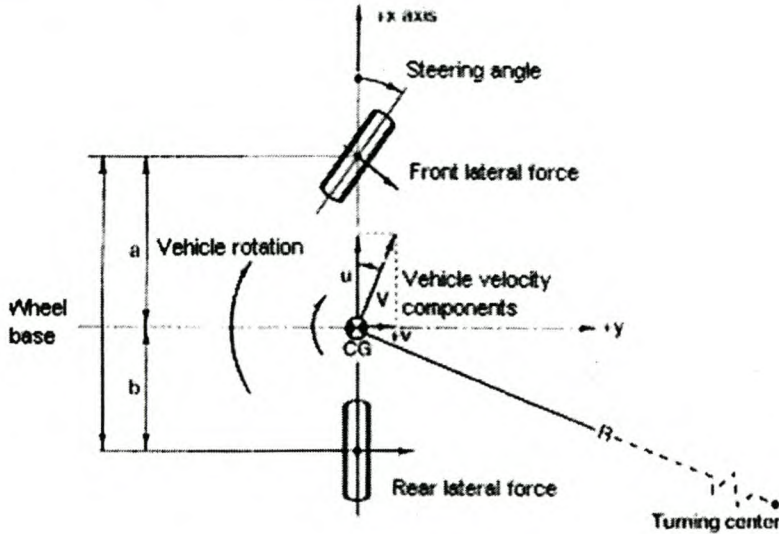
Figure 4.2 Bicycle model (Milliken, 1995)

4.3.1.2 Choice of control model

The racing driver is in control of the actual race car when circulating the track. A representative "driver" is needed to control the virtual vehicle while circuiting the virtual track in the software. The "driver" can be a mathematical model or control strategy. When considering that the main focus of the project is engine optimisation then it can be seen that the main requirements of the "driver" are:

- Consistency

For accurate comparison of lap times between different engine configurations it is important that the virtual driver has no room for human error. This requirement expels all driver models with variable properties, for example variable reaction time. The race car will circulate the race track on the ideal racing line.

- Simplicity

The same reasons that applied to the choice of software are also valid with the choice of control model. Calculation speed is directly influenced by control model complexity.

It was decided that the **friction ellipse** concept described in section 3.3.2.1 should be used. This means that the simulation program will try to drive the vehicle on the outer edge of the friction ellipse while staying on the racing line around the circuit.

21

4.3.1.3 Vehicle properties

In order to satisfy all the dynamic equations of the simulation the following properties concerning the vehicle are inputs to the model:

- Dimensions including wheelbase [m]
- Position of centre of gravity [m]
- Mass [kg]
- Drag coefficient
- Frontal area [m^2]
- Rotational inertia [kgm^2]
- Drive train efficiency
- Number of gears
- Gear and differential ratios
- Tyre size
- Rolling resistance coefficients
- Friction coefficients
- Brake deceleration [m/s^2]
- Engine torque curve
- Engine inertia [kgm^2]

This was done in the software program by entering the data in the blocks provided, ordered in categories by tabs as illustrated in Figure 4.3.
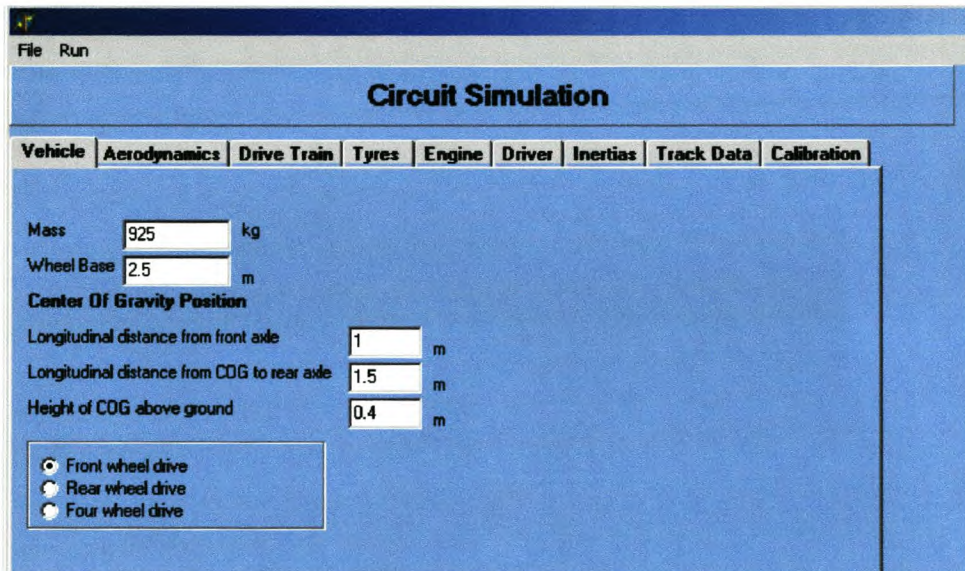
Figure 4.3 CircuitSim properties page

22

4.3.2 The track model

To optimise an engine for a race circuit by running a circuit simulation, it is necessary to program an accurate track model. The CircuitSim model consists of the following:

- Absolute position of the racing line
- Lengths of straights
- Gradients throughout the circuit
- Radii of all the corners
- Bank angles of all the corners

The method of gathering the above data will be discussed in the following section.

4.3.2.1 Method of gathering data

With the use of a Garmin 5 GPS it was possible to determine the layout of the circuit. Firstly the inner and outer edges of the circuit were measured followed by the racing line. By doing several laps around the Killarney race track (Western Cape) it was possible to get an average of the global layout. The relative error between the layouts of the measured laps did not exceed 5m. Garmin quotes an absolute positional accuracy of less than 15m (see Appendix C) but according to their website an accuracy of less than 10m is easily attainable in open sky conditions.

It was found that the altitude measurement of the GPS was not as accurate with the reading varying more than 10m at the start of each lap. There were reverted to the manual process of measuring gradients and bank angles using an inclinometer (see Figure 4.4).

Figure 4.4 Measurement of the Killarney circuit

After the data were collected, a CAD package was used to import the data points and do "curve fits" through the corners in order to determine the radii of the corner segments around the track. It was also possible to scale the CAD image and measure the length of each straight and corner segment of the racing line as illustrated in Figure 4.5.

Figure 4.5 CAD generated racing line of the Killarney race track

24

4.3.2.2 Usage of track data

The data are stored in a *.db file that lists the data according to distance, gradient, bank angle and radius. The length of each distance interval is determined by the number of measurements taken and complexity of the circuit. Corners will generally require shorter distance intervals than straights. This file is then imported into the main program where a pre-processor is used to determine the brake speed profile throughout the circuit in meter intervals. The brake speed profile is the theoretical maximum speed the vehicle can achieve at each position on the track before braking for the next corner commences and will be discussed in the next section.

4.3.4 Pre-Processor

By using the friction ellipse as the governing factor of the program it was necessary to built in a corner anticipating function in the program. This means that the vehicle will accelerate down a straight until it "sees" the corner approaching and starts braking exactly at the right moment to slow down and enter the corner at the maximum speed allowed by the friction ellipse.

This was done by programming a pre-processor that determines the braking limited speed profile around the track using the Milliken (1995) method. The vehicle will only accelerate until the simulated vehicle speed reaches this pre-determined braking limited speed profile and then follow this profile until the apex of the corner is reached. The vehicle will be on the limit of the friction ellipse from the start of braking until the apex of the corner. After the apex, the vehicle will start to accelerate following the allowable friction ellipse and engine power limitation.

4.3.4.1 The inputs

The racing line of the track was determined with the help of GPS measurements and a CAD model. Each corner was divided into several segments of changing radii. From Figure 4.5 it can be seen that the corner mostly starts with large radii that decrease until the apex of the corner is reached before the radii increase again as the next straight approaches.

Figure 4.6 shows the typical racing line through a 90-degree corner.
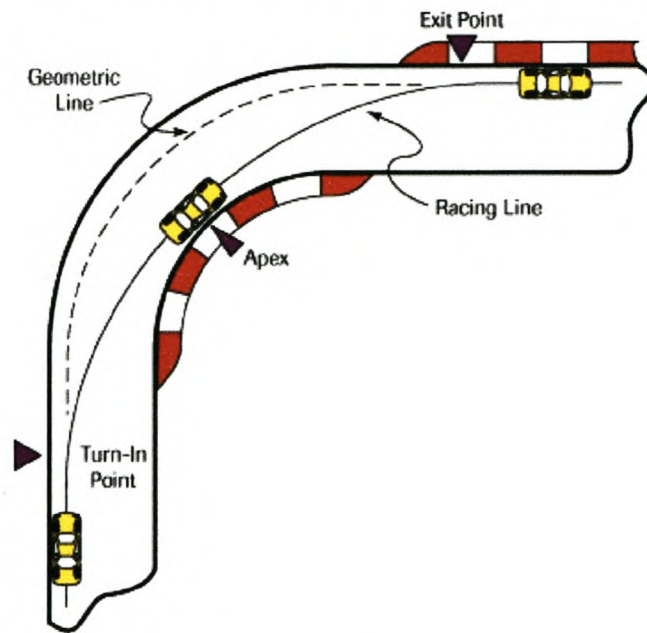
Figure 4.6 Approximate racing line through a corner

After studying the average deceleration of the expert racing driver in the braking zones around the track (see section 6.3.1) it was found that the value was much lower than the predicted value from the friction ellipse. Provision was made for maximum brake deceleration in the vehicle model in order to "shrink" the ellipse on the braking side. This was only an approximation, but it didn't affect the goal of engine optimisation due to the fact that the engine played little part in the braking zone. In short, the inputs to the mathematical model were:

- Tyre/road friction coefficient
- Rolling coefficient
- Mass of vehicle [kg]
- Gravity constant [m/s^2]
- Frontal area [m^2]
- Drag coefficient
- Maximum brake deceleration [m/s^2]
- Air density [kg/m^3]
- Bank angle [radians]
- Gradient [radians]
- Radius [m]
- Length of track segments [m]

4.3.4.2 The mathematical model

The first step of the pre-processor was to search for a corner in the lap. When a corner is located the next step is to search for the apex of the turn – radius segment with the smallest value. The steady state maximum speed is then determined:

a) Apex vehicle speed

Stage 1 Maximum vehicle speed without external forces.

The maximum speed [km/h] at which a vehicle can negotiate a constant radius turn was first approximated by summing the forces in the lateral direction and ignoring air and rolling resistance (See Appendix A for derivation):

$$V = \sqrt{\frac{-R_c g(\tan\theta + \mu)}{\mu\tan\theta - 1}} \qquad (4.1)$$

with

R_c = Corner radius [m]

θ = Bank angle [radians]

μ = Tyre/road friction coefficient

g = Gravitational constant [m/s^2]

Stage 2: Maximum vehicle speed with external vehicle forces considered.

The friction circle concept was used in the derivation where the grip at the vehicles front wheels is the limiting factor in a front wheel drive vehicle. The radius of this circle is the normal force on the front wheels multiplied with the friction coefficient.

Even at steady speed through a constant radius turn the front tyres must still provide a longitudinal force to overcome rolling, friction and gradient resistance where applicable. The final equation is shown below (see Appendix A for derivation):

$$V = \frac{-C - \sqrt{C^2 - 4TK}}{2T} \qquad (4.2)$$

where:

$$T = -0.25(\rho A C_d)^2 - \left(\frac{M_f \cos\theta}{R}\right)^2 + \left(\frac{\mu M_f \sin\theta}{R}\right)^2$$

$$C = \frac{2\mu^2 M_f^2 g\cos\theta\sin\theta}{R} - \frac{F_r \rho A C_d + 2M_f^2 \cos\theta g\sin\theta}{R} - F_g \rho A C_d$$

$$K = (\mu M_f g\cos\theta)^2 - F_g^2 - F_r^2 - 2F_g F_r - (M_f g\sin\theta)^2$$

27

with:

ρ = Air density [kg/m^3]

A = Frontal area [m^2]

C_d = Coefficient of drag

M_f = Mass on front axle [kg]

F_r = Rolling resistance force [N]

F_g = Gradient force [N]

After the apex speed is determined, using numerical integration it is possible to determine the maximum entry speed into each segment of the corner and speed through the corner by working backwards.

b) Corner entry speed

Using the Milliken (1995) method entails working backwards through the corner starting at the apex. A numerical integration method was used to calculate the new vehicle speed for the previous meter segment of the track.

At the apex of the corner the vehicle is at maximum lateral acceleration and travelling at constant speed. The friction ellipse strategy allows no longitudinal force to accelerate the vehicle. When the radius of the turn increases, the lateral force decreases for the same vehicle speed, and there is a surplus of traction available for longitudinal acceleration of the vehicle. This acceleration may not exceed the maximum brake deceleration specified by the user as explained in section 4.3.4.1. The vehicle is actually accelerated backwards to the corner entry.

As the vehicle speed increases in the new corner segment with constant radius the available longitudinal traction and therefore the force will decrease until the vehicle speed stabilises, if the segment length permits. The process will repeat itself for each new corner segment encountered. The smaller the corner segments the more realistic the braking limited speed profile will be.

The following numerical process was followed to determine brake speed profile for each corner segment:

- Determine the lateral force F_y [N]

$$F_y = \frac{MV^2 \cos\theta}{(3.6)^2 R_c} - Mg\sin\theta \qquad (4.3)$$

- Determine maximum longitudinal force F_{xmax} [N] according to the friction circle concept

$$F_{x\max} = \sqrt{(W\mu)^2 - (F_y)^2} \qquad (4.4)$$

where:

W = Vehicle weight [N]

- Determine resistance force F_{res} [N]

$$F_{res} = F_d + F_g + F_r \qquad (4.5)$$

where:

F_d = Aerodynamic drag force [N]

- Determine vehicle acceleration a_x [m/s^2] (backwards)

$$a_x = \frac{F_{x\max} - F_{res}}{M} \qquad (4.6)$$

- New vehicle speed V_{new} [km/h] for the previous meter of racing line (backwards)

$$V_{new} = \left(\sqrt{\left(\frac{V_{old}}{3.6}\right)^2 + 2a_x} \right) 3.6 \qquad (4.7)$$

This process was iterated until the whole corner entry braking limited speed profile was found. Once the maximum entry speed was known for each corner segment, as well as the entry speed at the start of the corner, it was possible to determine the braking limited speed profile down the straight until the next corner was reached.

c) Braking limited speed profile down the straights

With the corner entry speed known, the constant brake deceleration can be used to determine the braking limited speed profile down the straight until the next corner. This method repeats itself until a braking limited speed profile is found around the track. The vehicle will accelerate from the corner apex, as allowed by the friction ellipse, until its speed equals the speed of the braking limited speed profile determined. There after this speed profile will be followed until the apex of the next corner is reached. This is similar than a racing driver braking for the next corner.

The brake speed profile of the Killarney race track for the Ford Fiesta RSI resembles the pattern illustrated in Figure 4.7. Note that the peak values are the theoretical maximum speeds the vehicle could enter a straight, before braking commences, in order to negotiate the next corner successfully. The minimum values are the maximum apex vehicle speeds. From the track testing in chapter 6 it is evident that reaching the peak values are highly unlikely.
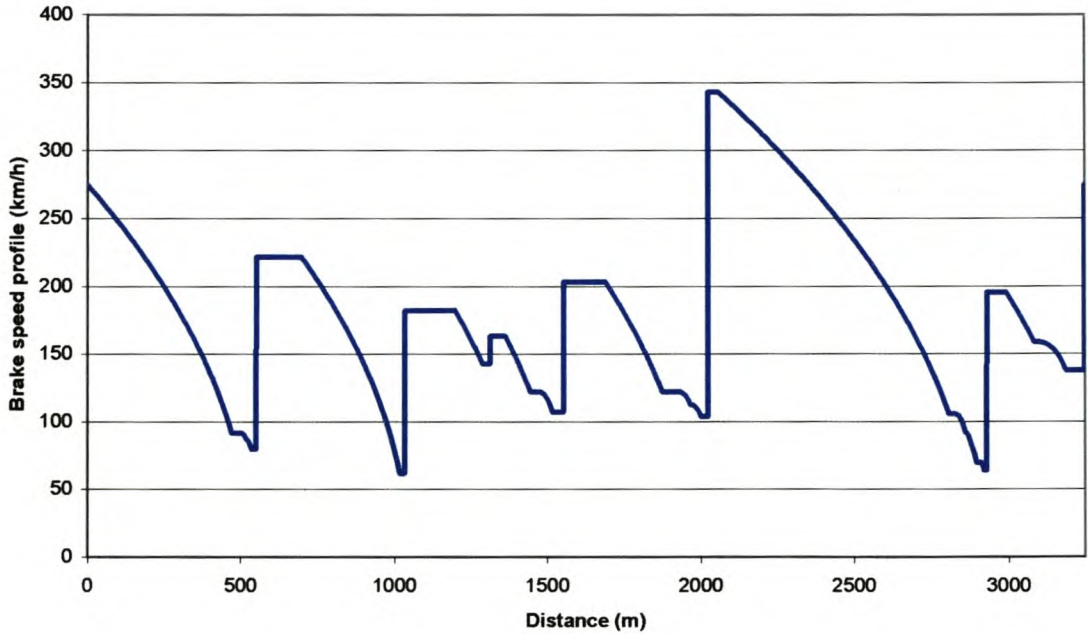
Figure 4.7 Killarney braking limited speed profile

4.3.5 Runtime calculations

To simulate a vehicle circuiting a track an advanced numerical process was used to determine the appropriate variables at each time step. Figure 4.8 summarizes the mathematical process of CircuitSim. The flow diagram of the signal processing can be seen in Figure 5.5.
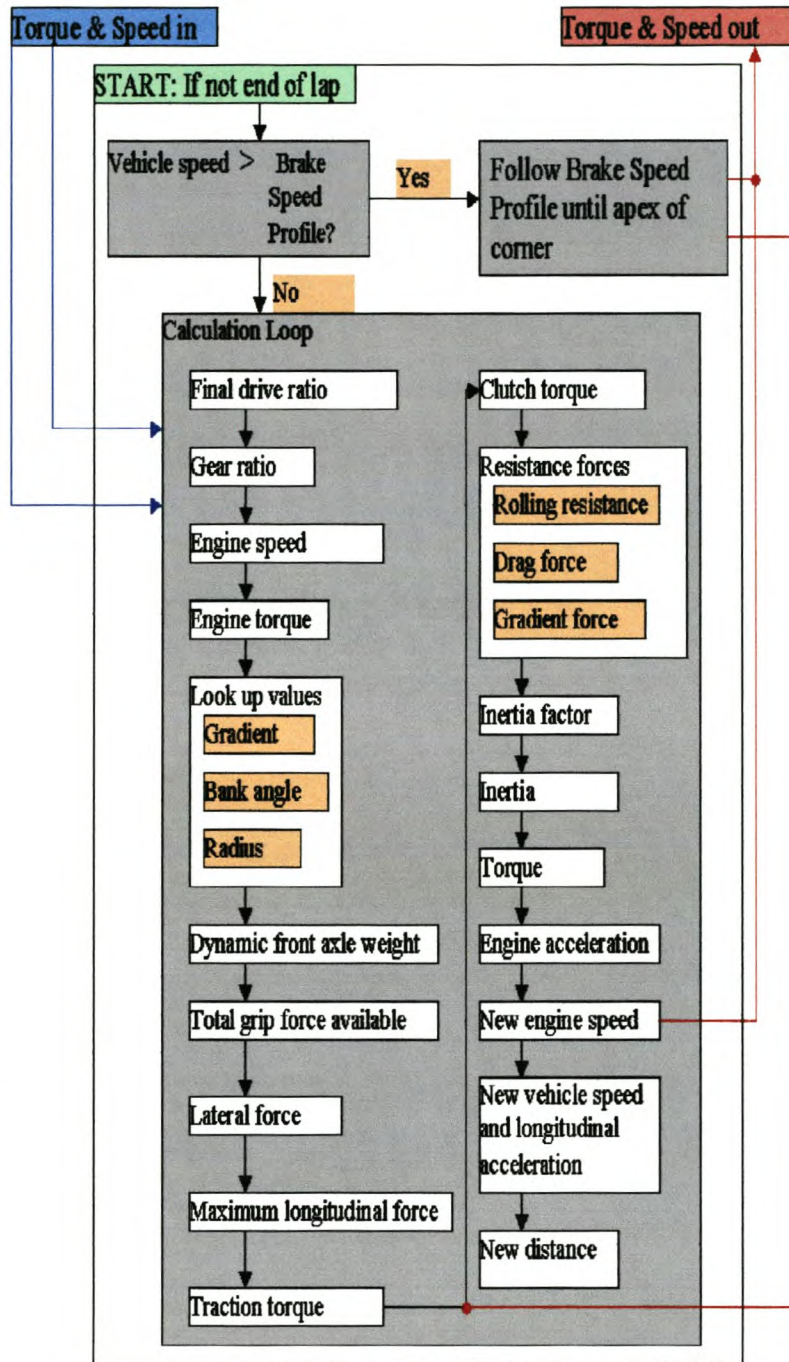
Figure 4.8 Calculation loop

31

To start off the process the following initial conditions were set:

Initial conditions

- Position along the track, X_i [m]
- Vehicle speed, V [m/s]
- Longitudinal acceleration, a_x [m/s²]

The following are determined in real time for each time step.

4.3.5.1 Final drive speed

Calculating the rotational speed of the wheels and multiplying it by the final drive ratio of the vehicle gives the final drive speed N_{fd} [rpm].

$$N_{fd} = \frac{25VG_f R_w}{3\pi} \tag{4.8}$$

4.3.5.2 Gear ratio

The selected gear of the vehicle at each position on the race track is a function of maximum engine speed, final drive speed and available gear ratios. For maximum power delivery from the engine it is necessary to keep the engine in the region where peak power is developed. The Ford RSI engine that was used developed peak power high up in the speed range (see Figure 7.13). It was beneficial to keep the engine speed as high as possible without exceeding the maximum allowable engine speed to maximise power output. With the final drive speed known, a nested If-statement was used to calculate which available gear ratio would result in the highest allowable engine speed. This is representative of an actual race driver.

$$G_f = f(N_{e\max}, N_{fd}, \textit{available gear ratios}) \tag{4.9}$$

4.3.5.3 Engine speed

The gear ratio multiplied with the final drive speed gives the engine speed N_e [rpm].

$$N_e = N_{fd}G_f \tag{4.10}$$

32

4.3.5.4 Engine torque

The engine delivers a torque that is delivered to the driven wheels by the drive train and leads to a tractive force. During real time simulation the actual torque delivered by the engine on the test bench is measured in real time. It is also possible to run the simulation "offline", hence using the torque values from the engine's torque curve. The two modes will now be discussed in more detail:

Mode 1:

The first mode runs the simulation "offline". There is no interaction with the hardware and the torque values are read from the engine's torque curve. The program uses engine speed as the input variable and relates the torque value (T_e) from a lookup table. This table is programmed beforehand with the actual torque values of the engine. It must be remembered that the torque curve of a vehicle is measured at steady state conditions so that engine inertia does not play a role in the actual values. During the "offline" simulation provision is made for engine inertia, which is not required for the "hardware in the loop" simulation. Figure 4.9 shows the torque input table for CircuitSim.
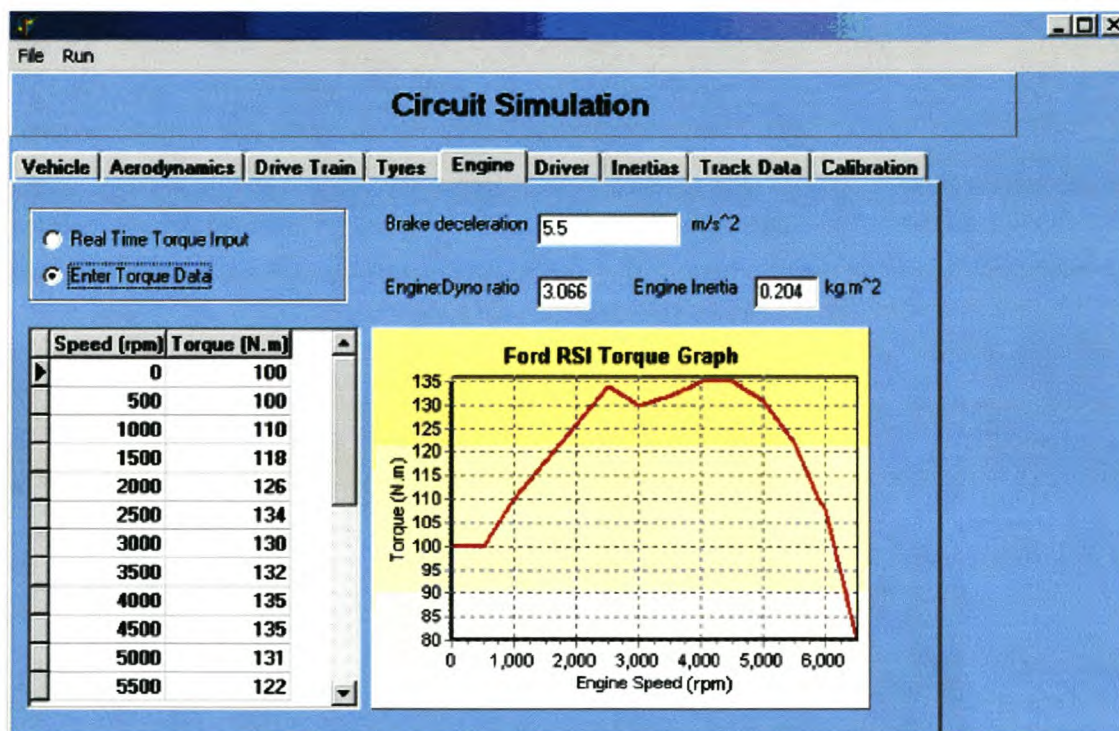
Figure 4.9 CircuitSim's torque input table

Mode 2:

The second mode is the real time simulation with "hardware in the loop", where the engine runs on the test bench. The torque value is measured by means of a torque hub between the engine and the dynamometer. This torque reading is in real time, and takes the engine inertia into consideration due to the dynamic nature of the simulation. This torque is the actual clutch torque, T_c.

4.3.5.5 Static front axle weight

The static front axle weight W_{fs} [N] is the part of the vehicle's static weight carried on the front axle when the vehicle is stationary. If the gradient [Φ] is small, then

$$W_{fs} = W\frac{c}{L} - W\frac{h}{L}\Phi \tag{4.11}$$

4.3.5.6 Extra weight on front axle due to bank angle

The extra normal force W_{fe} [N] on the wheels of a vehicle when negotiating a banked turn must be accounted for. This was done in the following way:

$$W_{fe} = M\frac{V^2}{(3.6)^2 R_c}\sin\theta\frac{W_{fs}}{Wf} \tag{4.12}$$

4.3.5.7 Dynamic front axle weight

The longitudinal acceleration of the vehicle will lead to a normal force shift between the front and rear axles of a vehicle. The dynamic front weight W_{fd} [N] was calculated as follows:

$$W_{fd} = W_{fs} - W\frac{a_x h}{L} + W_{fe} \tag{4.13}$$

4.3.5.8 Total grip available

This defines the force value F_c [N] of the friction circle radius on the front wheels of the vehicle.

$$F_c = W_{fd}\mu \tag{4.14}$$

4.3.5.9 Corner radius

The corner radius is obtained from a lookup table with distance as input variable. The lookup table is created before the simulation is run. Refer to Figure 4.5 for radii of the Killarney race track.

4.3.5.10 Lateral force at the front axle

The lateral force F_{yf} [N] was determined for the whole vehicle and then scaled to the front axle as shown in the next formula.

$$F_{yf} = (M \frac{V^2}{(3.6)^2 R} \cos\theta - W \sin\theta) \frac{W_{fd}}{W + W_{fe} \frac{W}{W_{fs}}} \tag{4.15}$$

4.3.5.11 Lateral acceleration

The lateral acceleration a_y [m/s^2] was determined in order to compare the predicted values with the actual measured data.

$$a_y = \frac{V^2}{(3.6)^2 R} \tag{4.16}$$

4.3.5.12 Maximum longitudinal force

The maximum longitudinal force F_{xmax} [N] was found by using the friction ellipse concept on the front wheels only for a front wheel drive vehicle.

$$F_{x max} = \sqrt{(W_{fd}\mu)^2 - (F_{yf})^2} \tag{4.17}$$

4.3.5.13 Traction torque

The traction torque T_t [Nm] was the torque calculated from the maximum longitudinal force as found by the friction ellipse. This torque is then divided by the overall transmission in order to compare it with the engine torque.

$$T_t = \frac{F_{x max} R_w}{G_{tf}} \tag{4.18}$$

4.3.5.14 Max torque T_c

The maximum clutch torque T_c [Nm] was the minimum of the traction and engine torque. This function guarantees that the driven wheels of the vehicle will never exceed their traction limits.

$$T_c = Min(T_t, T_c) \tag{4.19}$$

4.3.5.15 Rolling resistance

To increase the simplicity of the program it was decided to use the simplified method of determining rolling resistance. The rolling resistance force F_r [N] was calculated by multiplying the rolling coefficient with the normal force.

$$F_r = f_r W \qquad (4.20)$$

4.3.5.16 Drag force

Drag force F_d [N] was calculated by the formula as stated in Bosch GmbH (1993).

$$F_d = \tfrac{1}{2}\rho V^2 C_d A \qquad (4.21)$$

4.3.5.17 Mass factor

The "mass factor" is a term used to approximate all the rotational inertias of the drive train. This includes inertias of wheels, drive shafts, transmission and clutch. A representative number is often taken as (Gillespie, 1992):

$$f_m = 1 + 0.04 + 0.00025G_{tf} \qquad (4.22)$$

4.3.5.18 Inertia

J_v [kgm^2] was the effective vehicle rotational inertia as seen at the clutch. Equation 4.23 transforms the effective vehicle mass into a rotational inertia for use in the dynamic equations as stated by Conradie (2001). Note that the inertia is strongly dependent on gear ratio.

$$J_v = \frac{f_m M R^2}{G_{tf}^{\,2}} \qquad (4.23)$$

4.3.5.19 Torque

T_v [Nm] was the total vehicle load torque as seen at the clutch:

$$T_v = \frac{(F_r + F_d + F_g)R}{G_{tf}\eta_{tf}} \qquad (4.24)$$

36

4.3.5.20 Engine Angular acceleration

If one applies Newton's first law to the clutch interface, with the clutch disengaged, the equations can be written:

$$\alpha_e = \frac{T_e - T_c}{J_e} \tag{4.25}$$

$$\alpha_v = \frac{T_c - T_v}{J_v} \tag{4.26}$$

with

α_e = Engine angular acceleration [rad/s^2]

α_v = Equivalent vehicle angular acceleration [rad/s^2]

T_e = Engine torque [Nm]

T_c = Clutch torque [Nm]

T_v = Total vehicle load torque as seen at the clutch [Nm]

J_e = Engine inertia [kgm^2]

J_v = Equivalent total vehicle inertia [kgm^2]

When the clutch is fully engaged the above equations become:

$$\alpha_e = \alpha_v = \frac{T_e - T_v}{J_e + J_v} = \frac{T_c - T_v}{J_v} \tag{4.27}$$

4.3.5.21 New engine speed

The following Euler integration algorithm determined the new engine speed ω_e [rad/s] for the following time increment:

$$\omega_e = \omega_{e-1} + \Delta t \alpha_{e-1} \tag{4.28}$$

4.3.5.22 New vehicle speed

With the new engine speed known it was possible to determine the new vehicle speed V_{new} [km/h]:

$$V_{new} = \frac{(\omega_e 3600)R_w}{1000 G_{tf}} \tag{4.29}$$

37

4.3.5.23 New longitudinal acceleration

The longitudinal acceleration was determined in order to compare the predicted values with the actual measured data.

$$a_{xnew} = \frac{V_{new} - V_{old}}{3.6\Delta t}$$

(4.30)

4.3.5.24 New distance

The new distance s_{new} [m] was then calculated as:

$$s_{new} = s_{old} + \frac{(V_{old} + V_{new})}{2}\Delta t$$

(4.31)

4.3.6 Time increment

The success of the real time numerical integration method used to calculate the above variables depended on the accuracy of time step length. The numerical progress inevitably generates errors due to the finite length of the time increment but the error could be greatly reduced by using the smallest time step possible and measuring its length to a fine degree.

The programming language Delphi is a Microsoft Windows based application and the clocks available were not suitable for the real time nature of the simulation. The timing problem was overcome by using the onboard 2Mhz timer counter of the PC30FA data acquisition card (see section 5.4.1). A short algorithm was programmed to test for overflow when reading the clock value to assure accuracy.

The loop where all the above calculations were done, was allowed to run as fast as the 800Mhz CPU of the computer could achieve and the actual time increment was calculated by reading the value from the 2Mhz timer counter on the PC30FA data acquisition card. Typical time increments calculated during real time simulation varied between 0.054s and 0.061s. This equates to a 16-18Hz calculation loop frequency. During each loop the real time torque and speed signals were read, calculations done and the new speed and torque signals sent to the PLC. This showed that the chosen dynamic and track models allowed fast processing speed.

4.3.7 Visual Display

4.3.7.1 Run time

While the real time circuit simulation was running the display unit as illustrated in Figure 4.10 kept the user informed.
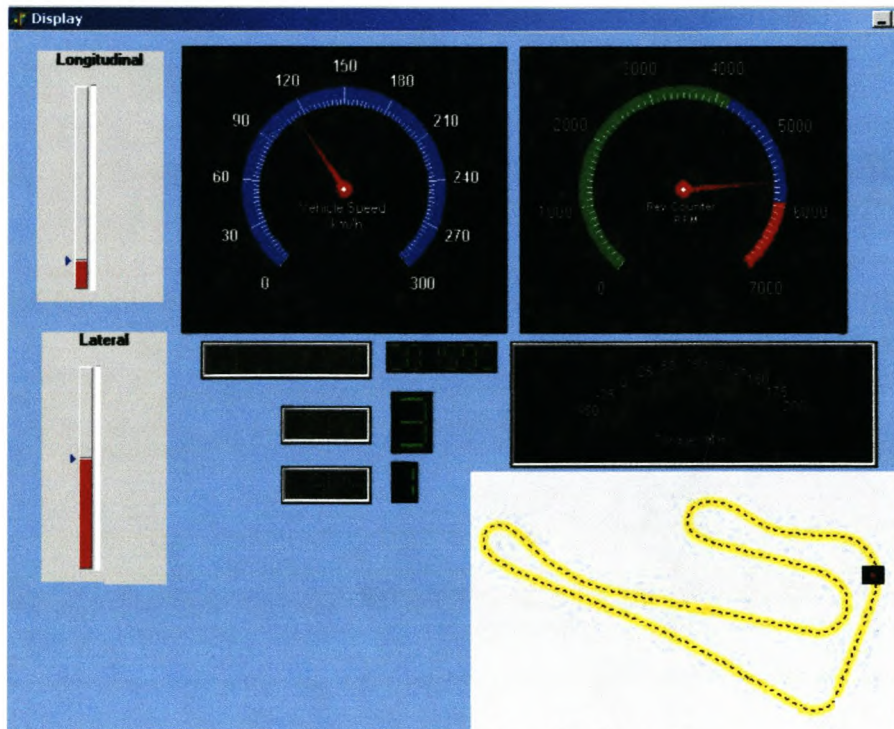
Figure 4.10 CircuitSim display unit

The unit displayed the following real time values:

- Vehicle speed
- Engine speed
- Distance
- Gear ratio
- Lap number
- Torque value
- Track position
- Longitudinal acceleration
- Lateral acceleration

4.3.7.2 Simulation report

After the completion of the simulation the following information was displayed to the user (see Figure 4.11):
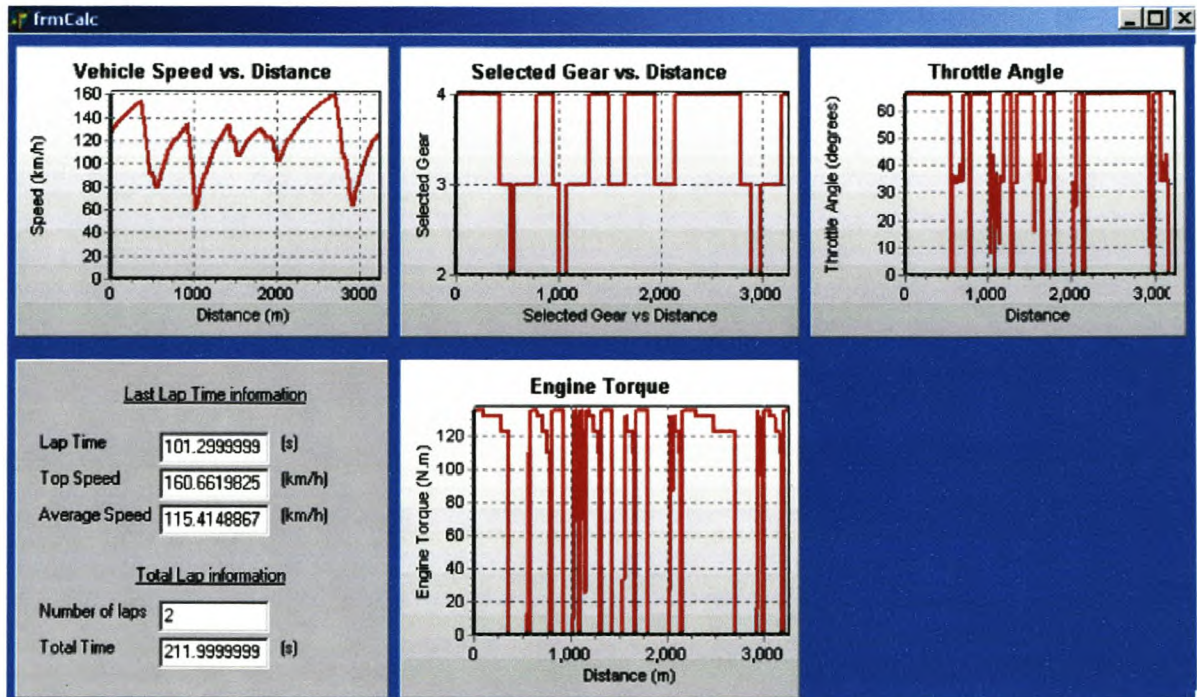
Figure 4.11 CircuitSim report back unit

The following information is reported:

- Vehicle speed vs. distance
- Gear ratio vs. distance
- Approximate throttle angle
- Real time engine torque vs. distance
- Lap time
- Top speed
- Average speed
- Number of laps
- Total time

The complete results were saved to a *.dbf file for easy analysis with the use of spreadsheets. An example of such a file can be seen in Appendix A.

5. Test system components

The Real Time Circuit Simulation used the same basic hardware set-up as used by Conradie (2001) for the dynamic engine test facility. The most important components will be discussed.

5.1 Regenerative DC dynamometer

The regenerative DC dynamometer is the main component of the CAE dynamic engine test facility (see Figure 5.1 below). The dynamometer is capable of absorbing and delivering power to the engine, thereby simulating most conditions encountered under normal driving operations.
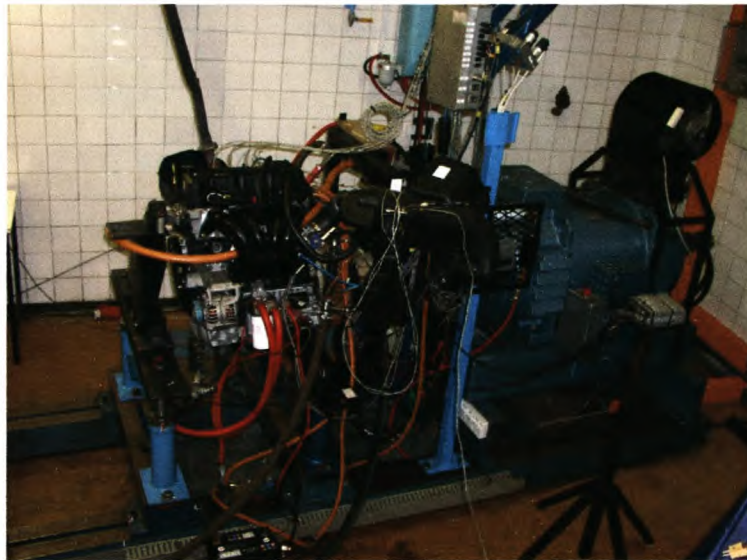
Figure 5.1 The CAE dynamic engine test stand

5.1.1 Electric motor

The DC motor coupled to the Siemens variable speed drive (discussed later) enabled engine speed and torque control. Table 5.1 lists the specifications of the electric motor (see Figure 5.2 for a photo of the CAE DC motor):

DC motor specifications:

Table 5.1 DC motor

Mode	Power [kW]	Speed [rpm]	Armature voltage [V]	Armature current [A]	Excitation voltage [V]	Excitation current [A]
Motor	154	5500	400	380	90	1.3
Generator	160	5500	400	380	95	1.4

41

Figure 5.2 CAE DC motor

5.1.2 DC dynamometer inertia

When performing dynamic engine simulation the ideal would be to use an electric motor with infinite power and zero inertia for the dynamometer motor. However this is not possible and the shortcomings of the system must be known and be accounted for.

Conradie (2001) used the load cell on the casing of the dynamometer to measure torque. When performing dynamic simulation it was necessary to use Newton's first law to determine the real time engine torque:

$$T_l = T_{lc} + J_d \alpha_d \qquad\qquad (5.1)$$

with

T_l = Load torque [Nm]
T_{lc} = Load cell torque [Nm]
J_d = Dynamometer inertia [kgm^2]
A_d = Dynamometer angular acceleration [rad/s^2]

One of the inputs when solving the equations was dynamometer inertia J_d. Conradie (2001) determined the inertia as 1.600 kgm^2 with the use of triangular speed functions. He measured reaction torque and dynamometer speed without an engine coupled to the dynamometer.

The circuit simulation used a torque flange (described in section 5.3.1) between the gearbox and dynamometer to measure the real time torque in the shaft between the engine and dynamometer. This gave instantaneous torque readings and eliminates the need to use the dynamometer inertia to calculate engine torque from the load cell.

5.1.3 Dynamometer specifications

For a dynamometer to be effective for dynamic engine testing it must be able to comply with certain requirements that are explained in the following sections:

- Control response
- Mass ratio
- Speed gradient

5.1.3.1 Control response

Control response is one of the most important parameters of a dynamic engine testing dynamometer. It is the parameter that determines how fast and with what degree of accuracy the dynamometer can follow specific speed and torque commands. These control responses are termed *amplitude frequency response* and *phase response* (Voos, 1992). The faster the dynamometer response, the better it is suited to dynamic simulations.

Conradie (2001) used a sinusoidal speed input signal with increasing frequency to determine the bandwidth of the dynamometer. The criteria for the cut-off frequency was 70.7% (-3dB) of the exciting amplitude and the phase response criteria was set at a maximum of -90°, as stated by Voos (1992).

The results of above tests (See Appendix B) showed that at low speed the control response was limited by torque and at high speed it was limited by power. The cut-off frequency was calculated at 2.15 Hz. This figure is quite low compared to the 16Hz quoted by Shafai and Geering (1989) and means that the system may not be totally suitable for all dynamic engine testing applications in its current state.

The standard CAE system was not ideal for dynamic engine testing due to its slow control response. Firstly, the maximum allowable dynamometer speed is only 5500rpm and for the circuit simulation the engine speeds wouldl be in excess of 6000rpm.

Secondly the other major draw back is the dynamometers inertia. This influences both the mass ratio and speed gradients negatively and could reduce the accuracy of a race simulation. Both of these shortcomings were alleviated by connecting the engine to the dynamometer through a gearbox with a reduction ratio. The ratio between the engine and dynamometer was 3.069:1. This allowed the engine speeds to reach the desired figures and reduced the effect of the dynamometer inertia by the square of the gear ratio as explained in the following section.

5.1.3.2 Mass Ratio

The mass ratio is defined as the ratio of moments of inertia:

$$m_r = \frac{J_d}{J_e} \qquad (5.2)$$

with

J_d = Dynamometer inertia [kgm^2]

J_e = Engine inertia [kgm^2]

The higher the mass ratio of the system, the more power must be available for sudden changes in engine speed. This is the case when gear changes must be simulated with a engaged clutch. The ratio of the CAE dynamometer system, with and without the gearbox, was compared with values from Voos (1992) for a typical 2L internal combustion engine with rotational inertia of 0.23 kgm^2 (see Table 5.2):

Table 5.2 Comparative mass ratios

	Hydrostatic unit	DC machine	AC machine	CAE DC dyno	CAE DC dyno with gearbox
m_r	0.16	1.39	1.96	6.96	0.739

It can be seen that the standard CAE system is inferior to the other systems due to its high inertia value, but with the inclusion of the gearbox compares very well with the other systems. This is due to the factor of 9 gain that the gearbox provides as shown in the following equation:

$$m_r = \frac{J_d}{J_e (3.069)^2} \qquad (5.3)$$

5.1.3.3 Speed gradient

The speed gradient $\dot{N}$ [rpm/s] of the dynamometer is defined as:

$$\dot{N} = \frac{dN}{dt} \qquad (5.4)$$

and indicates the speed gradient that the dynamometer can achieve. This is important for the simulation of an "open clutch" situation, as is the case during gear changes. In this situation zero torque must be simulated and the dynamometer must overcome its own inertia and follow the drop in engine speed, as it would drop during gear changes in a vehicle. Conradie (2001) determined the standard CAE system's speed gradient at 4700 rpm/s. Again the standard and modified CAE system was compared to the values of Voos (1992) as can be seen in Table 5.3.

44

Table 5.3 Comparative speed gradients

	Hydrostatic unit	DC machine	AC machine	CAE DC dyno	CAE DC dyno with gearbox
$\dot{N}$	1200	10800	8000	4700	14424

The low speed gradient value of the standard CAE system may hamper the simulation when fast ramp rates are demanded for example during gear changes. The inclusion of the gearbox improved this figure by a factor of 3 and enabled the CAE system to perform dynamic simulations.

5.2 Variable speed drive

Speed control of the dynamometer was achieved by a Siemens DC variable speed drive. This drive is fully regenerative and any absorbed power is returned to the electricity supply network. The technical specifications for the Siemens variable-speed DC drive are listed in Table 5.4. Although the Siemen speed drive was already calibrated the signal from and to the controller was verified using a strobe light.

Table 5.4 Technical specifications for Siemens variable speed drive

Serial no. 6RA2481-6DV62	Units	
Rated voltage/output	[V]	3-ph AC400 (+15%/-20%)
Rated supply voltage, field	[V]	2-ph AC400 (+15%/-20%)
Rated DC voltage	[V]	420
Rated DC current	[A]	400
Overload capability	[%]	Max. 150% rated DC current
Rated output	[kW]	168
Power loss at rated current	[W]	1250
Rated DC voltage	[V]	Max.325
Rated DC current	[A]	25
Control stability	[%]	Delta n = 0.1% of rated speed

5.3 Transducers and actuators

Transducers and actuators are used to obtain signals from and send signals to the system. The circuit simulation received two signals from the test bench namely engine speed (variable speed drive) and engine torque (torque transducer). When the calculation loop of the software is completed, the new torque and speed signals were sent to the PLC that controls the throttle actuator and input to the variable speed drive.

45

5.3.1 Torque transducer

The torque transducer is coupled directly to the shaft between the engine and dynamometer (see Figure 5.3) and gives instantaneous, real time, analogue torque signals. This is very important when doing dynamic engine testing, as the accuracy of the torque signal and frequency response will have a direct influence on the accuracy of the simulation.

The HBM torque flange has an internal calibration unit that supplies the sensor with 24 V. This equates to a torque reading of 2939 Nm of torque and was used to calibrate the unit.

See Appendix B for specifications of the torque flange.
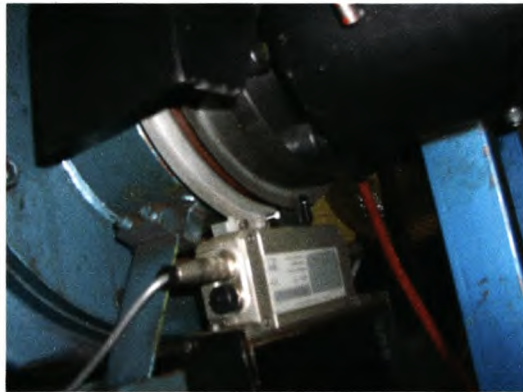
Figure 5.3 HBM T10F torque flange

5.3.2 Throttle actuator

The torque delivered by a spark ignition engine is controlled by the engine's throttle valve in the intake manifold. During the circuit simulation the throttle was controlled by output signals from the software program. The throttle actuator used was an ABB servo motor (see Figure 5.4) coupled to a Schenck controller.

Figure 5.4 ABB MC17HR0021 servo motor

46

5.4 Data processing systems

While the circuit simulation was running, data was acquired and processed at approximately 20Hz. The signals were processed as illustrated in Figure 5.5.
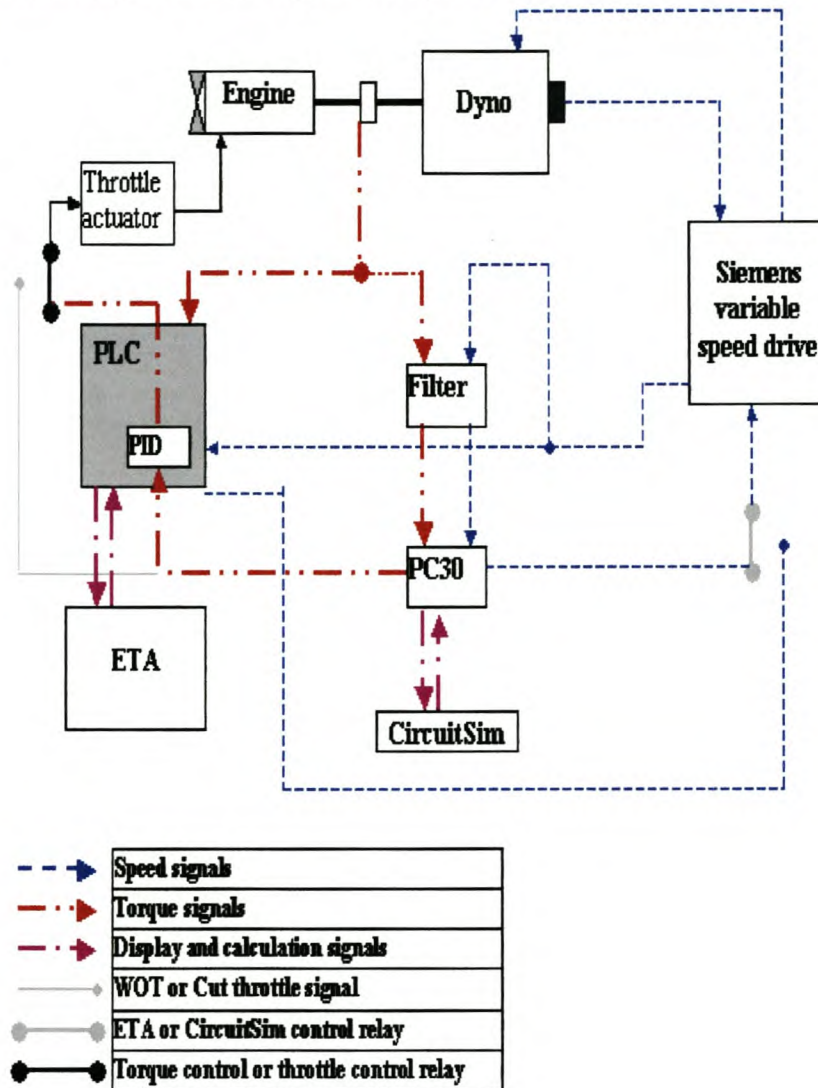
Figure 5.5 The CAE Dynamic engine test stand signal processing

The conventional steady state engine testing set-up was changed to accommodate the CircuitSim simulation program. The CircuitSim program used filtered real time torque and speed signals as inputs. CircuitSim's control over dynamometer speed was activated by a relay. Note that only ETA or CircuitSim could control dynamometer speed at a given moment in time. CircuitSim used the PLC's PID in order to achieve torque control by supplying torque set points directly to the PID register. CircuitSim also had the option of throttle control, for example during gear changes, by opening or closing the throttle control relay as seen in Figure 5.5. The following played a role in the data acquisition and processing.

47

5.4.1 PC30FA data acquisition card

The PC30FA (see Figure 5.6) is a high accuracy analogue and digital I/O board produced by Eagle Technology for IBM PC/AT and compatible series of computers. This card was used to acquire the engine speed and torque signal used for the software calculations and sent out the new speed and torque demand. See Appendix B for full specifications on the PC30FA card.
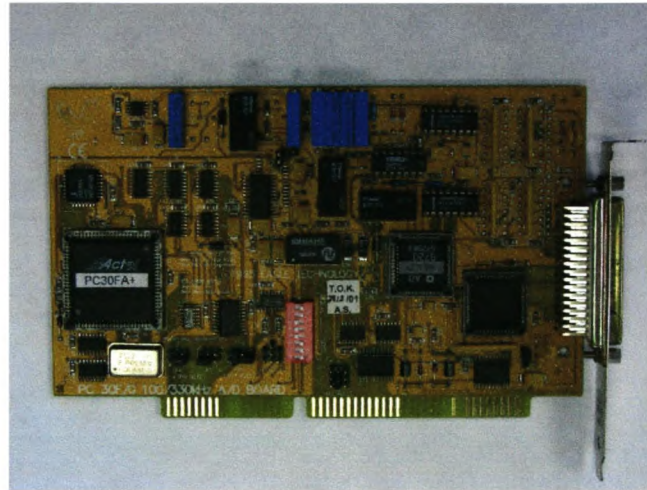
Figure 5.6 PC30 Data acquisition card

5.4.2 Anti-aliasing filter

The anti-aliasing filter is a low pass analogue filter through which data is sampled prior to being digitised. The basic concept is to attenuate frequencies above the Nyquist frequency, thus allowing only signals with the frequency content below half the sampling frequency to pass. This was done in order to reduce noise.

The dynamic response of the filter was determined by Conradie (2001) and the results can be seen in Figure 5.7
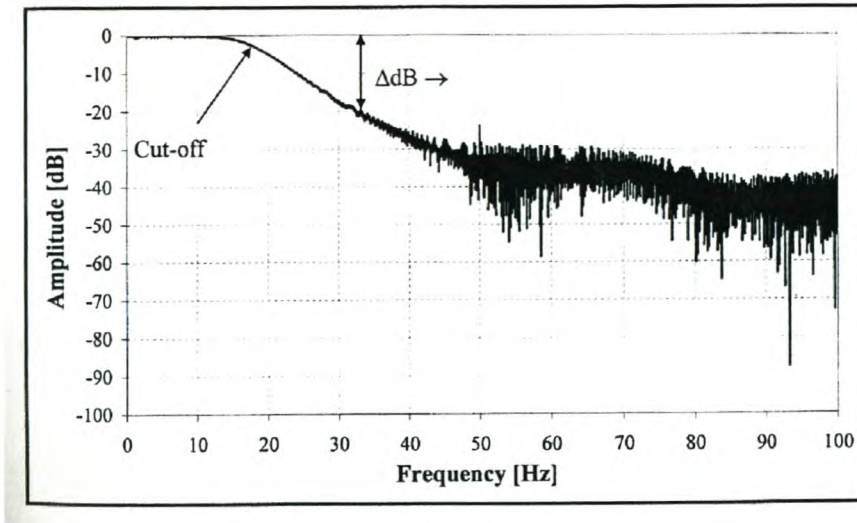
Figure 5.7 Dynamic response data of the anti-aliasing filter (Conradie, 2001)

The filter specifications can be seen in Table 5.5.

Table 5.5 Anti-aliasing filter specifications

Type	Butterworth
Response	Low-pass
Order	Fourth
Cut-off frequency	18Hz

5.4.3 System control computer

The system computer in a dynamic simulation is responsible for the total vehicle simulation. It reads the speed and torque inputs, does all the calculations while updating the graphical interface and sends out the new signals for the following time step.

The speed of the computer plays a significant role in the length of the time steps between computations and the overall accuracy of the simulation. The control computer used had the following specifications (see Table 5.6).

Table 5.6 Control computer specifications

Processor	800 MHz
Ram	128 Mbytes
Hard drive	20 Gbytes
Operating system	Microsoft Windows 2000

5.4.4 The PID controller

Common controllers in industry are proportional-plus-integral-plus-derivative (PID) controllers. The reasons for this is:

- Suitability to many control applications
- Low cost
- Ease with which they can be configured
- Configured to cater for most control requirements

According to Franklin et al. (2002) the first action is the **proportional** action. The relationship between the output of the controller u(t) and the error signal e(t) is:

$$u(t) = K_p e(t) \tag{5.5}$$

or in the Laplace domain:

$$\frac{U(s)}{E(s)} = K_p \tag{5.6}$$

K_p is the proportional gain constant. The proportional controller is essentially an amplifier with an adjustable gain.

The second action is the **integral** control action:

$$u(t) = K_i \int e(t) \tag{5.7}$$

or in the Laplace domain:

$$\frac{U(s)}{E(s)} = \frac{K_i}{s} \tag{5.8}$$

where K_i is the integral constant. The integral tends to eliminate offset errors.

The third action is the **derivative** control action. The magnitude of the controller output u(t) is proportional to the rate of change of the actuating error signal e(t):

$$u(t) = T_d \frac{de(t)}{dt} \tag{5.9}$$

Or in the Laplace domain:

$$\frac{U(s)}{E(s)} = T_d s \tag{5.10}$$

where T_d is the time derivative constant. The derivative term has a stabilising effect by correcting sudden errors.

The combined controller is represented in the Laplace domain by the following equations:

$$\frac{U(s)}{E(s)} = K_p(1 + \frac{1}{T_i s} + T_d s) \qquad\qquad (5.11)$$

The friction ellipse concept demanded accurate torque control, especially in the corners where the engine torque could easily overcome the available traction. The PID controller inside the PLC (see Figure 5.5) was utilised by supplying a value directly to its register. The end result was a very effective torque controller that limits engine torque to the maximum torque allowed by the friction ellipse.

6. Track Testing

The goal of any dynamic engine testing simulation is to represent real world conditions so accurately that it can minimize or even replace the need for real world testing. To perform accurate drive train optimisation for the Killarney race track, it was necessary to correlate the predicted data with actual data, which was measured to determine the viability of the Real Time Full Circuit Driving Simulation System. The measuring process will now be described.

6.1 Test Equipment

6.1.1 Test vehicle

The test vehicle was a Ford Fiesta RSI 1.6 (see Figure 6.1 below). This specific model is also raced in the local production car series. The vehicle tested was a standard production model except for the CAE aftermarket engine upgrade. The upgrade included a different camshaft, free flow exhaust manifold and remapped engine calibration. This is a very mild upgrade and increased the peak power from 70kW to 81kW. The specifications of the standard production vehicle can be seen in the Appendix C.

Figure 6.1 Ford Fiesta 1.6 RSI

6.1.2 Microstrain 3DM-G sensor

The 3DM-G is a three axis, gyro enhanced orientation sensor (see Figure 6.2). This sensor was placed near the centre of the vehicle with its x-axis aligned with the longitudinal axis and y-axis with the lateral axis of the vehicle.

This sensor has the capability to measure orientation, acceleration and angular rates in three dimensions. The sampling frequency of the sensor is 100Hz and all the data are time stamped. See Appendix C for complete specifications and calibration certificate.

Figure 6.2 MicroStrain orientation sensor

6.1.3 Global positioning system

The same GPS that was used to gather the track layout data was used again (see Figure 6.3). This time the absolute position and instantaneous velocity of the vehicle were recorded. See Appendix C for specifications.

Figure 6.3 Garmin 5 GPS

6.1.4 Engine control unit emulator

It was necessary to record all the engine parameters as the vehicle circuits the track to compare predicted values with measured results. In order to achieve this an engine control unit emulator was connected in place of the standard ECU. The data could now be recorded and saved in real time. See Appendix A for an example data file.

6.1.5 V-box system

This system also works on the principle of the GPS and records the absolute position, vehicle velocity and acceleration in real time at a rate of 20Hz (see Figure 6.4).

Although this was duplicating some of the previous data it provided a means by which the loss in accuracy of the GPS data, due to its slow data acquisition rate of 1 Hz, could be validated. This was done by plotting the results (illustrated in Figure 6.11). See Appendix C for specifications and example data file.

Figure 6.4 V-box data acquisition system

6.1.6 Summary of measurements taken

The summary of all the measurements taken can be seen in Table 6.1.

Table 6.1 Summary of measurements taken

Measurement	Equipment/sensor used
3-axis accelerations [m/s^2]	MicroStrain
3-axis angular accelerations [rad/s^2]	MicroStrain
3-axis orientations [degrees]	MicroStrain
3D global position [m]	Garmin 5 GPS, V-box
Vehicle speed [km/h]	Garmin 5 GPS, V-box
Engine speed [rpm]	Engine control unit emulator
Manifold pressure [Pa]	Engine control unit emulator

6.2 Test Procedure.

The test vehicle was set up with all the sensors mentioned in paragraph 6.1 and taken to Killarney race track (see Figure 6.5). Deon Joubert, a well known racing driver, volunteered to do three flying laps of the circuit. The first lap was completed and followed by a quick stop to save all the data. The next two flying laps were done in succession. The driver lapped consistently within two seconds.

Figure 6.5 Killarney race track

54

6.3 Results

6.3.1 Microstrain 3DM-G sensor

The longitudinal and lateral accelerations for one complete lap are illustrated in Figure 6.6. The measurements show start and finish at the beginning of the main straight. The Microstrain sensor starts recording when the power supply is switched on and therefore the 50s start time.
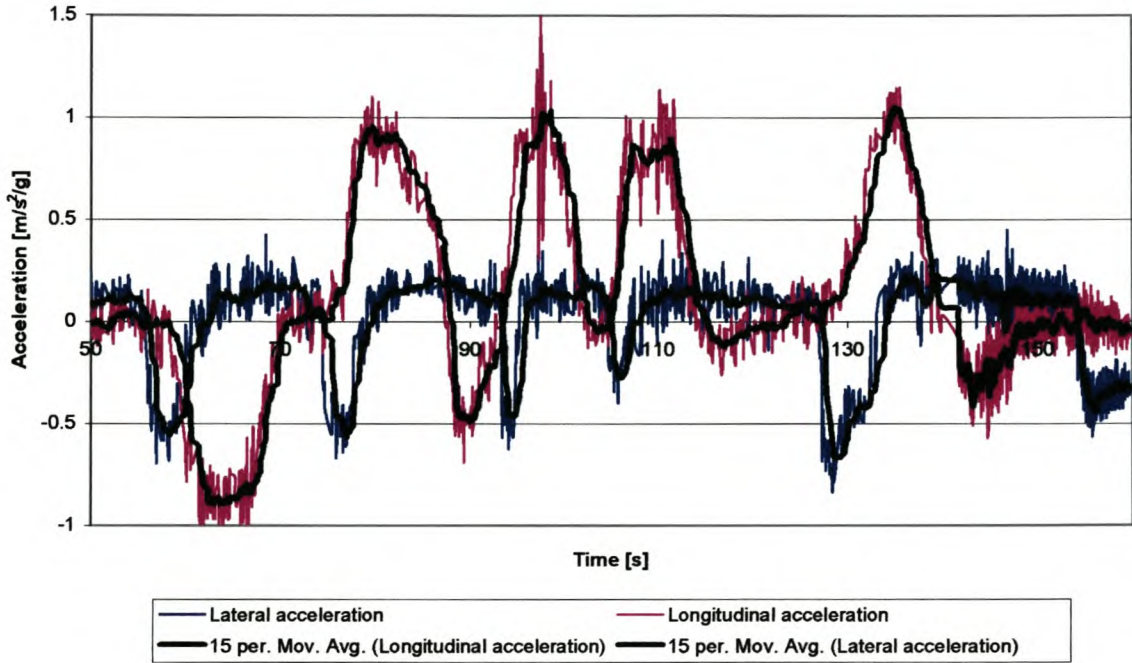
Figure 6.6 MicroStrain acceleration data

Lateral accelerations:

The pink graph shows the lateral acceleration of the vehicle when circling the track. The positive values above the x-axis represent right hand turns and the negative values represent left hand turns of which there is only one significant turn after the main straight. The expert racing driver was able to negotiate the turns at an average value of approximately 0.8g and a peak value of 1g.

Longitudinal accelerations:

The blue data represents the longitudinal accelerations of the vehicle around the track with the positive data being acceleration and the negative data being braking. The braking zones are easy to identify from the data and always follow after a straight.

55

All the sensors used were factory calibrated but it was decided to visually inspect the correlation between the V-box (GPS) system and MicroStrain system (Accelerometer) for the longitudinal acceleration. This can be seen in Figure 6.7.
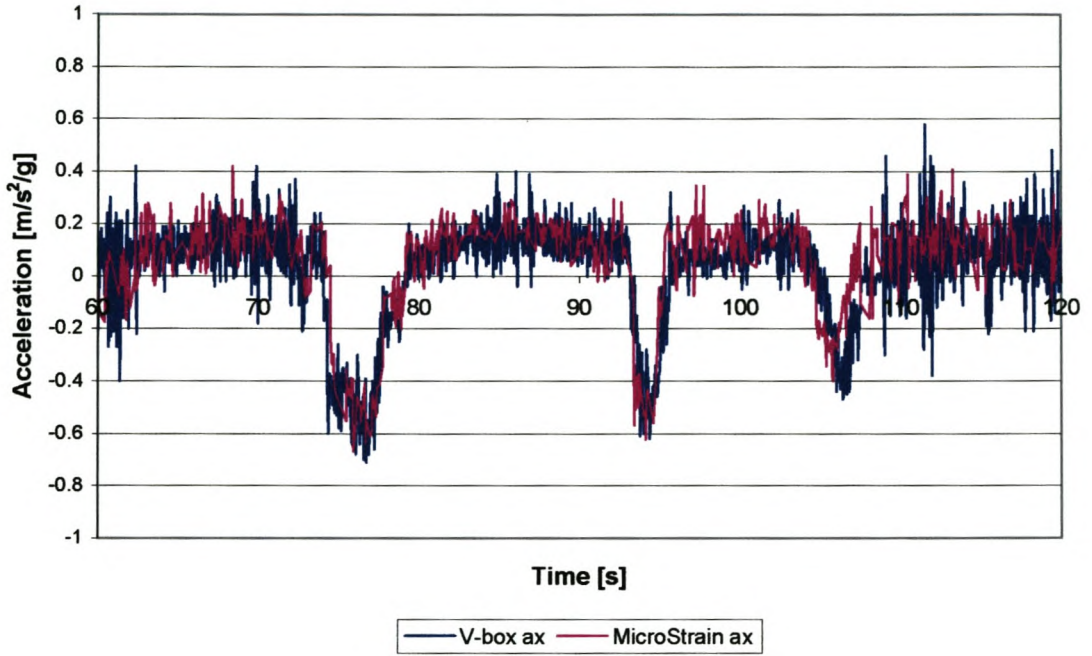
Figure 6.7 Longitudinal acceleration correlation

Only 60s of the lap is shown due to an erratic power supply of the V-box that led to zero vehicle speed readings (see Figure 6.11).

Friction circle concept:

To illustrate the friction circle concept the longitudinal and lateral acceleration were plotted on the x-axis and y-axis respectively. The result can be seen in Figure 6.8.
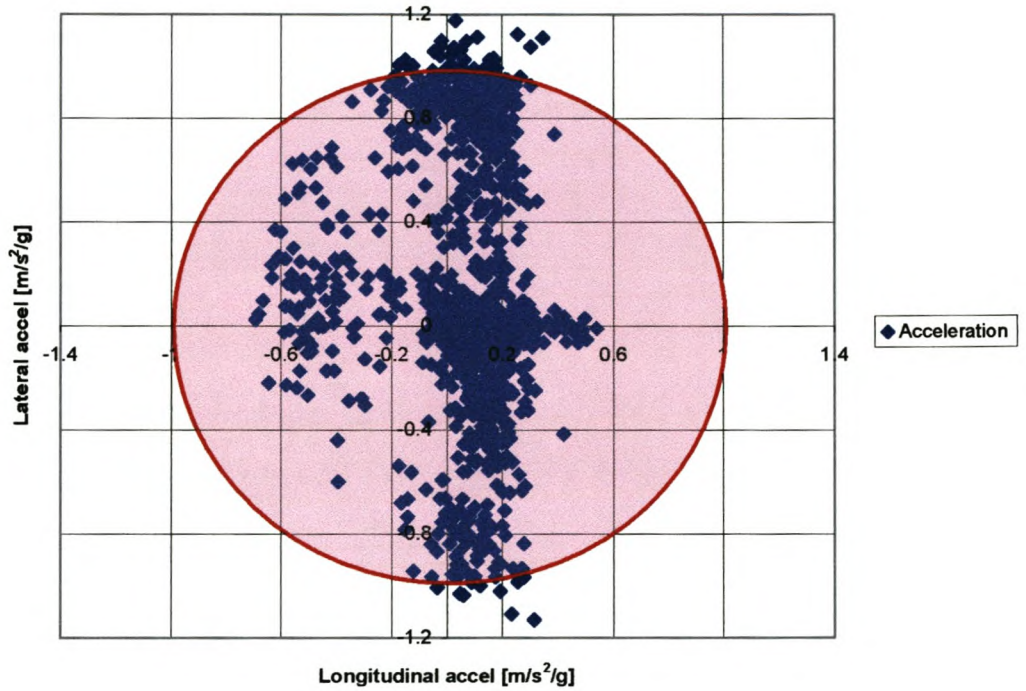
Figure 6.8 Friction circle graph

It can be seen from the figure that the vehicle spends most of the time accelerating in a straight line and on the friction circle limit while negotiating right handed turns.

For clarity the points were plotted for a left handed turn followed immediately by a right hand turn.

57

The results can be seen in Figure 6.9.
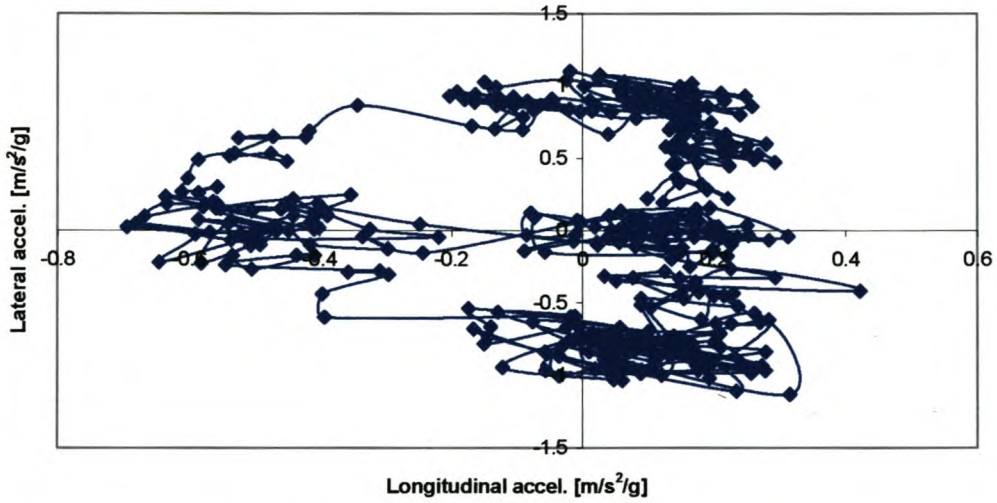
Figure 6.9 Deon Joubert's friction circle graph

The data points were linked in order to show the form of the ellipse. It can be seen that the race driver attempts to keep the vehicle close to the friction ellipse through the corners by braking and turning at the same time and accelerating when exiting the corner. The vehicle is very much power limited and this shows on the acceleration side (positive x-axis) where the "circle" is very flat. Milliken (1995) obtained the friction circle graph for Senna at the Adelade circuit as illustrated in Figure 6.10. Note the power to weight ratio and down force effects.
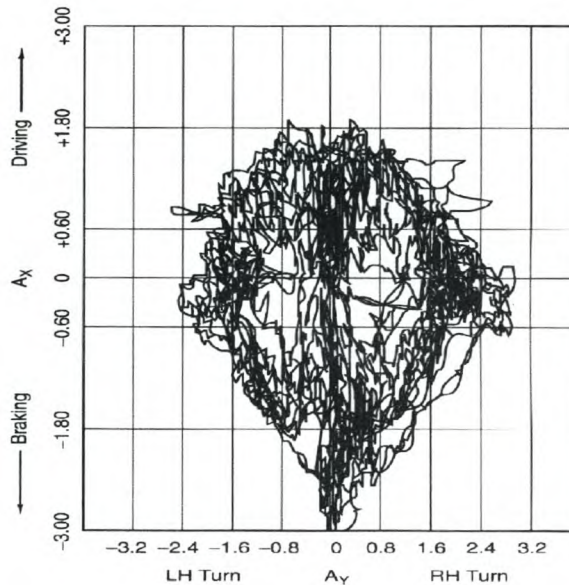
Figure 6.10 Senna's friction circle (Milliken, 1995)

58

6.3.2 Global positioning and V-box system

The main focus of the two systems was to capture instant vehicle speed while circuiting the track. The two speed profiles were plotted over each other to inspect relative accuracy at different data capturing frequencies. The comparative speeds can be seen in Figure 6.11.
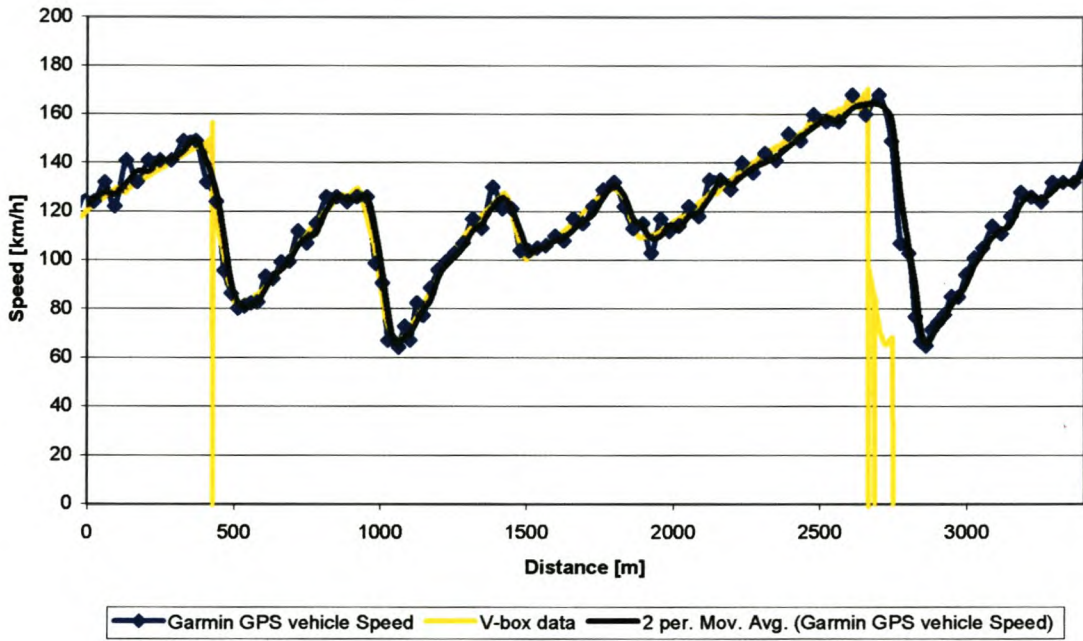
Figure 6.11 GPS and V-box vehicle speed

The sampling frequency of the V-box is 20 Hz compared with the Garmin GPS that only sample at 1Hz. When a moving average is applied to the Garmin GPS data, it correlates very well with the data collected by the V-box system. The zero speed-readings from the V-box data are due to erratic power supply. Fortunately most of the lap's data were still useful.

6.3.3 Engine control unit emulator

The main function of the engine control emulator was to capture engine speed and manifold pressure of the vehicle around the circuit and can be seen in Figure 6.12.

This data will be compared to the data gathered from the dynamic engine test stand.
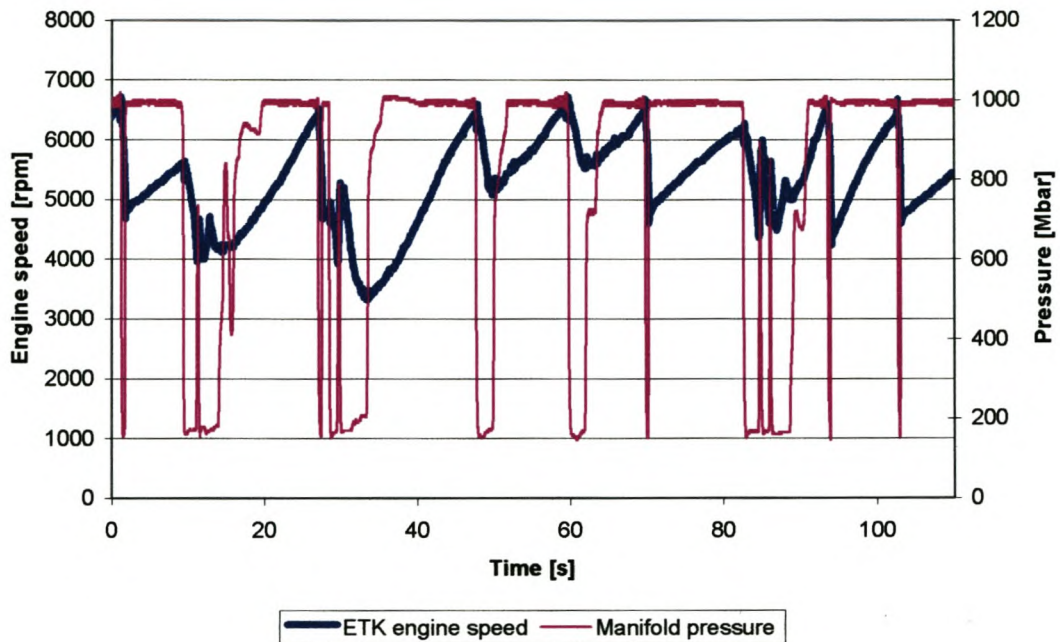
Figure 6.12 ETK track data

6.3.4 Conclusion

Vehicle speed measured by the Garmin GPS correlated with the V-box GPS system and vehicle acceleration measured by the V-box correlated with the MicroStrain accelerometer.

The goal of the track testing was to collect actual racing data in order to compare it with the simulated data. The correlation will validate the appropriateness of the simulation as an engineering tool for race engine optimisation.

60

7. Simulation results and correlation

In order to conduct simulation testing around the Killarney race circuit it was necessary to test and optimise the system. The process followed to achieve the goal of circuit simulation is described in the following sections.

7.1 Vehicle parameters

The vehicle parameters in Table 7.1 were based on typical values obtained from sources such as the road test of CAR magazine (November 2000). See Appendix for CAR magazine specification sheet. The focus of the project was engine optimisation and decisions will be based on comparative results, i.e. testing different engine configurations. If the vehicle properties closely resemble those of the actual vehicle and stay constant during the tests then it will be suitable for the real time simulation.

Table 7.1 Vehicle parameters

Vehicle Property	Value	Data source
Mass, M	925kg	CAR
Wheelbase, L	2.5m	CAR
Centre of gravity, b	1m	Assumption
Centre of gravity, c	1.5m	Assumption
Centre of gravity, h	0.4m	Assumption
Drive wheels	Front	Physical vehicle/CAR
Drag coefficient, C_d	0.35	Gillespie (1992)
Frontal Area, A	2.16	CAR
Vehicle drive train efficiency, η	90%	Assumption
Number of gears	5	Physical vehicle/CAR
Final drive ratio, G_f	4.06:1	CAR
Low gear	3.593:1	CAR
2nd	1.925:1	CAR
3rd	1.281:1	CAR
4th	0.951:1	CAR
5th	0.756:1	CAR
Tyre size	185/55 R14	Physical vehicle/CAR
Rolling resistance coefficient, f_r	0.15	Gillespie (1992)
Friction coefficient	1	Gillespie (1992)
Brake deceleration	5.5m/s^2	Track testing average
Engine dynamometer ratio	3.06	Physical value
Engine inertia, J_e	2.04kgm^2	Conradie (2001)
Gear change engine speed	6000rpm	Chosen value
Gear change time	0.5s	Chosen value

The assumptions made on the centre of gravity position were based on a 60:40 front to rear axle weight distribution. Drive train efficiency of 90% was assumed for the part of the drive train after the gearbox of the vehicle due to the fact that the torque measurement on the test stand was measured between the gearbox and the dynamometer. The gear change time and maximum engine speed are variables that were changed during the tests.

7.2 Straight-line performance

A progressive strategy was followed to develop the simulation system. The development started with straight-line performance. This simplified the simulation by eliminating lateral acceleration.

7.2.1 Method

A comparison was done by running the dynamic vehicle model off the standard engine's torque curve, with and without engine inertia as equation 4.27 shows, followed by a real time simulation with real time torque input from the engine on the test bench. The influence of engine inertia on data gathered from steady state testing will be shown. The length of the run was 1800 m.

7.2.2 Results

The three runs were plotted on one graph in Figure 7.1 for comparison.
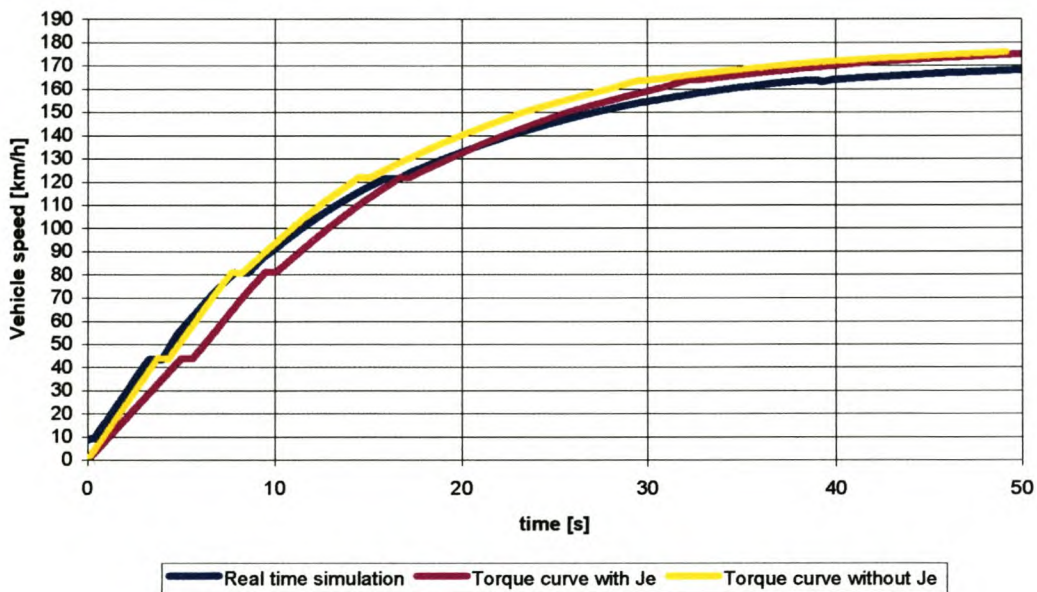
Figure 7.1 Comparative acceleration run vehicle speeds

Acceleration from a standing start was never an objective of the circuit simulation, as only "flying" laps was simulated. In order to produce the above graphs when running off the engine's torque curve, an initial torque was assumed for zero engine speed. During the real time simulation the acceleration from a standing start was replaced by a rolling start at idle speed. The mentioned pull away strategies compromised the 0-100km/h times. Gear change time was set at a modest 0.5s to lessen the impulse loading on the gearbox dynamometer set-up.

The summary of results in Table 7.2 below show that the real time simulation results correlate well with the data from CAR magazine. The kilometre sprint time differs less than 1s (2.76% error) and the top speed by 5km/h (2.79% error). It was decided that the real time data is accurate enough to illustrate the capabilities of the circuit simulation.

Table 7.2 illustrates the importance of including the engine inertia when using the torque curve attained from steady state engine testing. During the dynamic event of acceleration the engine's inertias tends to decrease the shaft output torque.

Table 7.2 Summary of acceleration results

Evaluation	Torque curve with J_e	Torque curve without J_e	Real time engine test	CAR magazine figures
0-100km/h	12.9s	11.0s	11.46s	10.33s
1 km sprint	33.7s	32.1s	32.94s	32.03s
Top Speed	177km/h	177km/h	172km/h	179km/h

The comparative engine speeds for the acceleration runs are illustrated in Figure 7.2. Note that the fictitious vehicle without engine inertia shifts to 5th gear 10s before the real time simulation model.
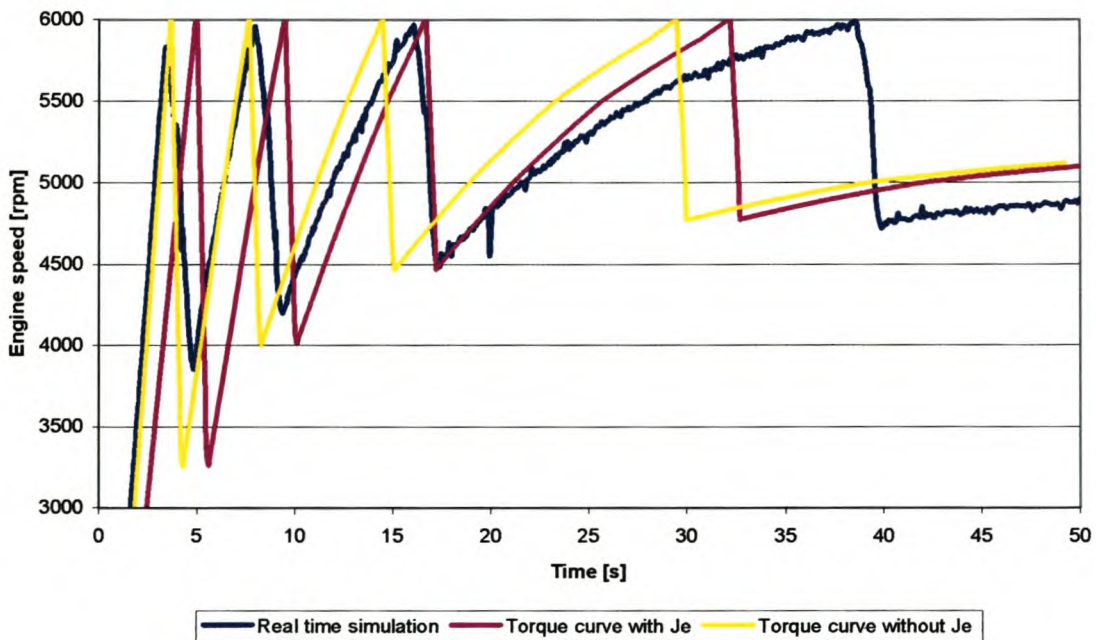
Figure 7.2 Comparative acceleration run engine speeds

It is clear that the simulated engine speed with "hardware in the loop" lags behind the speeds predicted from the torque curves (as does the vehicle speed). The reason for this is the torque output of the real engine is lower than the torque values that the "steady state" database predicts.

63

This is clearly shown in Figure 7.3. The zero torque values represent gear changes in the vehicle model. The model started in first gear and accelerated at Wide Open Throttle (WOT) through the gears. The variables in Table 7.1 were held constant for all the tests.
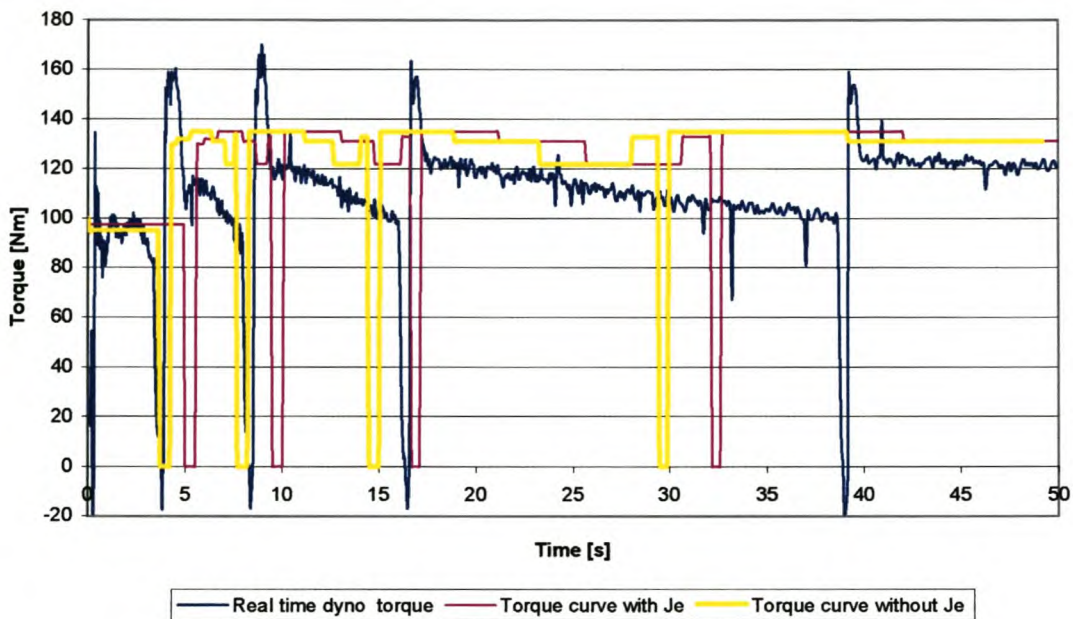
Figure 7.3 Acceleration run torque graphs

The reasons for the lower torque values of the real time simulation with "hardware in the loop" compared to the values from the steady state torque curve are:

- Gearbox attached to real engine with efficiency loss.
- Mechanical inertia.
- Flow inertia.
- Thermo dynamical inertia.

During gear changes in an actual vehicle the clutch is disengaged and zero torque will be transferred. The DC dynamometer was simulating gear changes with an engaged clutch, which makes it impossible to achieve exactly zero torque at the clutch interface. A strategy was followed whereby cutting the throttle by the correct amount during simulated gear changes resulted in near zero torque readings as can be seen in Figure 7.3.

The torque spike measured after each gear change resulted from engine inertia. The dynamometer ramps down the engine speed during each up shift as to simulate linear clutch engagement. A similar torque pulse occurs in an actual race car. When a racing driver releases the clutch swiftly after each up shift, a jolt can be felt through the vehicle, as the clutch speed has to meet up with the engine speed.

64

7.3 Cornering simulation

In order to test the simulation of cornering a number of short "test tracks" were programmed.

7.3.1 Corner entry

As explained earlier the vehicle will accelerate down the straight until the vehicle speed exceeds the brake speed calculated by the pre-processor. The vehicle will follow this predetermined profile until the corner apex is reached. A fictitious corner was programmed with several small corner segments with decreasing radii, Ranging from 100 m to 20 m. The vehicle speed when entering the corner will be 105 km/h and will decrease as allowed by the values of the pre processor described in section 4.3.4. The real time simulated vehicle speed is shown in Figure 7.4.
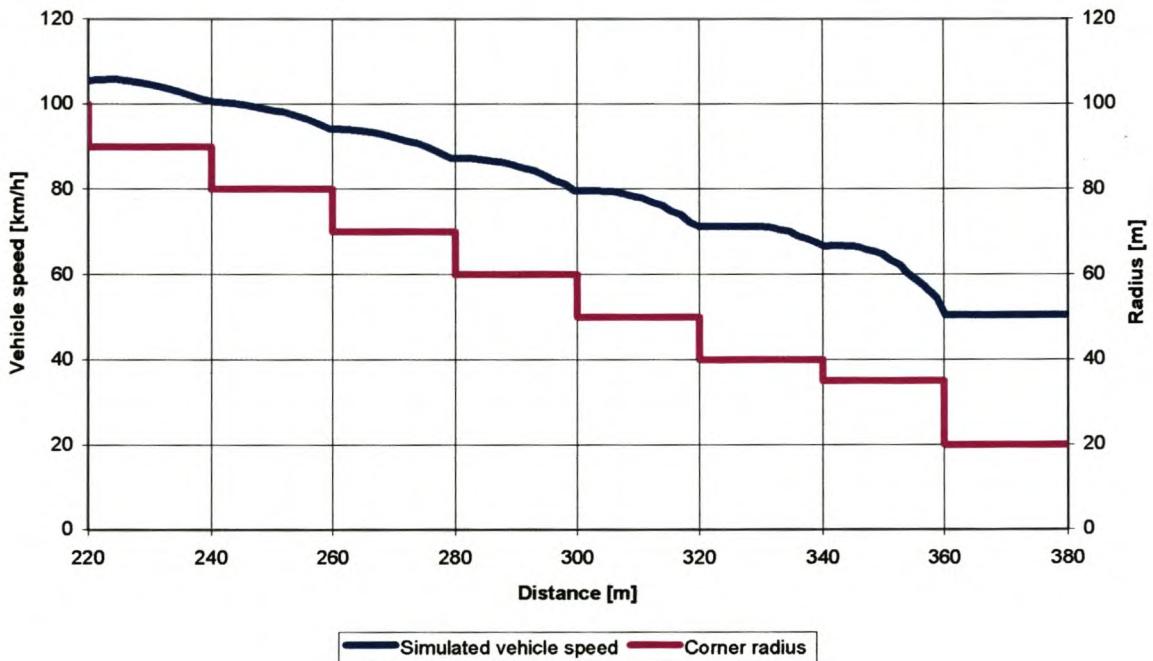
Figure 7.4 Vehicle entry speed for small corner segments

It can be seen how the vehicle speed adapts to the new corner radii. The smaller the corner segments the more the vehicle speed will tend to be a gradual curve.

65

7.3.2 Corner Apex

The vehicle follows the brake profile until it reaches the corner apex at the theoretical maximum speed possible. Engine torque must be controlled in the apex to overcome friction, aerodynamic, rolling and gradient forces enabling the vehicle to maintain a constant speed. According to the friction circle concept the vehicle will be close to the maximum lateral force possible with an offset to positive traction force due to the traction force mentioned. Figure 7.5 illustrates this. The lateral acceleration decreases as the vehicle speed decreases in the corner segment before the apex (400 m). When the vehicle enters the apex it is at maximum lateral acceleration (constant lateral acceleration) as allowed by the friction ellipse.
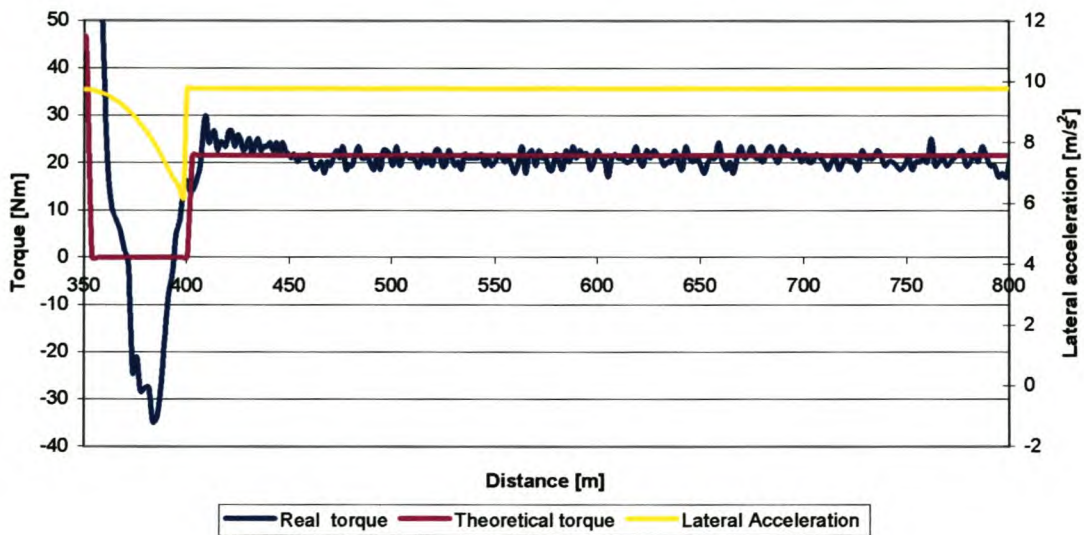
Figure 7.5 Apex torque control

The PID controller of the PLC manages to follow the theoretical value very well with minimal overshoot in the positive torque region. The negative torque is due to a sudden throttle cut during a gear change to select the optimal gear ratio for the desired apex speed.

7.3.3 Corner Exit

When the vehicle is exiting a corner the radius of each new corner segment will gradually increase therefore, according to the friction circle method, also increasing the possible traction force. The torque control capability of the simulation was tested by subjecting it to a corner with three long exit segments with different radii. The results are shown in Figure 7.6.

The vehicle will accelerate in every new corner segment until the friction circle concept limits the traction force due to the increasing lateral force. The vehicle will

66

continue at constant speed until the next corner segment (see yellow line on graph for vehicle speed).
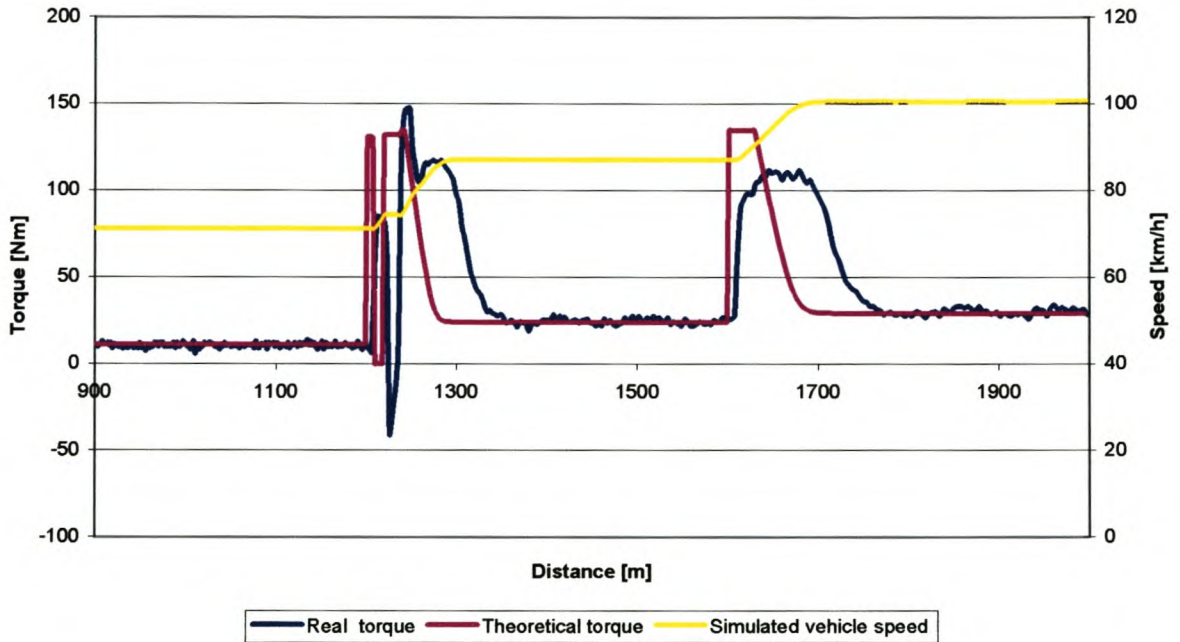
Figure 7.6 Torque control on corner exit

The first torque spike is due to a gear change. It looks as if the real torque value lags behind the theoretical value after each radii increase. The fact is because the vehicle speed in the real simulation does not increase as rapidly as in the theoretical simulation therefore allowing more torque possible later into the corner segment. The effect of the friction circle concept is illustrated in Figure 7.7.
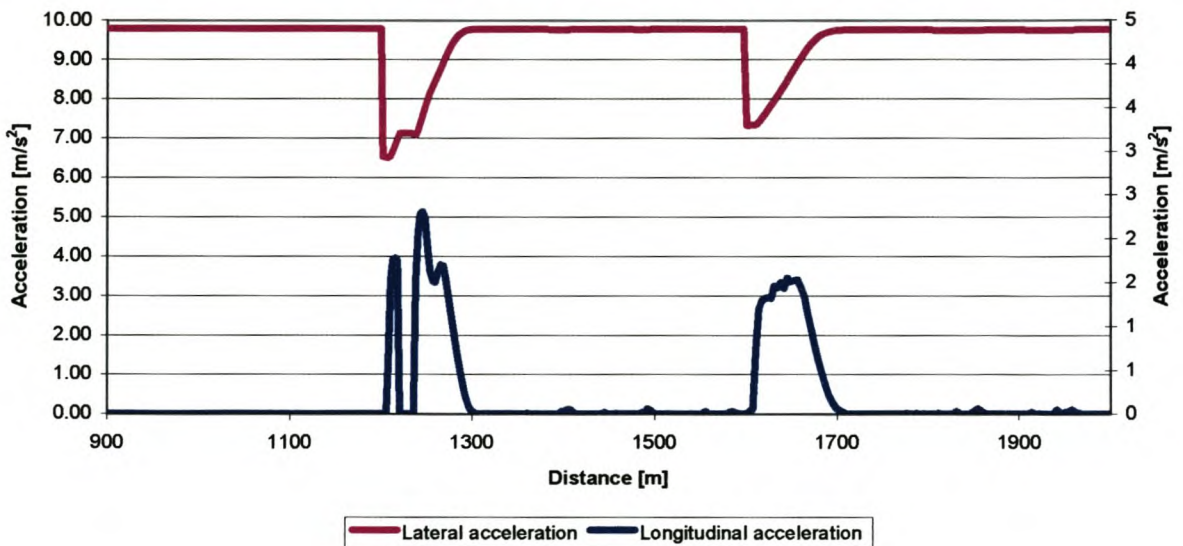
Figure 7.7 Corner exit accelerations

67

As the corner radius increases lateral force decreases for the same vehicle speed and the friction circle method allows tractive force to be increased and therefore leads to the longitudinal acceleration peaks shown in Figure 7.7. As the vehicle speed increases the lateral force increases again and longitudinal acceleration is limited. Note that the first longitudinal acceleration spike is due to the gear change.

7.3.4. Speed demand

During the discussion of the hardware in chapter 5 it was evident that the standard CAE DC dynamometer set up is not ideal for dynamic engine testing in its standard form. A solution was found by running the engine through a gearbox with a 3.069:1 ratio. A piece of track was programmed to analyse the ability of the new dynamometer set-up to follow a speed demand. The simulated vehicle accelerated until it reached a corner. Braking commenced followed by acceleration as the vehicle was exiting the corner. The results are shown in Figure 7.8.
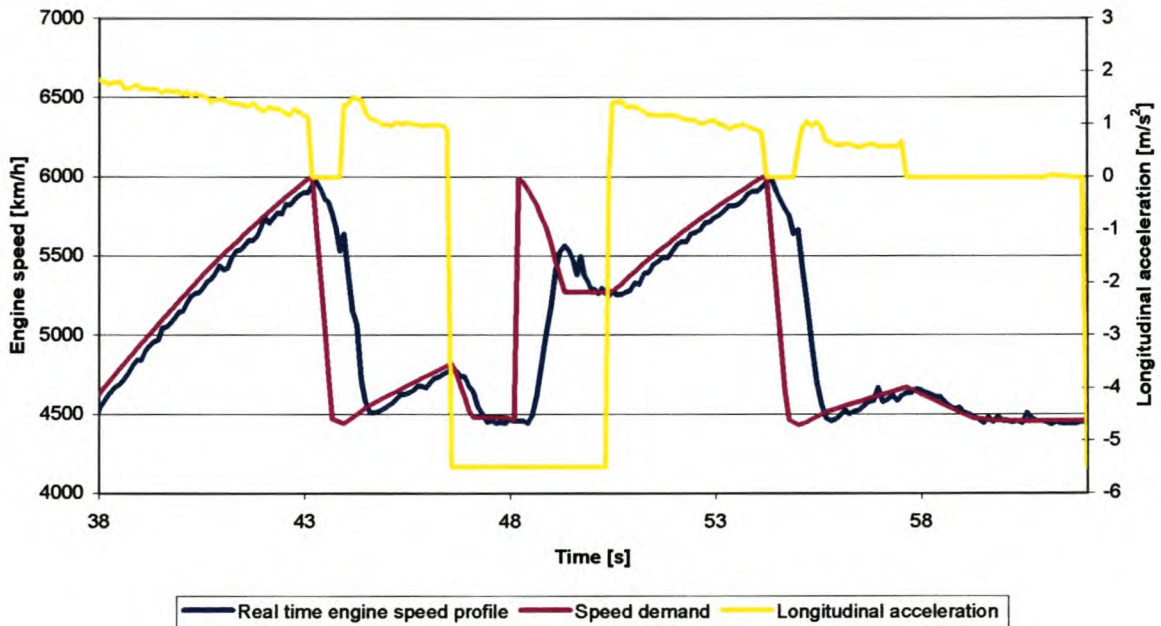
Figure 7.8 Speed demand

It is illustrated in Figure 7.8 that the dynamometer was unable to follow the speed demand when high ramp rates were required. When studying the above graph in more detail it is evident that that the greatest speed lag occurred during gear changes (zero longitudinal acceleration) and braking (negative longitudinal acceleration). The speed difference during braking wouldn't make any difference to lap time since the vehicle is following a predetermined speed profile. The high speed rate demand during braking is the "driver" using engine braking by selecting suitable gear ratios as he brakes. The lag when changing gear seems to be constant for each gear change therefore still makes the comparative nature of the circuit simulation valid.

68

7.4 Repeatability evaluation

One of the characteristics of an accurate simulation is repeatability. The real time nature of the simulation inevitably leads to some degree of discrepancy in results. Variable factors such as atmospheric conditions will influence the real time circuit simulation. A procedure was followed in order to test the repeatability of the system. Ten real time simulated laps were run around an experimental lap of the Killarney race track. Six laps were run on the 24th of November followed by another four laps one week later to conclusively prove the repeatability of results. Comparative vehicle speeds around the track are shown in Figure 7.9.
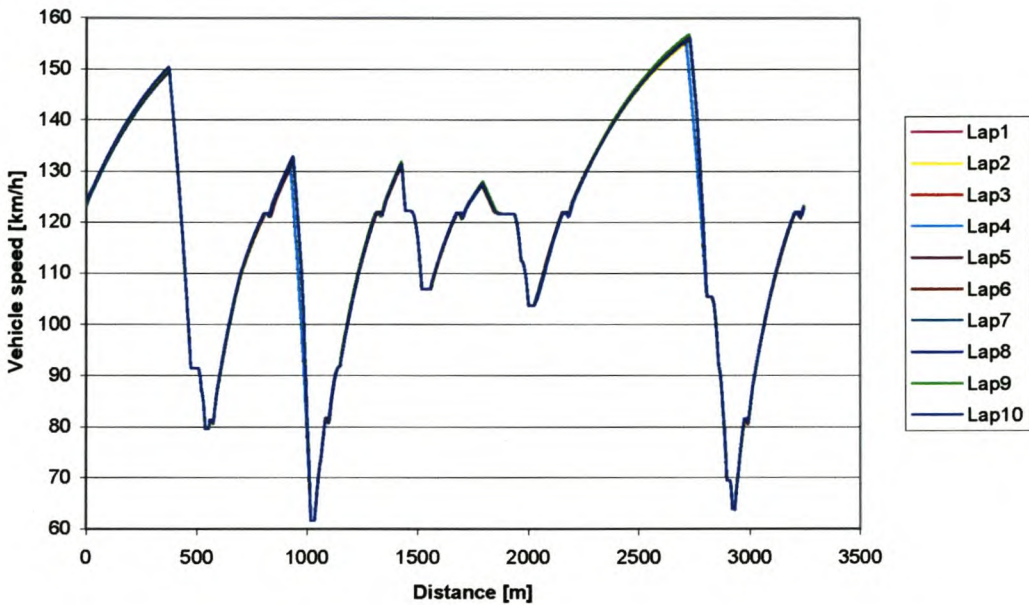
Figure 7.9 Repeatability of vehicle speed

Statistical analysis

The analysis was done on the average vehicle speed for each lap.

Sample mean: 114.276 km/h
Sample median: 114.302 km/h
Sample range: 0.257 km/h
Sample standard deviation: 0.091 km/h

From Figure 7.9 it is evident that the maximum difference in vehicle speed at any moment in time was less than 3 km/h.

Figure 7.10 shows the comparative engine speeds for the ten virtual laps.
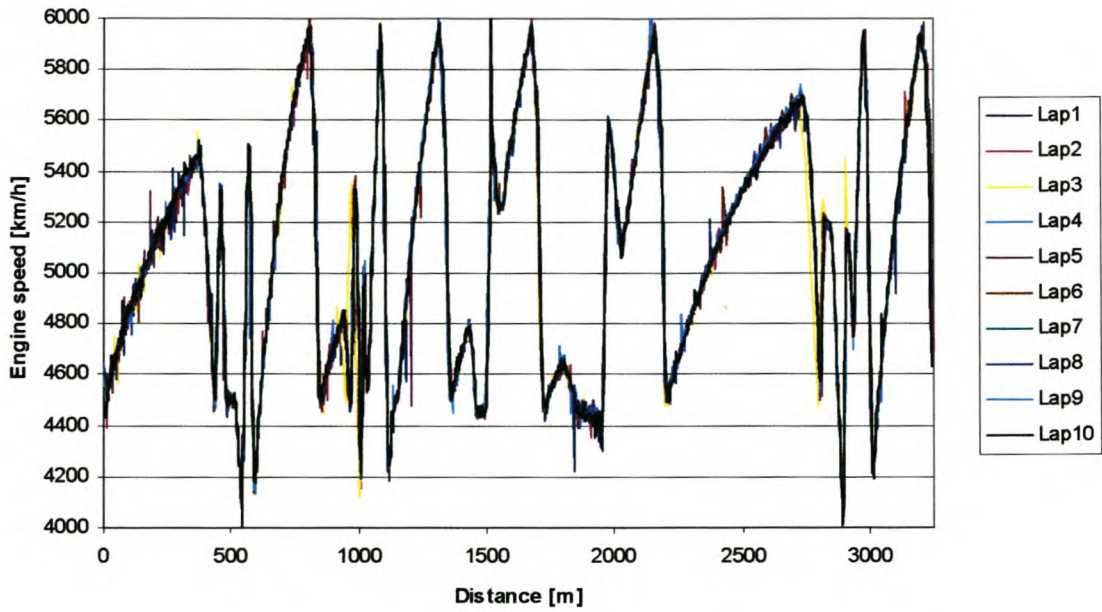
Figure 7.10 Repeatability of engine speed

The comparative real time engine torque measured for the ten virtual laps is illustrated in Figure 7.11.
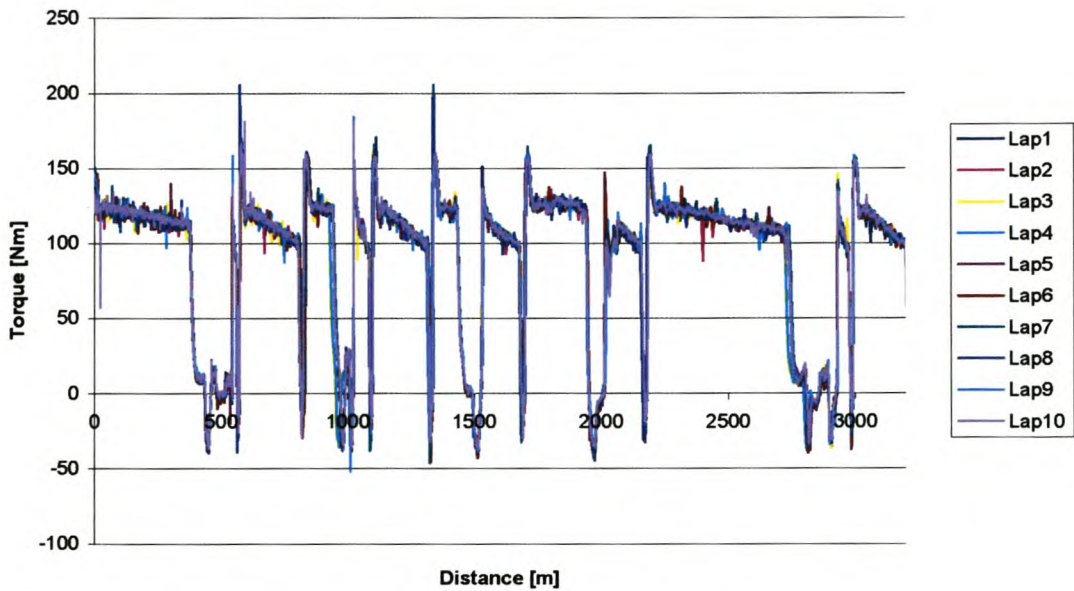
Figure 7.11 Repeatability of engine torque

When one takes into consideration the dynamic real time nature of the simulation, then all of the results shown in Figures 7.9-7.11 visually indicate a high degree of repeatability.

70

The main criterion for the optimisation of a race engine and drive train set-up is to minimize lap times. It is therefore vital that the simulation predicts the similar lap times for the same engine and drive train configuration. This is also illustrated by the virtual lap times that were measured as illustrated in Figure 7.12.
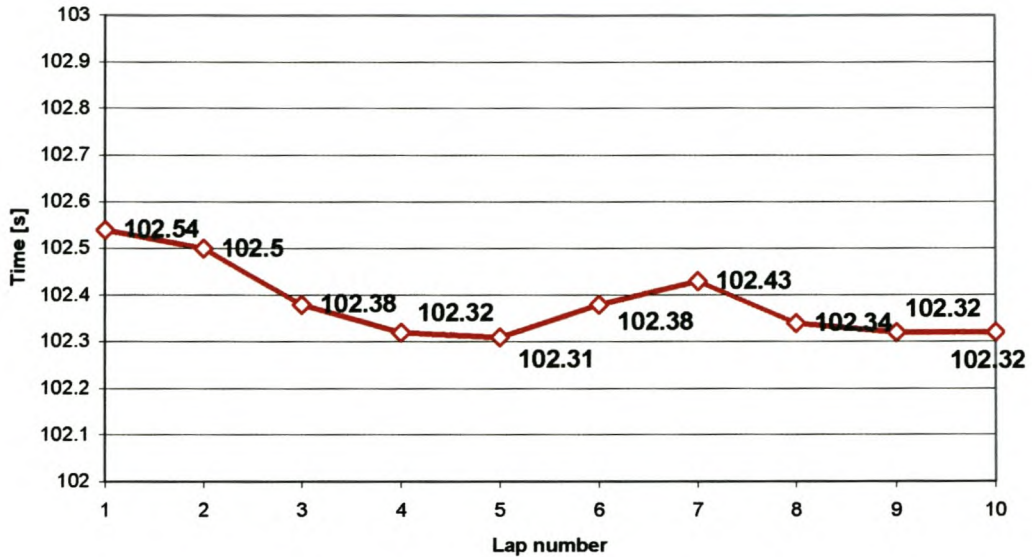
Figure 7.12 Repeatability lap times

Statistical analysis

Sample mean: 102.384 s
Sample median: 102.36 s
Sample range: 0.22 s
Sample standard deviation: 0.0814 s

The lap times showed a high degree of repeatability with the difference in lap time between the fastest and slowest lap measured only being 0.22 (sample range). This means that the maximum error in repeatability of the real time dynamic simulation is only 0.2%. According to the repeatability study the circuit simulation provides repeatable results and can be used for comparative studies.

71

7.5 Comparative simulation with different engine configurations

7.5.1 Objective

The objective of the comparative simulation is to test the effect on overall lap time for different engine configurations by running the Real Time Full Circuit Driving Simulation System. Comment will be made on the suitability of each configuration for the circuit tested.

7.5.2 Method

Two engine configurations of the Ford Rocam 1.6 mentioned earlier were used as a power source of the circuit simulation. A number of real time simulated laps were run around the Killarney circuit in each configuration while keeping all simulation variables constant.

Configuration 1: Standard engine

The engine was the standard Rocam 1.6 engine as found in the Ford Fiesta and Icon range. This engine was also used to calibrate the signals of the simulation program when the interaction between the software and hardware had to be done.

Configuration 2: Modified engine

One of CAE's projects was to increase the performance of the standard 1.6 Rocam unit. This performance upgrade included:

- Different camshaft
- Modified air box
- Free flow exhaust manifold
- Adjustment to ECU values

The engine in the Ford Fiesta RSI that was used for the track testing had the CAE performance upgrade installed. It was decided to exchange the standard parts of the engine on the test bench for the modified parts in the Ford Fiesta in order to test the comparative capability of the simulation. This was done to bring the standard engine specification as close as possible to that of the vehicle's engine. Even the vehicle's exhaust system was transferred to the test cell.

Power curves were done on both engines to show the difference in power output as illustrated in Figure 7.13.
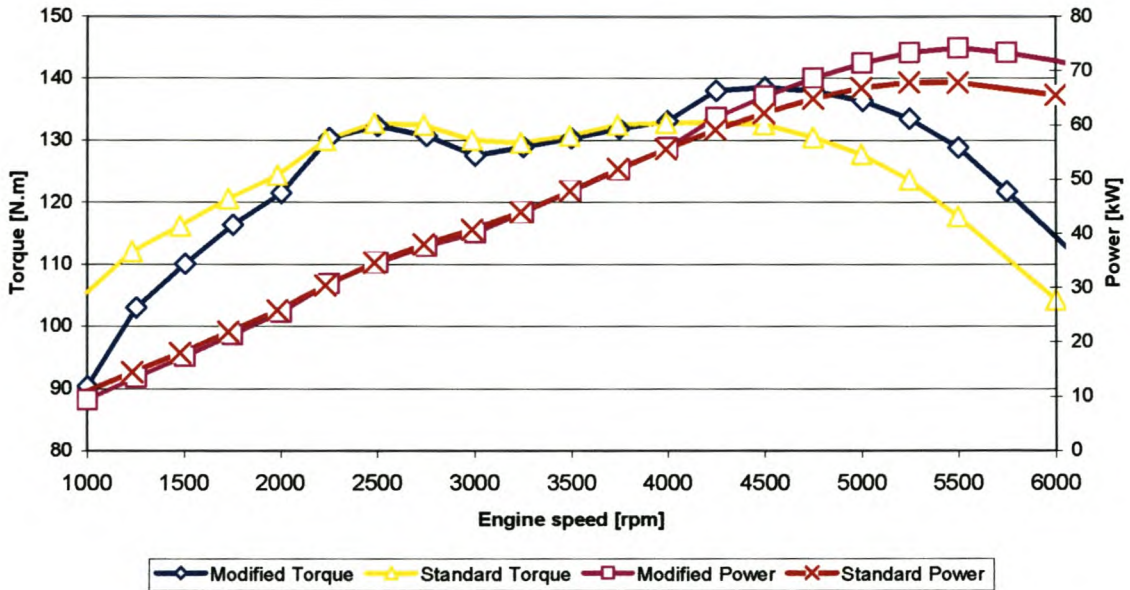
Figure 7.13 Comparative power curves

The main difference can be seen in the high-speed range. Tests conducted previously without a gearbox showed the peak output of the standard engine at 70kW and 81kW for the modified unit.

7.5.3 Lap time results

Several real time simulated laps were run with each configuration and lap times were compared. Both engines were restricted to 6000 rpm maximum speed. The predicted lap time was shown in Figure 7.14.
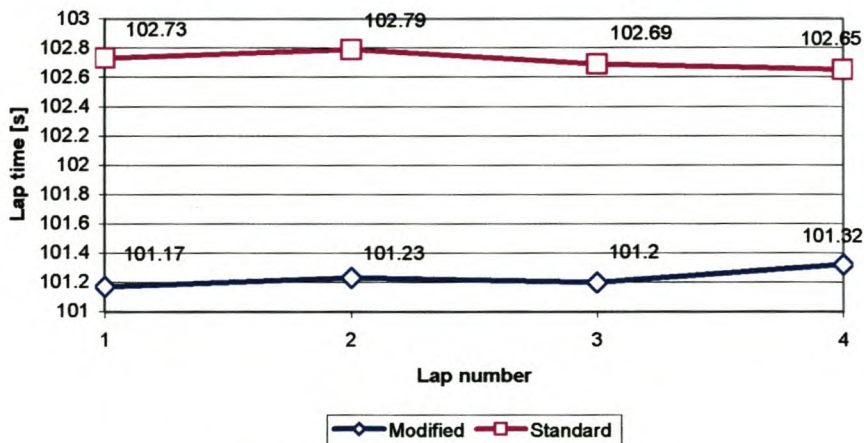
Figure 7.14 Comparative lap times

73

With the average difference in lap time being 1.5s, it is clear that the modified vehicle will have a distinct advantage on the race track. At an average lap speed of 115km/h the modified vehicle will gain 48m per lap on the standard vehicle. In order to analyse where the modified vehicle improves on the standard vehicle an analysis of the following was made:

Vehicle speed around the track as shown in Figure 7.15:
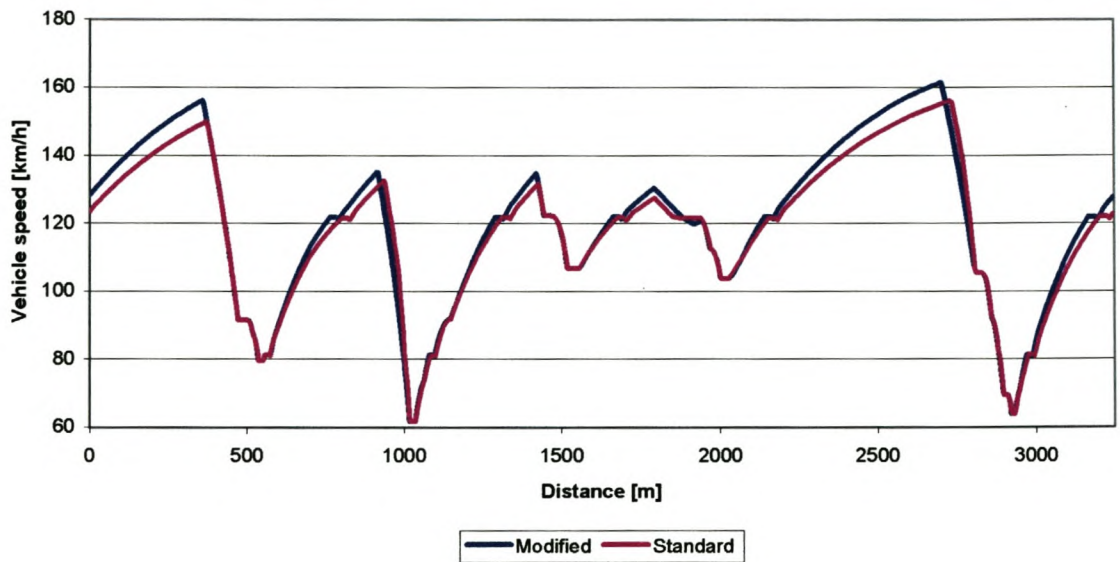
Figure 7.15 Comparative vehicle speed vs. distance

As expected the corner speeds are much the same with the superior power of the modified unit only apparent during acceleration. This lead to a difference in simulated top speed of 5.4 km/h at the end of the back straight.

This is due to increased torque available as shown in Figure 7.16.
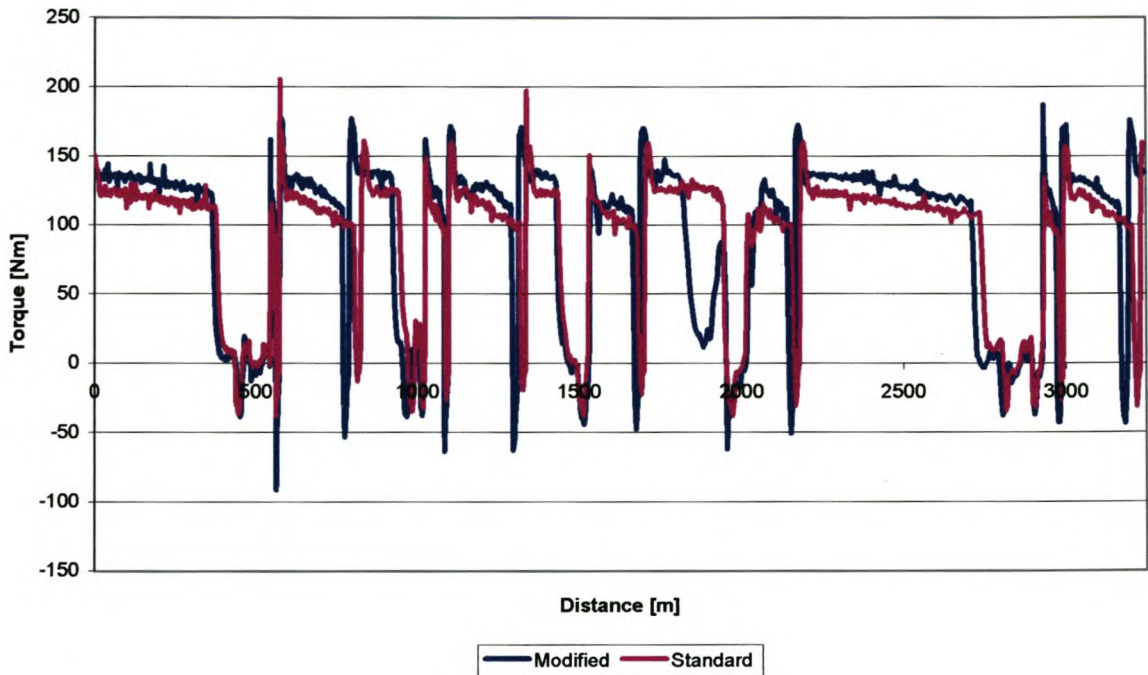
Figure 7.16 Comparative torque vs. distance

The discrepancy in torque values at approximately 1800 m was an extra gear change that is required for the higher simulated vehicle speed of the modified vehicle.

7.5.4 Conclusion

The Real Time Full Circuit Driving Simulation System predicts a definite improvement in lap time for the modified engine.

7.5.5 Additional simulation

It was decided to include a straight-line acceleration run to clearly show the performance advantage of the modified unit. The acceleration runs were done from a rolling start in first gear at idling speed.

See Figure 7.17 for comparative vehicle speeds.
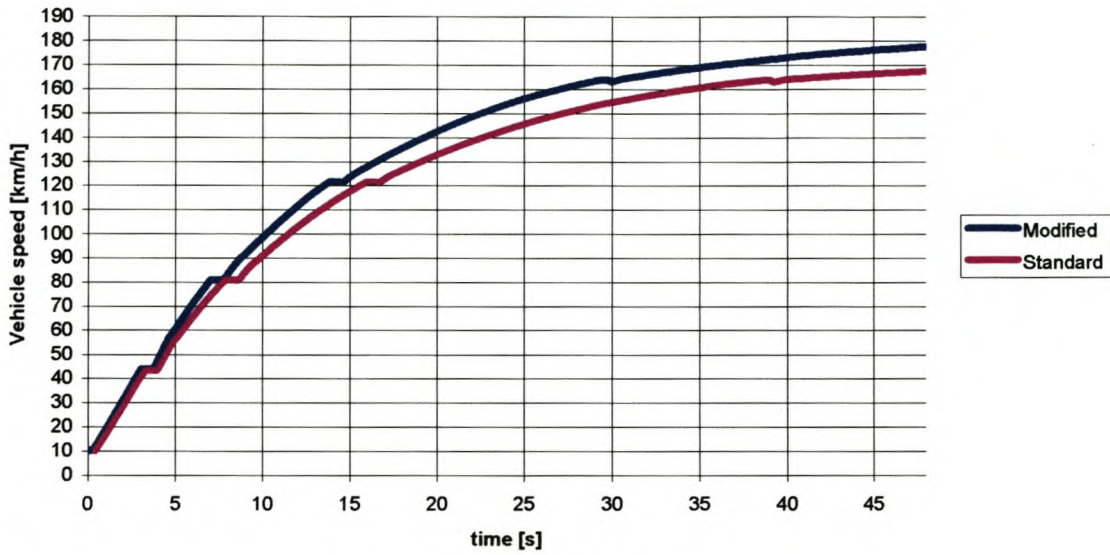
Figure 7.17 Acceleration run: vehicle speed

From the graph above the advantage is clear and the modified vehicle will reach 100 km/h **1.26 s faster** than the standard powered vehicle. Figure 7.18 illustrates the comparative engine speed – note the phase shift due to superior acceleration of modified unit:
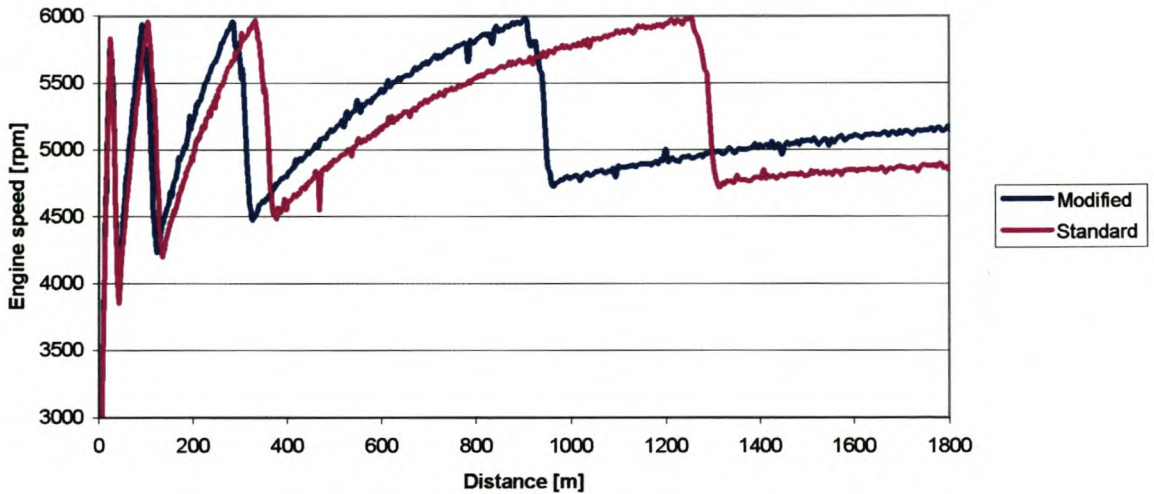
Figure 7.18 Acceleration run: engine speed

The acceleration runs confirms the advantage of the modified unit and illustrates another capability of the Real Time Full Circuit Driving Simulation System.

76

7.6 Correlation with track data

7.6.1 Objective

For the circuit simulation to be a valid representation of a vehicle circling the Killarney race track, it is important to look at the correlation of the simulated data compared to the data collected during track testing.

7.6.2 Method

The method used entails running the circuit simulation using the exact engine configuration as used in the test vehicle for the track testing. This enabled the direct comparison of all engine and vehicle parameters.

7.6.3 Results

Predicted lap times were measured and Table 7.3 summarises the results.

Table 7.3 Lap time correlations

Lap number	Circuitsim value (simulation test)	GPS value (physical test)
1	100.51 s	104 s
2	100.58 s	102 s
3	100.41 s	102 s
4	100.41 s	
5	100.49 s	
6	100.54 s	
Average	100.49 s	102.67 s

The objective of the circuit simulation is not the prediction of absolute lap time but rather engine set-up optimisation by studying comparative results. A difference in average lap time of 2.18s equates to a 2.1% error and is acceptable for comparative type studies. The reason for the difference might be slightly inaccurate track data in the simulation software and the fact that the friction circle concept leads to a "perfect" driver model. By using a "bicycle" model the lateral weight shift experienced when cornering is also not accounted for in the simulation.

The vehicle speed correlation around the track is shown in Figure 7.19.
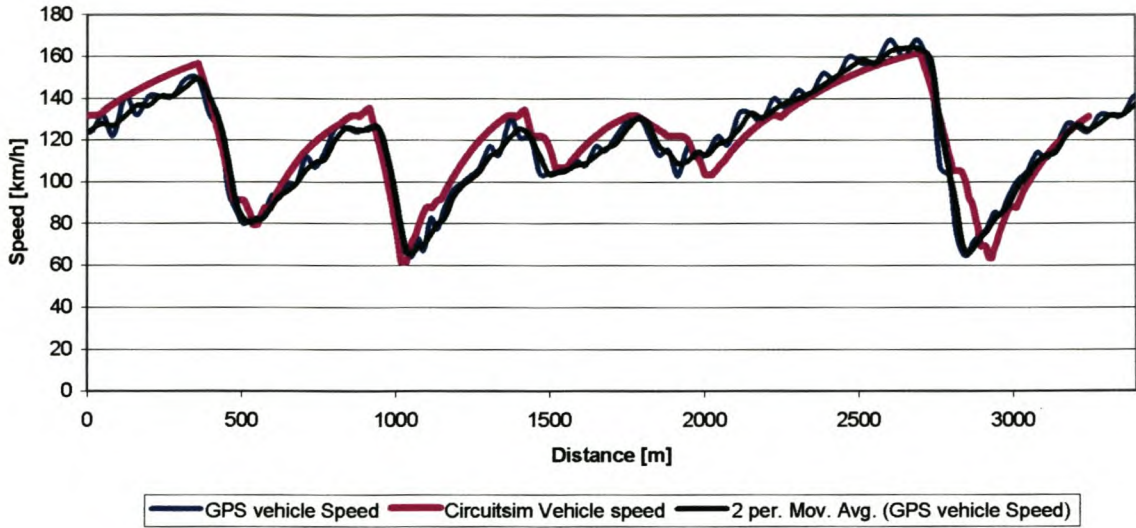
Figure 7.19 Vehicle speed correlation

Overall the vehicle speed correlated well with a 2.46 km/h difference in average speed between the simulated and track data. The average simulated vehicle speed was slightly higher than the physical GPS data, which resulted in faster lap times. The phase shift of the corners might be due to slightly inaccurate track data.

The longitudinal acceleration correlation can be seen in Figure 7.20
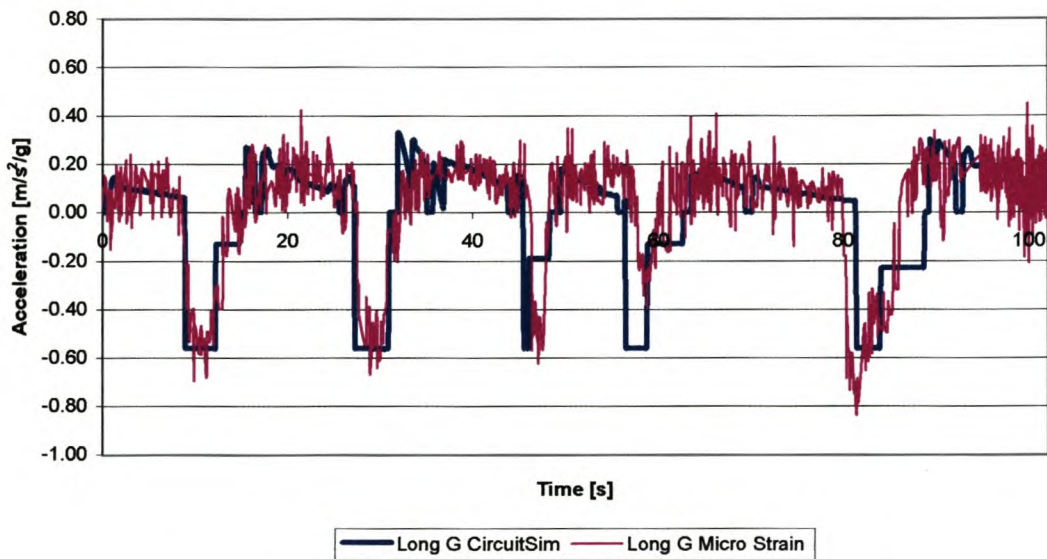
Figure 7.20 Longitudinal acceleration correlation

The simulation limited maximum deceleration to 5.5 m/s^2 as specified by the user in order to correlate with the actual braking performance. The second simulated

78

deceleration step is an average value of deceleration predicted by the friction circle concept that the simulated vehicle experiences when entering a corner.

With the aim of analysing the cornering behaviour of the simulated vehicle the correlation between vehicle's lateral acceleration was carried out. The lateral acceleration is shown in Figure 7.21. The perfect driver of the circuit simulation entered the corners at maximum lateral acceleration as allowed by the friction ellipse. The expert racing driver utilized a safer approached by entering the corners at speeds below the maximum theoretical values and therefore lower lateral accelerations.
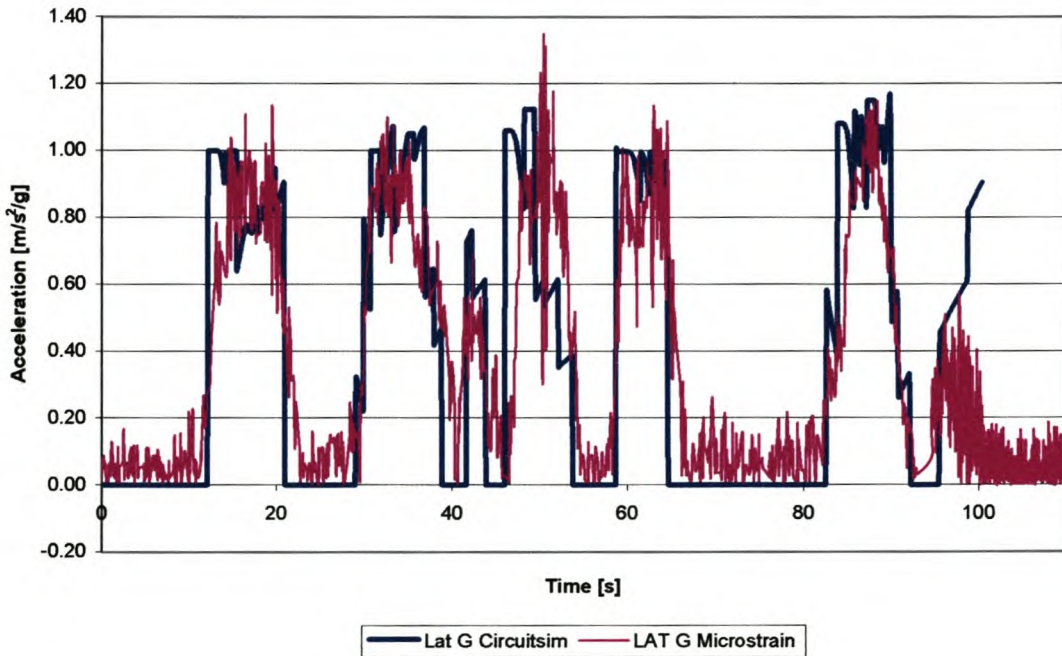
Figure 7.21 Lateral acceleration correlation

The circuit simulation does not account for left or right hand turns due to the simplified bicycle model used, therefore the absolute value of the measured data was used to do the correlation. Overall the average value of the simulated accelerations was higher than that of the measured data and this also led to the higher vehicle speed and faster lap time of the simulation. It must be remembered that the simulation used the friction circle as the governing factor and this in turn leads to a "perfect" driver. This is required for comparative tests but will lead to somewhat faster lap times than are possible in real life.

The engine data correlation is illustrated in Figure 7.22.
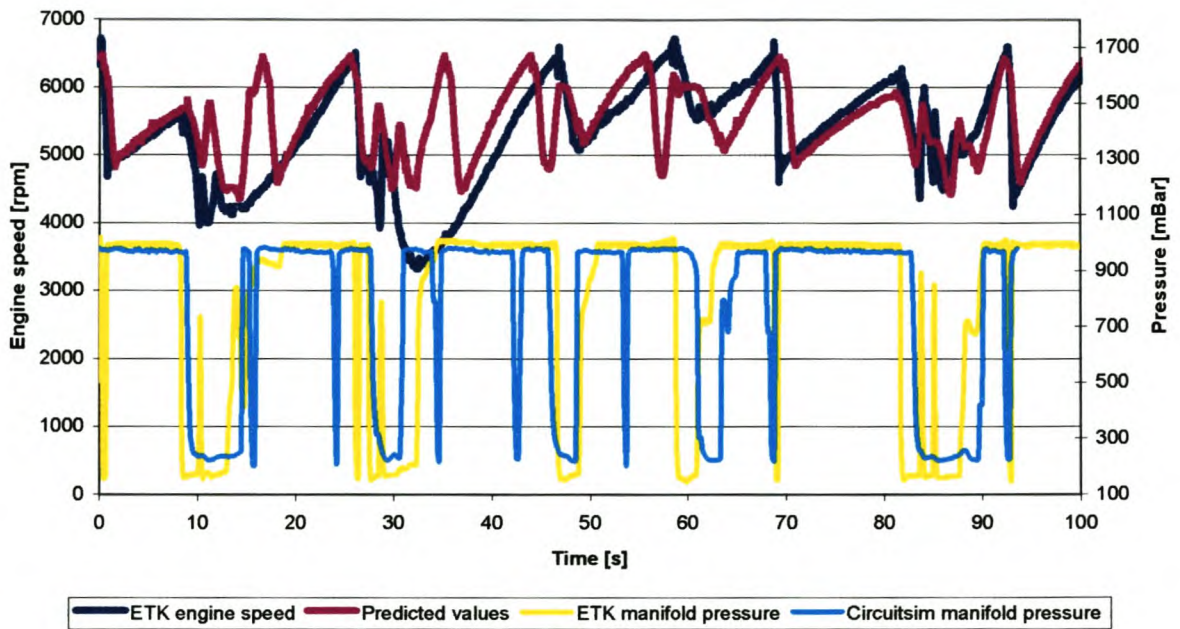
Figure 7.22 Engine data correlation

It was apparent from the literature study conducted that the engine speed correlation is the most difficult to achieve. The main reason for this is that a human (driver) is in control of the engine speed around a circuit and to simulate human behaviour is not easy. The engine speed still correlated well throughout most part of the lap with the exception at approximately 18 s and 35 s. This was due to the intelligent gear change strategy that the experienced racing driver employed.

According to the graph shown in Figure 7.23 the racing driver kept the car in 3rd gear at 18 s and 35 s while opting to shift to 5th gear without reaching the maximum speed in 4th gear at stages. The circuit simulation will always strive to extract maximum power from the engine and will opt for a lower gear if possible – even when negotiating a turn.

80

The race driver has knowledge of the circuit and opts for a higher gear, while compromising power, to exclude a gear change at a later stage in the circuit. This behaviour is difficult to predict and could only be implemented after studying the style of a certain driver.
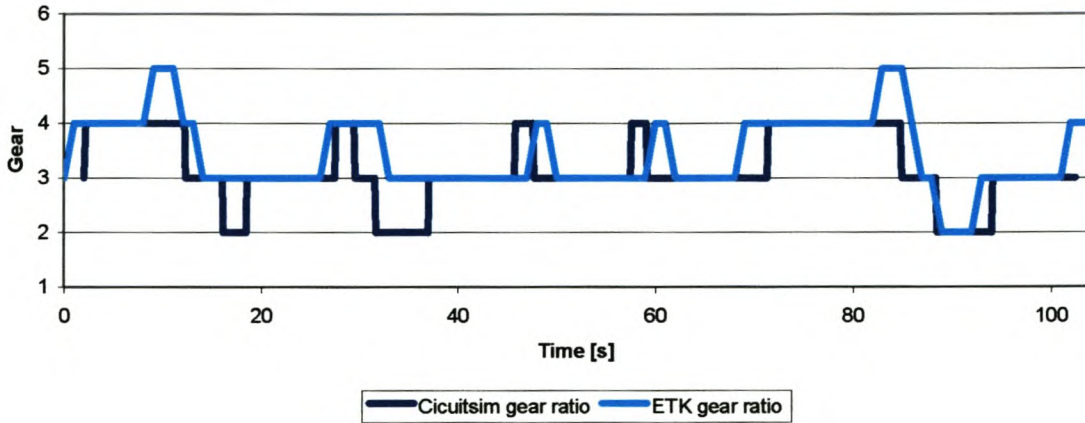
Figure 7.23 Gear ratio correlation

7.6.4 Conclusion

One of the objectives of this project was to develop a dynamic vehicle, race track and traction model and integrate it in a Real Time Full Circuit Driving Simulation System. The only way to verify the accuracy and appropriateness of the model was to compare it with actual data measured at the race track.

The results correlated well with predicted lap times only differing by approximately 2% from the actual lap times. This will allow the simulation to be used as an effective engineering tool for race engine optimisation for the Killarney race track.

7.7 More simulation applications

Although the circuit simulation was programmed with the first objective being engine optimisation, the simulation has numerous off line (see section 4.3.5.4 mode 1) possibilities and applications. All the variables concerning the virtual vehicle can be adjusted in order to see its difference in predicted lap times. By running the simulation off line, i.e. from the torque curve data, a good indication of possible improvement in lap times may be found with minimum time and cost penalties. When a gain is found, a real time simulation on the dynamometer could give a more accurate prediction. Although only actual track testing will confirm the gain, according to all the previously stated results, chances are that the gain would be transferred to the track. One variable that can be changed in order to use the available engine power of a race car more effectively around the race track is final drive ratio.

7.7.1 Method

Optimise the final drive ratio by running off line simulations for different final drive ratios.

7.7.2 Results

The deciding factor for any change to the vehicle's drive train is lap time. The final drive ratio was varied from 3.2 to 5 with the standard 4.06 in between. It can be seen from Figure 7.24 that an optimising strategy would have to be followed in order to achieve the most favourable value. The range of the difference between the slowest and fastest lap is 0.5 s, which is a lot in racing terms. The round-off error that is apparent in the lap times is due to the 0.1 s time increment that the off line simulation is run at. The accuracy of the predicted lap time will increase with a smaller time increment with an increase in computing time. Without the circuit simulation this would be impossible to visualise due to the complex nature of the problem.
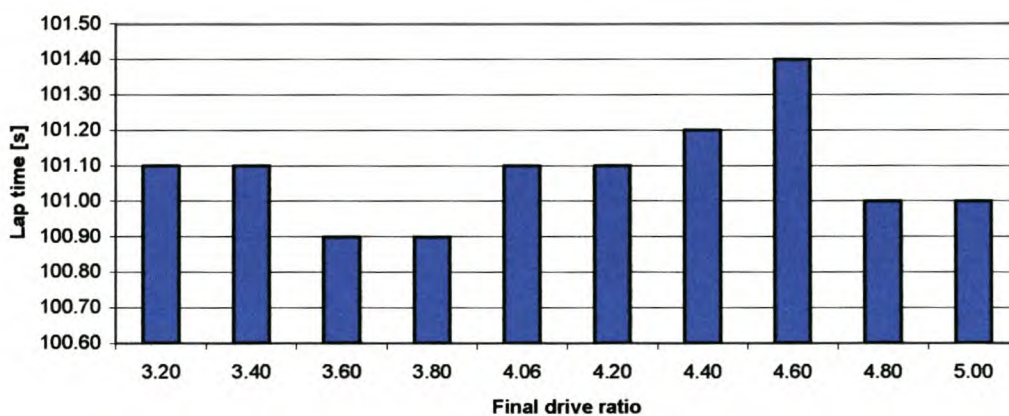
Figure 7.24 Final drive ratio variation

82

When one considers the engine speed around the track as shown in Figure 7.25 for the 3.6 and 4.6 ratios, it shows the intricate nature of the problem. The ratios alter the speed range around the track and would load the engine in dissimilar ways.
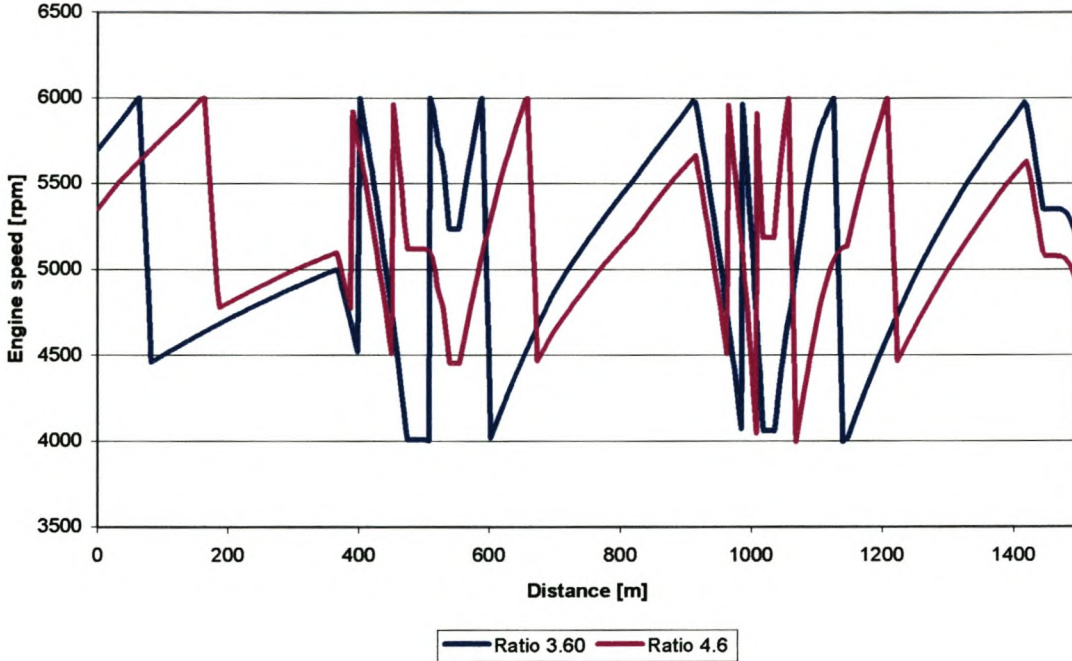
Figure 7.25 Final drive ratio variation engine speed

7.7.3 Conclusion

The circuit simulation can be used off line to examine the influence of various vehicle parameters on lap times. This will give a good indication of which variable will influence the lap time most and where the focus of optimisation must be.

83

8. Conclusion and recommendations

8.1 Conclusion

During the completion of the **Real Time Full Circuit Driving Simulation System** the following was achieved:

- An appropriate vehicle model was programmed using Delphi.

- The three dimensional race track layout was successfully modelled and used as input to the simulation program.

- The friction circle traction strategy was successfully employed and resulted in a good driver model, which is essential for comparative studies.

- The simulation was successfully linked to the hardware of the CAE dynamic engine test facility.

- Real time circuit simulations were run with good repeatability and correlation with actual race data measured.

The **Real Time Full Circuit Driving Simulation System** proved itself as an invaluable engineering tool and took dynamic engine testing to a new level with a vast number of opportunities to be explored

8.2 Recommendations

The following will improve the circuit simulation.

8.2.1 Test system components

- Low inertia AC or DC dynamometer.

Any dynamic engine testing simulation is severely limited by the inertia of the electric motor. The CAE dynamic engine testing facility will benefit from acquiring a state of the art AC asynchronous dynamometer for example the AVL DynoExact APA 100 series.

- Control computer.

The computer used has a 800MHz CPU which is slow by modern standards but is suited to connect with the PC30 data acquisition card. When a faster machine is used it will speed up the real time calculation process and increase the accuracy of the simulation. An example of such a system is a Pentium 4, 3.4GHz processor with four 80 Gig hard drives that runs in parallel. This will allow fast processing and rapid hard drive access.

8.2.2 Circuit simulation program

- Track data.

The circuit simulation used the track data as input and combining it with the dynamic vehicle model predicts lap times. The more accurate this data is the more accurate the simulation will be. During the track testing a standard GPS was the major source of data capturing but is not accurate enough to capture the precise racing line. The elevation data could not be used and therefore there was reverted to the manual process of inclination measurement. By finding more appropriate techniques the accuracy of the simulation can be improved on. The latest GPS system with WAAS technology claims a positional error of less than 3m.

- Cornering strategy.

The simulation uses corner segments with varying radii as described earlier to predict corner speeds. Increasing the number of segments will improve the simulation but the ideal would be to use a continuous varying curve to represent a turn. The simulation also assumed that a vehicle's speed would decrease through a corner until the apex and then increase again. This might not always be the case when complex corners are encountered.

- Dynamic vehicle model.

The dynamic vehicle model used was very simple to increase real time calculation speed by keeping calculations simple without the need for iterative techniques. With the availability of faster computers it might be worth the effort to use a more complex model to include suspension set up.

- Control strategy.

The friction circle was the governing factor of the software simulation and excluded the use of virtual driver models. If the object of the tests is to simulate human drivers, then driver models would have to be included in the software.

- Data capturing.

During the real time simulation program data were written to files. The speed of the process might be improved if the data were stored in a buffer and streamed to the files at a later stage.

References

Allen R.W., Rosenthal T.J., Klyde D.H. and Christos J.P., 2000, Vehicle and tire modelling for dynamic analysis and real-time simulation, SAE paper no. 2000-01-1620.

Alles S., Swick C., Hoffman M., Mahmud and Lin F., 1994, A real-time hardware-in-the-loop vehicle simulator for traction assist, International Journal of Vehicle Design Vol 15 no. 6.

Bosch GmbH, 1993, Automotive Handbook, Third Edition, 323-324, 483-488.

Brown D.G. and Thompson S., 1983, A novel approach to engine torque and speed Control, SAE paper no. 831302.

Cassidy J.F. and Rillings J.H., 1972, Transient engine testing by computer control, SAE paper no. 720454.

Conradie P.A., 2001, The development of a dynamic engine testing facility, M.Sc Eng, University of Stellenbosch, published.

Day T. and Metz L.D., 2000, The simulation of driver inputs using a vehicle driver Model, SAE paper no. 2000-01-1313.

Fullmer R.R., Tuken T. and Van Gerpen J.H., 1992, Adaptive Torque Control of a Diesel Engine for Transient Test Cycles, SAE paper no. 920238.

Franklin G.F., Powell J.D. and Emami-Naeini A., 2002, Feedback Control of Dynamic Systems, Fourth edition, Prentice Hall.

Gallacher A.M. and Krebi W.H., 1995, Dynamic engine testing: Why? SAE paper no. 952301.

Gillespie T.D., 1992, Fundamentals of vehicle dynamics, SAE inc, ISBN 1-56091-199-9.

Hong C., 1995, An automotive dynamic performance simulator for vehicle power train system design, International. Journal of Vehicle Design Vol 16.

Jacobs O.L.R., 1996, Introduction to control theory, Oxford science publications.

Jacobson B., 1995, On vehicle driving cycle simulation, SAE paper no. 950031.

Leonhardt S., Schmidt C., Voigt K. and Iserman R., 1992, Real-time simulation of drive trains for use in dynamical engine test stands, American Control Conferance.

Milliken, W.F. and Milliken D.L., 1995, Race car vehicle dynamics, SAE inc. ISBN 1-56091-526-9.

Noble A.D., Beaumont A.J. and Mercer A.S., 1988, Predictive control applied to transient engine testbeds, SAE paper no. 880487.

Pacejka E., Bakker E. and Lidner L., 1989, A new tire model with an application in vehicle dynamics studies, SAE paper no 890087.

Setright L.J.K., 1972, Automobile tyres, Halstead press SBN 412 09850 4.

Shafai E. and Geering H.P., 1989, Emulation of vehicle dynamics on an engine test bench, American Control Conference.

Siegler B., Deakin A. and Crolla D., 2000, Lap time simulation: comparison of steady state, quasi-static and transient racing car cornering strategies, SAE paper no. 2000-01-3563.

Vehicle Dynamics Terminology, 1976, SAE J670e.

Voigt K.U., 1991, A control scheme for a dynamical combustion engine test stand, Technical University of Darmstadt, Institute of Control Engineering, Germany.

Von Thun H., 1987, A new dynamic combustion engine test stand with real-time simulation of the vehicle drive line, SAE paper no. 870085.

Voos W., 1992, Dynamic engine testing, SAE paper no. 920254.

Appendix A

A.1 Pre-processor: Stage 1 derivation

Summation of forces in the lateral direction when a vehicle negotiates a turn at the maximum possible speed results in the following equations:
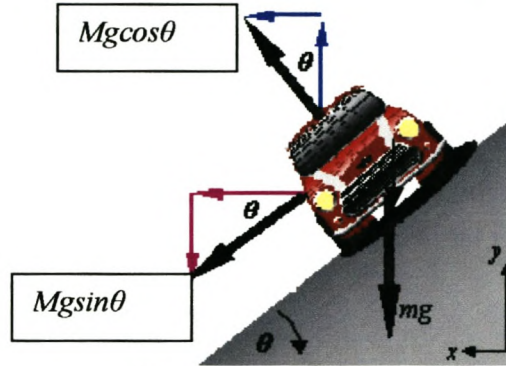
Figure A.1 Vehicle on banked turn

$$-Mg\sin\theta - (Mg\cos\theta + \frac{MV^2}{R}\sin\theta)\mu + \frac{MV^2}{R}\cos\theta = 0 \qquad (A.1)$$

$$Divide\ by: -M\cos\theta \qquad (A.2)$$

$$\therefore g\tan\theta + \mu g + \frac{\mu V^2}{R}\tan\theta - \frac{V^2}{R} = 0 \qquad (A.3)$$

$$\therefore g(\tan\theta + \mu) + \frac{V^2}{R}(\mu\tan\theta - 1) = 0 \qquad (A.4)$$

$$\therefore V^2 = -\frac{Rg(\tan\theta + \mu)}{\mu\tan\theta - 1} \qquad (A.5)$$

$$\therefore V = \sqrt{\frac{Rg(\tan\theta + \mu)}{1 - \mu\tan\theta}} \qquad (A.6)$$

88

A.2 Pre-processor: Stage 2 derivation

The following derivation is done using the bicycle model as basis and implements the friction circle concept on the front wheels of a front wheel drive vehicle. When a vehicle is cornering at maximum constant speed on a constant radius bend then the longitudinal force present at the tyre contact patch of the driven wheels equals the rolling, drag and gradient resistance:

$$F_x = F_r + F_g + F_d \tag{A.7}$$

with

$$F_r = Wf_r \tag{A.8}$$

$$F_g = W\sin\theta \tag{A.9}$$

$$F_d = \tfrac{1}{2}\rho V^2 C_d A \tag{A.10}$$

The lateral force present at contact patch of the front wheels equals:

$$F_{yf} = \frac{M_f V^2 \cos\theta}{R} - M_f g\sin\theta \tag{A.11}$$

According to the friction circle concept the total force available equals the normal force present at the contact pact multiplied by the friction coefficient:

$$F = \left(M_f g\cos\theta + \frac{M_f V^2 \sin\theta}{R} \right)\mu \tag{A.12}$$

Applying the friction circle formula yields:

$$F^2 = F_x^2 + F_{yf}^2 \tag{A.13}$$

After substituting the above in equation A.10 the only unknown in the equations is V, which can be solved by various means and leads to:

$$V = \frac{-C - \sqrt{C^2 - 4TK}}{2T} \tag{A.14}$$

with

$$T = -0.25(\rho A C_d)^2 - (\frac{M_f \cos\theta}{R})^2 + (\frac{\mu M_f \sin\theta}{R})^2$$

$$C = \frac{2\mu^2 M_f^2 g\cos\theta\sin\theta}{R} - \frac{F_r \rho A C_d + 2M_f^2 \cos\theta g\sin\theta}{R} - F_g \rho A C_d$$

$$K = (\mu M_f g\cos\theta)^2 - F_g^2 - F_r^2 - 2F_g F_r - (M_f g\sin\theta)^2$$

A.3 Sample of a output file *.dbf:

Table A.1 is an example of the output file that is generated when the simulation runs.

Table A.1 Output.dbf

TIME	DISTANCE	ENG_SPEED	VEH_SPEED	GEAR_RATIO	MAX_TORQUE	THROT_POS	LONG_G	LAT_G
5.400	53.01	4475.50	62.77	2.00	126.23	65.83	2.94	0.00
5.464	54.15	4509.00	63.46	2.00	124.61	65.83	2.88	0.00
5.530	55.29	4601.20	64.13	2.00	127.04	65.83	2.94	0.00
5.596	56.47	4643.20	64.82	2.00	126.23	65.83	2.84	0.00
5.661	57.66	4685.10	65.50	2.00	123.00	65.83	2.88	0.00
5.728	58.85	4752.10	66.17	2.00	125.42	65.83	2.88	0.00
5.796	60.09	4802.40	66.87	2.00	124.61	65.83	2.87	0.00
5.860	61.36	4852.70	67.57	2.00	125.42	65.83	2.84	0.00
5.928	62.57	4877.90	68.22	2.00	121.38	65.83	2.77	0.00
5.994	63.86	4961.70	68.90	2.00	125.42	65.83	2.88	0.00
6.060	65.13	5003.60	69.58	2.00	124.61	65.83	2.80	0.00
6.128	66.41	5045.60	70.25	2.00	123.00	65.83	2.74	0.00
6.194	67.75	4995.30	70.92	2.00	116.52	65.83	2.77	0.00
6.260	69.05	5129.40	71.58	2.00	118.95	65.83	2.69	0.00
6.330	70.37	5204.80	72.22	2.00	121.38	65.83	2.75	0.00
6.396	71.78	5255.10	72.91	2.00	121.38	65.83	2.76	0.00
6.463	73.12	5297.00	73.57	2.00	120.57	65.83	2.79	0.00
6.531	74.50	5364.10	74.24	2.00	118.95	65.83	2.70	0.00
6.598	75.91	5389.30	74.90	2.00	118.95	65.83	2.69	0.00
6.665	77.31	5422.80	75.55	2.00	121.38	65.83	2.65	0.00
6.733	78.72	5489.90	76.19	2.00	115.71	65.83	2.51	0.00
6.800	80.16	5506.60	76.80	2.00	121.38	65.83	2.55	0.00
6.870	81.60	5590.50	77.42	2.00	113.29	65.83	2.53	0.00
6.938	83.11	5624.00	78.05	2.00	111.67	65.83	2.49	0.00
7.005	84.59	5682.70	78.66	2.00	113.29	65.83	2.51	0.00
7.081	86.06	5724.60	79.27	2.00	110.05	65.83	2.43	0.00
7.148	87.74	5758.10	79.94	2.00	105.19	65.83	2.41	0.00
7.216	89.24	5825.20	80.52	2.00	106.81	65.83	2.37	0.00
7.284	90.76	5858.70	81.10	3.00	108.43	0.00	0.00	0.00
7.352	92.29	5992.90	81.10	3.00	103.58	0.00	0.00	0.00
7.423	93.83	5942.60	81.10	3.00	79.30	0.00	0.00	0.00
7.465	95.42	5867.10	81.10	3.00	-0.81	0.00	0.00	0.00
7.509	96.37	5791.70	81.10	3.00	-59.88	0.00	0.00	0.00
7.551	97.36	5758.10	81.10	3.00	-20.23	0.00	0.00	0.00
7.594	98.31	5791.70	81.10	3.00	-49.36	0.00	0.00	0.00
7.637	99.28	5800.00	81.10	3.00	-33.99	0.00	0.00	0.00
7.680	100.25	5758.10	81.10	3.00	-29.13	0.00	0.00	0.00
7.724	101.21	5741.40	81.10	3.00	-25.08	0.00	0.00	0.00
7.767	102.21	5716.20	81.10	3.00	-19.42	0.00	0.00	0.00
7.811	103.17	5665.90	81.10	3.00	-12.14	65.83	0.00	0.00
7.854	104.16	5632.40	81.00	3.00	-13.76	65.83	0.00	0.00

Appendix B

B.1 Determination of cut-off frequency

Figure B.1 show the dynamometer bandwidth and cut-off frequency determination by Conradie (2001) for the CAE dynamic engine test facility. The tests were run at a nominal speed of 5000rpm and oscillation amplitude of 400 rpm. The frequency at which the magnitude of the output signal was 3dB less than that of the input signal was taken as the cut-off frequency for this test. The cut-off frequency was determined at 2.15Hz
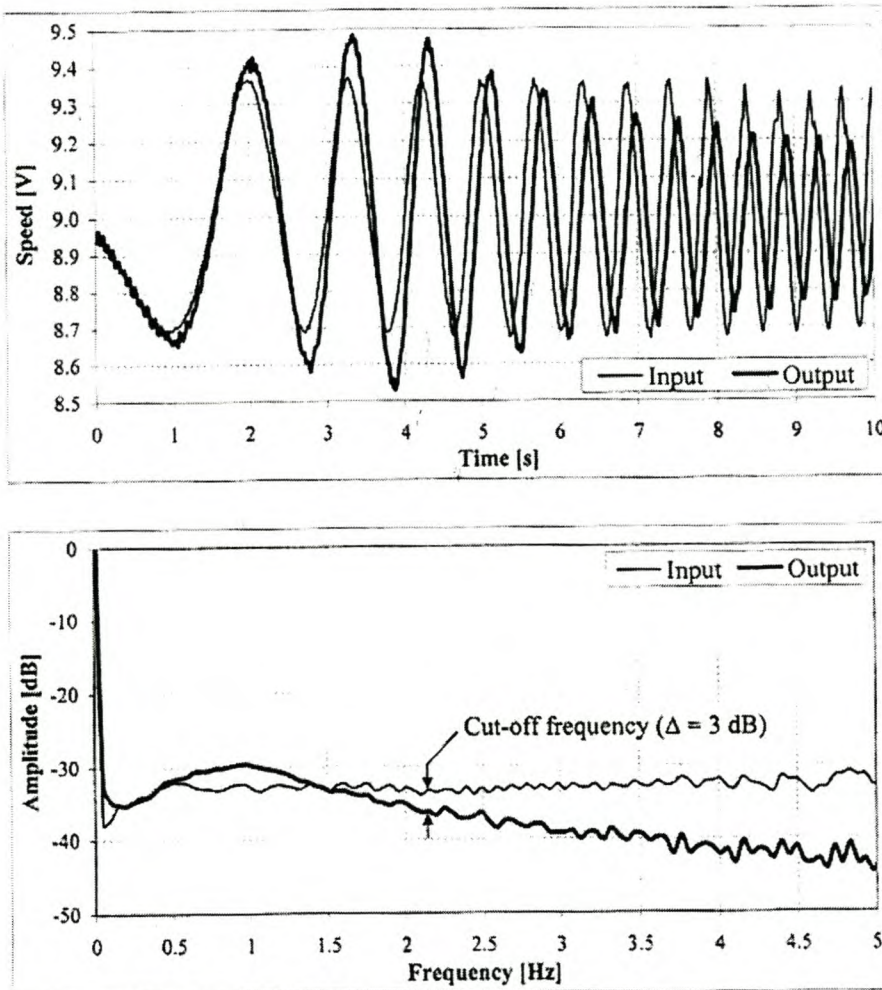
Figure B.1 Cut-off frequency

B.2 Torque flange specifications:

For the Real Time Full Circuit Simulation the 5k transducer was used.

Table B.1 Torque flange sheet 1

Specifications

Type		T10F								
Accuracy class		0.1								
Torque measuring system										
Nominal (rated) torque M_nom	N·m	50	100	200	500	1k	2k	3k	5k	10k
for reference only	ft–lb	37.5	75	150	375	750	1500	2250	3750	7500
Nominal (rated) sensitivity (nominal (rated) signal range between torque = zero and nominal (rated) torque)										
Frequency output	kHz	5								
Voltage output	V	10								
Characteristic tolerance (deviation of the actual output quantity at M_nom from the nominal (rated) signal range)										
Frequency output	%	± 0.1								
Voltage output	%	± 0.2								
Output signal at torque = zero										
Frequency output	kHz	10								
Voltage output	V	0								
Nominal (rated) output signal										
Frequency output										
with positive nominal (rated) torque	kHz	15 (5V symmetric[1]/12V asymmetric[2])								
with negative nominal (rated) torque	kHz	5 (5V symmetric[1]/12V asymmetric[2])								
Voltage output										
with positive nominal torque	V	+10								
with negative nominal torque	V	–10								
Load resistance										
Frequency output	kΩ	≥2								
Voltage output	kΩ	≥5								
Long–term drift over 48h										
Voltage output	mV	≤± 3								
Measurement frequency range										
Voltage output	Hz	0 ... 1000 (–3dB)								
Group delay time										
Frequency output	ms	0.15								
Voltage output	ms	0.9								
Residual ripple Voltage output	%	0.4 (peak-to-peak)								
Temperature influence per 10 K in the nominal (rated) temperature range										
on the output signal, related to the actual value of signal span										
Frequency output	%	< ± 0.1								
Voltage output	%	< ± 0.2								
on the zero signal, related to the nom. sensitivity										
Frequency output	%	< ± 0.1	< ± 0.05							
Voltage output	%	< ± 0.2	< ± 0.15							
Power supply (version KF1)										
Excitation voltage (square wave)	V	54 ± 5% (peak-to-peak)								
Release of calibration signal	V	80 ± 5%								
Frequency	kHz	approx. 14								
Max. current consumption	A	1 (peak-to-peak)								
Preamplifier excitation voltage	V	0/0/+15								
Preamplifier, max. current consumption	mA	0/0/+25								
Power supply (version SF1/SU2)										
Nominal (rated) supply voltage (protective low voltage)	V (DC)	18 ... 30; asymmetric								
Current consumption in measuring mode	A	< 0.9								
Current consumption in start-up mode	A	< 2								
Nominal (rated) power consumption	W	< 12								
Linearity deviation including hysteresis, related to the nominal (rated) sensitivity										
Frequency output	%	< ± 0.1 (< ± 0.05 optional)								
Voltage output	%	< ± 0.1 (< ± 0.07 optional)								

[1] RS 422 complementary signals: factory settings version SF1/SU2
[2] Factory settings version KF1 (no switching possible)

92

Table B.2 Torque flange sheet 2

Nominal (rated) torque M_{nom}	N·m	50	100	200	500	1k	2k	3k	5k	10k
for reference only	ft–lb	37.5	75	150	375	750	1500	2250	3750	7500
Rel. standard deviation of the repeatability										
according to DIN 1319, by reference to variation of the output signal	%					$< \pm 0.03$				
Calibration signal					approx. 50% of M_{nom} value given to the identification plate					
Tolerance of calibration signal	%					$< \pm 0.05$				
Speed measuring system										
Measuring system					optical, by means of infrared light and metallic slotted disc					
Mechanical increments	Number			360				720		
Positional tolerance of the increments	mm					± 0.05				
Tolerance of the slot width	mm					± 0.05				
Pulses per rotation										
adjustable	Number		360; 180; 90; 60; 30; 15				720; 360; 180; 90; 60; 30; 15			
Output signal	V				5 symmetric (RS 422 complementary signals) 2 square wave signals 90° phase shifted					
Load resistance	kΩ					≥ 2				
Minimum speed for sufficient pulse stability	rpm					2				
Group delay time	µs					< 5 typ. 2.2				
Max. permissible axial displacement between rotor and stator	mm					± 2				
Max. permissible radial displacement between rotor and stator	mm					± 1				
Hysteresis of reversing the direction of rotation [3] with relative vibrations between rotor and stator										
Torsional rotor vibrations	Degree					$<$ approx. 2				
Radial stator vibrations	mm					$<$ approx. 2				
Permitted degree of soiling, in the optical path of the sensor fork (lenses, slotted disc)	%					< 50				
Protection against scattered light						by fork and infrared filter				
General data										
EMC										
EMI (Immunity) (EN50082–2)										
RF enclosure	V/m					10				
RF common mode	Vpp					10				
Magnetic field	A/m					100				
Burst	kV					2/1				
ESD	kV					4/8				
EME (Emission) (EN55011; EN55022; EN55014)										
RFI voltage						Class A				
RFI power						Class B				
RFI field strength						Class B				
Degree of protection according to EN 60529						IP 54				
Weight, approx. Rotor		0.9	0.9	1.8	3.5	3.5	5.8	7.8	14.0	15.2
Rotor with speed measuring system		1.1	1.1	1.8	3.5	3.5	5.9	7.9	14.1	15.3
Stator		1.1	1.1	1.2	1.2	1.2	1.3	1.3	1.4	1.4
Reference temperature	°C | °F					+23 |73.4|				
Nominal (rated) temperature range	°C | °F					+10...+60 |+50...+140|				
Service temperature range	°C | °F					–10...+60 |+14...+140|				
Storage temperature range	°C | °F					–20...+70 |–4...+158|				
Impact resistance, test severity level to IEC 68; part 2-27; IEC 68-2-27-1987										
Number of impacts	n					1000				
Duration	ms					3				
Acceleration (half–sine)	m/s²					650				
Vibration resistance, test severity level to IEC 68, part 2-6; IEC 68-2-6-1982										
Frequency range	Hz					5...65				
Duration	h					1.5				
Acceleration (amplitude)	m/s²					50				

[3] Can be switched off

93

Table B.3 Torque flange sheet 3

		50	100	200	500	1k	2k	3k	5k	10k
Nominal (rated) torque M_{nom}	N·m	50	100	200	500	1k	2k	3k	5k	10k
Nominal (rated) speed (x1000)	rpm	15	15	15	12	12	10	10	8	8
Load limits[4]										
Limit torque, related to M_{nom}	%	400				200				160
Breaking torque, related to M_{nom}	%	>800				>400				>300
Axial limit force	kN	2	2	4	7	7	12	14	22	31
Lateral limit force	kN	1	1	3	6	8	15	18	30	40
Bending limit moment	N·m	70	70	140	500	500	1000	1600	2500	4000
Oscillation bandwidth according to DIN 50100 (peak-to-peak) [5]	kN·m	0.16	0.16	0.32	0.8	1.6	3.2	4.8	8.0	12.0
Mechanical values										
Torsional stiffness C_T	kN·m/rad	160	160	430	1000	1800	3300	5100	9900	15000
Torsion angle at M_{nom}	Degree	0.018	0.036	0.027	0.028	0.032	0.034	0.034	0.029	0.038
Maximum excursion at axial limit force	mm	< 0.03								
Additional max. concentricity error at lateral limit force	mm	< 0.01			< 0.02			< 0.03		
Additional plane-parallel deviation at bending limit moment	mm	< 0.2								
Balance quality-level to DIN ISO 1940		G 6.3								
Max. limits for relative shaft vibration (peak-to-peak)[6]	µm	$s_{max} = \dfrac{4500}{\sqrt{n}}$								
Mass moment of inertia of the rotor										
I_V (about axis of rotation) x10⁻³	kg·m²	1.3		3.4	13.2		29.6	41	110	120
I_V with speed system x10⁻³	kg·m²	1.7		3.5	13.2		29.6	41	110	120
Proportional mass moment of inertia (measuring-body side)	%	51		44	39		38	33	31	33
Proportional mass moment of inertia with speed measuring system (measuring-body side)	%	40		43	39		38	33	31	33
Max. permissible static eccentricity of the rotor (radially) [7]	mm	± 2								
Permissible axial displacement between shaft and housing [7]	mm	± 2			± 3					

94

B.3 PC30 data acquisition card specifications:

Table B.4 PC30 sheet1

Table 1	Analog Inputs
Number of Channels Number of Channels with simultaneous sample/hold	16 single-ended or 8 differential (software selectable) 16 single ended only
Resolution	12-bits (1 in 4096)
Total System Accuracy (absolute accuracy)	±1 bit LSB (for Gain of 1)
Linearity: Integral Differential	±0.05% FS ±¼ LSB max.
A/D Input Voltage - Ranges	±5V, ±10V, 0 to 10V (PC30G, PC30GA) ±5V, ±10V (PC30F, PC30FA) ±5V (PC30GAS4, PC30GAS16, PC30FAS4, PC30FAS16)
Data Acquisition Rate	PC30G: 100kHz, PC30F: 330kHz (G<1000) PC30G: 100kHz, PC30F: 100kHz (G=1000)

Input Impedance:
   On Channel
   Off Channel
	
	10M/20pF
	10M/100pF

Offset Voltage Input Bias Current Input Bias Offset Drift	±5 LSB adjustable to 0 ±100 pA/°C ±30ppm/°C

Input Gains:
   Ranges
   Gain Error
   Gain Accuracy
   CMRR for various
   gains
   Monotonicity
	
	1, 10, 100, 1000 or 1, 2, 4, 8 (S/W selectable)
	Adjustable to 0
	0.25% max, 0.05% typical for gains < 1000
	
	1% max, 0.1% for g=1000
	0 to 70°C

Temperature Drift: Full Scale Error Drift Bipolar Zero Drift Gain	 6 ppm/°C (PC30Fx) 1 ppm/°C (PC30Fx) ±30 ppm/°C

95

Table B.5 PC30 sheet 1b

Table 1	Analog Inputs
Input Over voltage Protection	±12V
A/D FIFO Buffer Size	16 samples
Channel Gain/Queue Length	31

A/D Clock:
    Internal Clock
    Clock frequency tolerance
    Clock Drift
    Internal Clock Divider
    External Clock
    External Trigger
    Channel List (queue) Length
    Block Scan Mode
	2 MHz or 8 MHz (software selectable)
	0.01%
	
	10 ppm/°C
	2 x 16 bit stages
	TTL compatible
	TTL compatible
	
	31
	Up to 256 channels per block; all channels converted at max. thruput on each clock pulse

Noise Levels (p-p)	G=1: ±1 bit; G=10: ±1 bit; G=100: ±2 bits Noise levels will vary according to environmental conditions
Data Acquisition Modes	Polled I/O, Interrupts, Single and Dual Channel DMA

Table B.6 PC30 sheet 2&3

Table 2	Analog Outputs
Number of channels	4
Resolution	Two 12-bit, two 8-bit
Accuracy	±1 LSB (12-bit), 0 LSB (8-bit)
Differential Nonlinearity	±1 LSB max.
Output Ranges	±5V, ±10V, 0 to 13 V (software selectable)
Offset Error	Unipolar: ¼ LSB typical, 1 LSB max. (12 bit) Bipolar: ½ LSB typical, 2 LSB max. (12 bit)
Gain: Ranges Error	x1, x2 2 LSB typical, 5 LSB (12 bit)
Settling time to ½ LSB	10 µs max. in a Load of 500 p, 2 kΩ
Throughput Rate	500 kHz (depending on computer)
Temperature Drift	100 ppm/°C of full scale
Max. Current Output Source	5 mA maximum
Monotonicity	0 to 70°C

Table 3	Digital I/O
Number of I/O Lines	24 in 3 ports (8255 PPI)
Voltage Compatibility	TTL
Interface Selection	Programmable for simple I/O, strobed I/O or handshake I/O
Max. Input Voltage	5.5V
Max. Current Source/Sink	±1 mA

Table B.7 PC30 sheet 4 - 8

Table 4	Timer/Counter Specifications
Resolution	16 bits
Voltage Compatibility	TTL
Number of Counters	3 (2 used for A/D timing)

Table 5	PC Interface
Base Address	0 - 1FFF DIP Switch selectable
Number of Registers	32 8 bit registers
Interrupts	Register selectable for end of conversion, DMA block or timer
DMA	Dual channel jumper selectable to levels 5, 6 or 7
I/O Connector	50-way female D-type (same as PC30 series)

Table 6	Environmental Specifications
Operating Temperature	0 to 70°C
Storage Temperature	-55 to 150°C
Relative Humidity	5% to 95% noncondensing

Table 7	Power Requirements
+5 V	500 mA typ.
+12 V	100 mA typ.
-12 V	100 mA typ.

Table 8	Physical
Dimensions	193 mm long, 111 mm high (excluding gold edger connector, DB50 connector and bracket)

Appendix C
C.1 Ford Fiesta RSI Specifications (Car, 2001):

Ford Fiesta 1,6 RSi ★★★★☆

SPECIFICATIONS

ENGINE:

Cylinders	four in-line, transverse
Fuel supply	electronic fuel injection
Bore/stroke	82/75,48 mm
Cubic capacity	1 594 cm³
Compression ratio	9,5 to 1
Valve gear	s-o-h-c
Ignition	electronic
Main bearings	five
Fuel requirement	unleaded

ENGINE OUTPUT:

Max power ISO (kW)	70
Power peak (r/min)	5 500
Max usable r/min	6 175
Max torque (N.m)	137
Torque peak (r/min)	2 500

TRANSMISSION:

Forward speeds	five
Low gear	3,593 to 1
2nd gear	1,925 to 1
3rd gear	1,281 to 1
4th gear	0,951 to 1
Top gear	0,756 to 1
Reverse gear	3,615 to 1
Final drive	4,060 to 1
Drive wheels	front

WHEELS AND TYRES:

Road wheels	14x6,0J alloy
Tyre make	Continental Sport Contact
Tyre size	185/85 R14
Tyre pressures (front)	210 to 250 kPa
Tyre pressures (rear)	180 to 280 kPa

BRAKES:

Front	discs
Rear	drums
Hydraulics	dual circuit
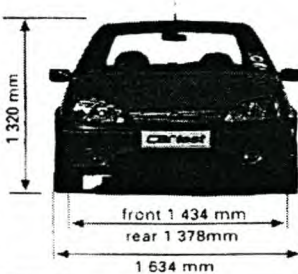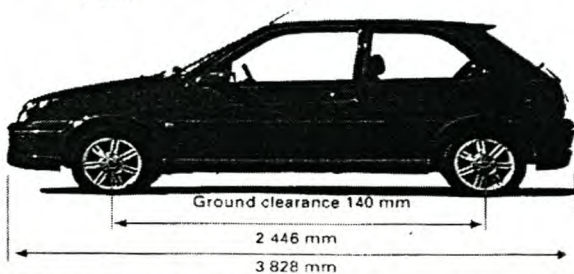
STEERING:

Type	variable rate rack-and-pinion, power assisted
Lock to lock	2,8 turns
Turning circle	9,9 metres

SUSPENSION

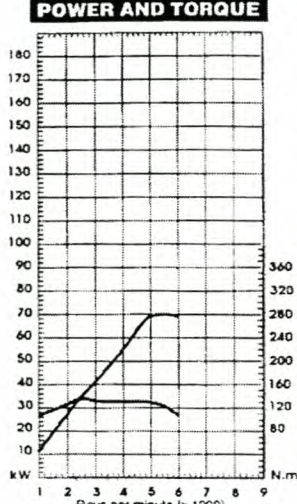|	
Front	MacPherson struts, lower wishbones, anti-roll bar
Rear	torsion beam, strut-type coil spring/damper units

CAPACITIES:

Seating	4/5
Fuel tank	42 litres
Boot space	224 dm³
Utility space	856 dm³

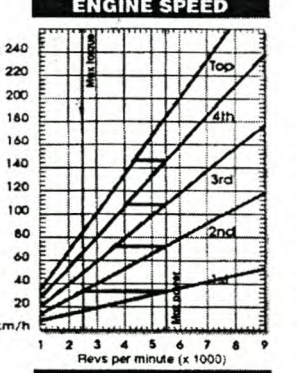**WARRANTY AND SERVICE INTERVALS:**
12 months/100 000 km
Service every 15 000 km

TEST CAR FROM:
Ford Motor Company of Southern Africa
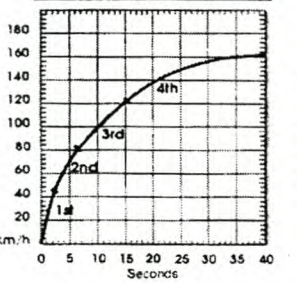
L6 RSi

POWER AND TORQUE

ENGINE SPEED

ACCELERATION

TEST RESULTS

MAXIMUM SPEED (km/h):

True speed	179 at 5 360 r/min in top gear
Speedometer reading	185

(Average of runs both ways on a level road)

Calibration:	60	80	100	120
True speed:	56	76	96	116

Odometer error   0,39 per cent under

ACCELERATION (seconds):

0-60	4,00
0-80	6,50
0-100	10,33
0-120	14,88
1 km sprint	32,03
Terminal speed	157,5 km/h

OVERTAKING ACCELERATION (seconds):

	3rd	4th	Top
40-60	3,24	5,00	6,90
60-80	3,47	4,95	7,12
80-100	3,61	5,48	7,63
100-120	5,06	6,45	9,63
120-140	–	7,81	12,34

FUEL CONSUMPTION (litres/100 km):

60	4,51
80	5,40
100	6,54
120	8,18
*Fuel index	9,16 litres/100 km
	10,92 km/litre

Estimated tank range   459 km
(*Calculated overall consumption)

BRAKING TEST:
From 100 km/h

Best stop	3,1
Worst stop	3,8
Average of 10 stops	3,4

(Measured in seconds with stops from true speeds at 30-second intervals on a good bitumenised surface.)

RESERVE POWER (in top):

Speed	kW available	kW used	Total kW
80	20	10	30
100	22	18	40
120	21	23	44
140	19	39	58

GEARED SPEEDS (km/h):

Low gear	33*	44
2nd gear	72*	81
3rd gear	108*	122
4th gear	146*	164
Top gear	184*	206

(Calculated at engine power peak* – 5 500 r/min and at max. usable r/min – 6 175 r/min.)

INTERIOR NOISE LEVELS (db, A-weighted):

	Mech	Road
Idling	33	–
60	51	–
80	53	60
100	56	63
120	59	65

PERFORMANCE FACTORS:

Power/mass net (W/kg)	75,68
Frontal area (m²)	2,16
km/h per 1 000 r/min (top)	33,43
Mass as tested (kg)	925

(Calculated on "mass as tested", gross frontal area, gearing and ISO power output)

TEST CONDITIONS:

Altitude	at sea level
Weather	warm, light wind
Fuel used	95 octane unleaded
Test car's odometer	3 187

1 320 mm

front 1 434 mm
rear 1 378mm
1 634 mm

Ground clearance 140 mm
2 446 mm
3 828 mm

CAR November 2001

Figure C.1 Ford RSI specification

98

C.2 MicroStrain specifications:

Orientation Range	360 degrees full scale (FS), all axes (Matrix, Quaternion modes)
Angular Velocity Range	+/-300 degrees/second (max)
A/D Resolution	12 bits
Dynamic Compensation	Closed loop digital control (0 to 50 Hz)
Orientation Angle Resolution	< 0.1 degrees (angle resolution specifications taken at most aggressive filter setting)
Temperature Drift single axis:	+/0.025%/degrees Celsius
Nonlinearity	0.23% full scale (tested in static conditions)
Repeatability	0.10 degrees
Accuracy	+/-5 degrees typical for an arbitrary angular orientation (accuracy specifications taken at constant ambient temperature; tested with known sine and step inputs including angular rates to 300 degrees/second)
Output Modes	Matrix, Quaternion, Scaled Sensor Bits
Sensor Range Gyros:	+/-300 degrees/second FS (full scale)
Accelerometers:	+/- 2 G's FS
Magnetometers:	+/-1 Gauss FS
Digital Outputs	RS-232, RS-485
Output Data Rate	100 Hz (digital RS-232)
Serial Data Rate	19,200 baud; 38,400 baud; 115,200 baud
Supply Voltage	5.2 VDC min, 12 VDC max
Supply Current	90 milliamps typical
Connectors	One keyed LEMO for RS-232 Two keyed LEMOs for RS-485
Operating Temperature	-40 to 70 degrees C with enclosure -40 to +85 degrees C without enclosure
Enclosure (w/tabs)	64mm by 90 mm by 25mm 2.5" by 3.5" by 1.0"
Weight	40 grams with enclosure
Shock Limit	1000g unpowered, 500g powered

CERTIFICATE OF CALIBRATION

This document certifies that the equipment referenced below meets published specifications.

Model Number: __3DM-G__

Serial Number: ___1024___   Calibration Date: __8/27/2002__

Description: _Gyro-Enhanced Inclinometer_   Calibration Technician: _____

MicroStrain, Inc.

310 Hurricane Lane, Suite 4
Williston, VT 05495-3211
USA
Ph (802) 862-6629, Fax (802) 863-4093
www.microstrain.com
info@microstrain.com

For any questions concerning this certificate, please call MicroStrain, Inc. for an application engineer.

Figure C.2 Microstrain calibration certificate

C.3 Garmin 5 GPS specifications:

Receiver: WAAS enabled, 12 parallel channel GPS receiver continuously tracks and uses up to 12 satellites to compute and update your position
Acquisition times:

- Warm: Approximately 15 seconds
- Cold: Approximately 45 seconds
- AutoLocate®: Approximately 5 minutes

Update rate: 1/second, continuous
GPS accuracy:

- Position: < 15 meters, 95% typical*
- Velocity: 0.05 meter/sec steady state

DGPS (USCG) accuracy:

- Position: 3-5 meters, 95% typical
- Velocity: 0.05 meter/sec steady state

DGPS (WAAS) accuracy:

- Position: < 3 meters, 95% typical
- Velocity: 0.05 meter/sec steady state
- Dynamics: 6g's

C.4 V-box specifications:

Specification

Velocity

Accuracy	0.1 Km/h (averaged over 4 samples)
Units	Km/h or Mph
Update rate	20 Hz
Maximum velocity	1000 Mph
Minimum velocity	0.1 Km/h
Resolution	0.01 Km/h

Distance

Accuracy	0.05% (<50cm per Km)
Units	Metres / Feet
Update rate	20Hz
Resolution	1cm
Height accuracy	6 Metres 95% CEP**
Height accuracy with DGPS	2 Metres 95% CEP**

Absolute Positioning

Accuracy	3m 95% CEP**
Accuracy with DGPS	1m 95% CEP**
Update rate	20 Hz
Resolution	1 cm

Heading

Resolution	0.01°
Accuracy	0.1°

Time

Resolution	0.01 s
Accuracy	0.001 s

Acceleration

Accuracy	0.5%
Maximum	20 G
Resolution	0.01 G
Update rate	20Hz

Memory

Internal memory	1 Mbyte battery backed SRAM
Recording time	Approx 55 minutes logging all GPS channels
External memory support	Compact Flash type 1
Recording time	Dependant on CF capacity. Approx 4.3 megabytes per hour used while logging all GPS channels.

Outputs

CAN Bus

Bit rate	250Kbits ,500Kbits & 1Mbit selectable baud rate
Identifier type	Standard 11bit 2.0A
Data available	Satellites in view, Latitude, Longitude, Velocity, Heading, Altitude, Vertical velocity, Distance, Longitudinal acceleration & Lateral acceleration

Analogue

Voltage range	0 to 5Volts DC
Default setting *	0.0125Volts per Km/h (0 to 400Km/h)
Accuracy	0.1 Km/h @ 100Km/h

Digital

Frequency range	DC to 44.4Khz
Default setting *	25Hz per Km/h (0 to 400Km/h)
Accuracy	0.01Km/h @ 100Km/h

* The range settings can be adjusted by the user in software

Power

Input Voltage range	6-18v DC
Current	Typically 560mA

101